CHAPTER 20

SOLUTION METHODS FOR NONGRAY EXTINCTION COEFFICIENTS

20.1 INTRODUCTION

In the preceding chapters on solution methods for the radiative equation of transfer within participating media we have exclusively dealt with gray media, that is, media whose radiative properties (absorption coefficient κ, scattering coefficient σ_s, and phase function Φ, as well as emittance of boundary surfaces ϵ) do not vary across the electromagnetic spectrum. We noted that most relationships also hold true for a nongray medium on a spectral basis (i.e., as long as the simplification of radiative equilibrium is not invoked). While the assumption of gray surfaces made in the net radiation method of Chapters 5 (diffusely reflecting surfaces) and 6 (partly specular reflecting surfaces) is often a good one over the relatively small relevant part of the spectrum, this is nearly never the case for participating media. Molecular gases below ionization temperatures (discussed in detail in Chapter 11) absorb and emit over a multitude of very narrow spectral lines, which may overlap and form vibration–rotation bands. The result is an absorption coefficient that oscillates wildly within each band, and is zero between bands. Similarly, the discussion of radiative properties of suspended particles (Chapter 12) has shown that their absorption and scattering properties may also oscillate strongly across the spectrum (see, for example, Fig. 12-3). However, if particles of varying sizes are present, as is usually the case, the spectral oscillations tend to be damped out so that the assumption of a gray medium becomes a reasonable one. Like molecular gases, semitransparent solids and liquids often display strong absorption bands in the infrared due to photon–phonon coupling, with weak absorption coefficients between bands. Therefore, we conclude that the simplification of a gray participating medium is, except for particle suspensions with variable sizes, a poor assumption that may lead to very significant errors in the analysis. It behooves the engineer to realize that accurate solutions to the equation of transfer (such as exact solutions in two or three dimensions), as opposed to simple approximate ones (such as the P_1-approximation in one or two dimensions), may be meaningless unless the spectral variation of radiation properties is taken into account.

Unfortunately, consideration of spectral variations of radiation properties tends to considerably increase the difficulty of an already extremely difficult problem, or at least make their numerical solution many times more computer-time intensive. All solution methods discussed

thus far, whether exact or approximate, are poorly suited for the consideration of nongray properties. In general, radiative heat flux, divergence of heat flux, and/or incident radiation must be evaluated for many, many spectral locations, followed by numerical quadrature of the spectral results. This process will always involve the guessing of a temperature field, followed by an iterative procedure. This statement is true even for the case of radiative equilibrium, since the condition $\nabla \cdot \mathbf{q} = 0$ holds only for total heat flux, but not for spectral heat flux: While it is true that each volume element must emit as much radiative energy as it absorbs, the re-emission of energy must not occur at the same wavelength; the wavelengths of absorption are determined by the local absorption coefficient and by the wavelengths of the incoming radiation (and, thus, depend on the temperature of the *surrounding* medium), while the wavelengths of emission are determined by the local absorption coefficient and the *local* temperature.

In principle, if detailed information is given for the spectral extinction coefficient of the participating medium, such as contained in the high-resolution HITRAN [1] and HITEMP [2] databases for molecular gases, accurate determination of radiative fluxes and sources can be made. In practice, the rapid spectral variation of the gas absorption coefficient requires approximately one million spectral evaluations for such "line-by-line" (LBL) calculations, making them impractical for all applications except as benchmarks for the evaluation of more approximate models. In the field of combustion, the earliest full-spectrum heat transfer line-by-line calculations were perhaps carried out by Denison and Webb [3–5], looking at one-dimensional slabs of water vapor–nitrogen mixtures with prescribed simple temperature profiles and constant water vapor concentration, using the HITRAN92 database. Rivière *et al.* [6] investigated a one-dimensional layer of air at $T > 10000\,\mathrm{K}$, and Pierrot and coworkers [7, 8] considered one-dimensional layers of mixtures containing H_2O and/or CO_2 with various simple temperature and concentration profiles (steps, linear, parabolic), using the French database [9, 10]. Similarly, Marin and Buckius [11] used the HITRAN92 database, while the later papers of Solovjov and Webb [12] and Modest and Zhang [13–16] used the HITEMP 1995 database [17]. A one-dimensional homogeneous slab containing CO was considered by Solovjov and Webb [18]. All these line-by-line calculations were generated as benchmarks for approximate global models, which will be discussed later in this chapter. Somewhat different line-by-line calculations were carried out by Tang and Brewster, looking at Elsasser-model lines superimposed on the exponential wide band model [19], and Monte Carlo-generated line-by-line results for a CO_2 mixture with linear-anisotropically scattering particles [20], both again for a one-dimensional slab. In nonequilibrium aerospace applications virtually all calculations to date have been line-by-line, one-dimensional, and decoupled, since no spectral models were available until very recently. The earliest calculations were done by Park using NEQAIR [21]. Most planetary entry calculations have used this database in uncoupled fashion, e.g., Olynick and coworkers evaluated radiative fluxes for the FIRE II [22] and Stardust [23] missions, Olejniczak [24] considered radiative heating during aerocapture on Titan (one of Jupiter's moons), etc. Optimized LBL schemes have recently been reported by da Silva [25] and Feldick and coworkers [26], the latter closely coupled to a hypersonic flow code. The only two-dimensional line-by-line heat transfer calculations to date appear to have been carried out by Modest and Zhang [13, 14, 16], who considered an axisymmetric combustion chamber with strong spatial variations in temperature and concentration of methane, water vapor, and carbon dioxide, and by Hartung and Hassan [27], who applied the modified differential approximation of Section 16.8 to hypersonic entry problems.

The complexity and time consumption of nongray property treatment may be decreased considerably if one considers limiting situations, or if some simple approximations are made for the spectral dependence of the absorption and/or scattering coefficients. In the following we shall first consider the simplest method, known as the *mean beam length method*, in which the entire participating medium is assumed to be a single isothermal zone that exchanges heat with finite surface areas, much like the net radiation method of Chapter 5, followed by the semigray approximation, which is a gray model, but uses different spectrally weighted property values for emission and absorption. Next the *box model* is discussed, in which the absorption coefficient

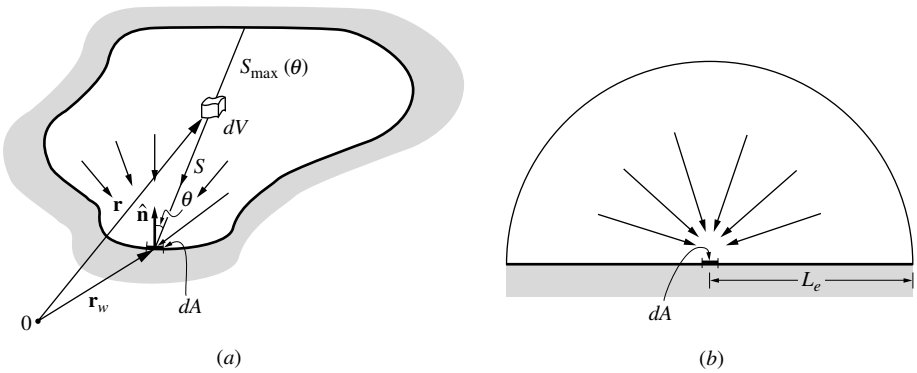

FIGURE 20-1
Isothermal gas volume radiating to surface element: (*a*) arbitrary gas volume, (*b*) equivalent hemisphere radiating to center of its base.

is assumed to attain a finite number of values that remain constant over finite wavenumber regions. This is followed by several sections that deal much more rigorously with the band nature of molecular gases, but are more or less limited to one-dimensional, plane-parallel, nonscattering media confined between black plates, culminating with the weighted-sum-of-gray-gases model, which is a very simple, accurate, and powerful method. Finally, global models based on high-resolution databases and on the *k*-distributions described in Chapter 11 will be described, which allow very accurate determination of radiative heat transfer in arbitrary geometries, including reflecting walls and/or scattering media.

20.2 THE MEAN BEAM LENGTH METHOD

The idea of a *mean beam length* was first advanced by Hottel [28] for the determination of radiative heat fluxes from an isothermal volume of hot combustion gases to cold black furnace walls. With some difficulty the method may be extended to include the effects of hot and gray walls. We include here only a brief discussion of the method, primarily for historical reasons and since the notion of a mean beam length is sometimes employed by other methods (see, for example, the box model in the next section). A somewhat more detailed account has been given by Hottel [28] and Hottel and Sarofim [29]. Today, with the availability of fast digital computers the method is somewhat outdated and is commonly replaced by the related zonal method, discussed in detail in Chapter 18, which allows not only for hot and gray walls, but also for a number of isothermal subvolumes within the enclosure.

Definition of Mean Beam Lengths

Consider a hot, isothermal, nonscattering gas volume radiating toward a black area element dA on its surface, as shown in Fig. 20-1*a*. The spectral heat flux arriving at and absorbed by dA from a volume element is equal to the spectral emission by dV into all (4π) directions $\times$ the fraction intercepted by $dA \times$ the fraction transmitted along the path from dV to dA. Thus, from equation (10.51) the spectral heat flux arriving at dA from all volume elements may be written as

$$q_\eta \, dA(\mathbf{r}_w) = \int_V (4\pi\kappa_\eta I_{b\eta} \, dV) \times \left(\frac{dA \cos\theta}{4\pi S^2} \right) \times e^{-\kappa_\eta S},$$

or

$$q_\eta(\mathbf{r}_w) = I_{b\eta} \int_V e^{-\kappa_\eta S} \frac{\kappa_\eta \cos\theta \, dV}{S^2}, \tag{20.1}$$

where we have chosen wavenumber η as the spectral variable. We notice that, in general, the heat flux from a hot gas volume arriving at a surface element dA is proportional to the blackbody intensity $I_{b\eta}$ and a factor which depends on the spectral absorption coefficient as well as on the geometry of the medium. While the integral factor will not be trivial to evaluate for most geometries, it is readily determined for a hemispherical volume radiating to the center of its base, dA, as shown in Fig. 20-1*b*. For this case $S = r$ and $dV = r^2 \sin\theta \, dr \, d\theta \, d\psi$, leading to

$$q_\eta = I_{b\eta} \int_{\psi=0}^{2\pi} \int_{\theta=0}^{\pi/2} \int_{r=0}^{R} e^{-\kappa_\eta r} \kappa_\eta \cos\theta \sin\theta \, dr \, d\theta \, d\psi = \pi I_{b\eta} (1 - e^{-\kappa_\eta R}) = \pi I_{b\eta} \epsilon_\eta, \tag{20.2}$$

where we have employed the definition for the spectral emissivity of an isothermal layer, equation (10.13). It is clear that the radiative heat fluxes arriving at dA, either from an arbitrary volume V or from a hemisphere of radius R, may be made equal if an appropriate value for the radius of the hemisphere is chosen. Thus, as far as the spectral, hemispherical irradiation onto dA is concerned, there is no difference whether the emission originated from an arbitrary volume or from an equivalent hemisphere of the correct radius $R = L_e$, where L_e is known as the mean beam length. Therefore, the definition of the mean beam length for an arbitrary volume irradiating an infinitesimal surface element dA is, from equations (20.1) and (20.2),

$$\frac{q_\eta}{\pi I_{b\eta}} = 1 - e^{-\kappa_\eta L_e} = \int_V e^{-\kappa_\eta S} \frac{\kappa_\eta \cos\theta \, dV}{\pi S^2}. \tag{20.3}$$

Note that the magnitude of the mean beam length depends on absorption coefficient as well as on geometry.

It is also common to define a mean beam length for an arbitrary volume irradiating a finite surface, by replacing the local heat flux q_η in equation (20.1) by a surface-averaged value, or

$$\frac{q_{\eta,\text{av}}}{\pi I_{b\eta}} = 1 - e^{-\kappa_\eta L_e} = \frac{1}{A} \int_A \int_V e^{-\kappa_\eta S} \frac{\kappa_\eta \cos\theta \, dV}{\pi S^2} dA. \tag{20.4}$$

Example 20.1. Determine the mean beam length for an isothermal gas layer of thickness L radiating to (*a*) an infinitesimal surface element, (*b*) an entire bounding surface.

Solution

The mean beam length may be evaluated by first finding from equation (14.40) the radiative heat flux hitting a surface element, or by integrating equation (20.3) directly. Choosing the latter for illustrative purposes, we express V in terms of a cylindrical coordinate system with its origin at dA. Thus, $dV = 2\pi r \, dr \, dz$, $S = \sqrt{r^2 + z^2}$, and $\cos\theta = z/S$, leading to

$$\frac{q_\eta}{E_{b\eta}} = \frac{1}{\pi} \int_{z=0}^{L} \int_{r=0}^{\infty} e^{-\kappa_\eta S} \frac{\kappa_\eta z \, 2\pi r \, dr \, dz}{S^3}.$$

By replacing the integration variable r by S, this expression becomes, with $r \, dr = S dS$,

$$\frac{q_\eta}{E_{b\eta}} = 2 \int_{z=0}^{L} \int_{S=z}^{\infty} e^{-\kappa_\eta S} \frac{\kappa_\eta z \, dS dz}{S^2} = 2\kappa_\eta \int_{z=0}^{L} E_2(\kappa_\eta z) \, dz,$$

where the definition for the exponential integral has been employed [see equation (14.31) or Appendix E]. Integrating, we obtain

$$\frac{q_\eta}{E_{b\eta}} = -2E_3(\kappa_\eta z)\Big|_0^L = 1 - 2E_3(\kappa_\eta L),$$

which, of course, would also have followed immediately from equation (14.40), if only emission from the medium had been considered ($T_1 = T_2 = 0$).

Thus, from equation (20.3), the mean beam length from the gas layer to a surface element dA is

$$L_e = \frac{1}{\kappa_\eta} \ln \frac{1}{2E_3(\kappa_\eta L)}.$$

The mean beam length for the entire surface, equation (20.4), is the same since, for this one-dimensional problem, local and average heat flux are identical.

Mean Beam Lengths for Optically Thin Media

Equations (20.3) and (20.4) are generally not trivial to evaluate and, for nongray media, the integrations need to be carried out for different absorption coefficients if total rather than spectral heat fluxes are desired (as is usually the case). However, the relationships become much simpler if optically thin media are considered, i.e., if $\kappa_\eta L \ll 1$, where L is a characteristic dimension of the medium. If we expand the exponents in equations (20.3) and (20.4), and drop terms of order κ_η^2 and higher, we find the mean beam length for an optically thin volume radiating to a point on its surface, L_0, is

$$1 - (1 - \kappa_\eta L_0) = \frac{1}{\pi} \int_V 1 \times \frac{\kappa_\eta \cos\theta \, dV}{S^2},$$

or

$$L_0 = \frac{1}{\pi} \int_V \frac{\cos\theta \, dV}{S^2}. \tag{20.5}$$

If we express the volume in terms of a spherical coordinate system centered at dA, with S as the radius, we may write $dV = S^2 \, dS \sin\theta \, d\theta \, d\psi = S^2 \, dS d\Omega$, and equation (20.5) becomes

$$\begin{aligned} L_0 &= \frac{1}{\pi} \int_{\psi=0}^{2\pi} \int_{\theta=0}^{\pi/2} \int_{S=0}^{S_{\max}(\theta,\psi)} \cos\theta \sin\theta \, dS d\theta \, d\psi \\ &= \frac{1}{\pi} \int_{2\pi} S_{\max}(\hat{\mathbf{s}}) \cos\theta \, d\Omega. \end{aligned} \tag{20.6}$$

Similarly, from equation (20.4), the mean beam length for an optically thin volume radiating to a finite surface is

$$L_0 = \frac{1}{\pi A} \int_A \int_{2\pi} S_{\max}(\mathbf{r}_w, \hat{\mathbf{s}}) \cos\theta \, d\Omega \, dA. \tag{20.7}$$

By employing physical arguments, one finds that the solution of equation (20.7) is trivial for the case that A is the entire area bounding the volume V: The total emission from the entire volume is, from equation (10.54), $4\pi\kappa_\eta I_{b\eta} V$. Since, for an optically thin medium, no self-absorption occurs, all of this energy must be absorbed by the (black) bounding surface. Therefore, the average heat flux onto the surface is

$$q_\eta = 4\pi\kappa_\eta I_{b\eta} V/A$$

and, from equation (20.3) (with $\kappa_\eta L_0 \ll 1$),

$$\frac{q_\eta}{\pi I_{b\eta}} = \kappa_\eta L_0 = 4\kappa_\eta V/A$$

or

$$L_0 = 4\frac{V}{A}. \tag{20.8}$$

The mean beam lengths for optically thin media, L_0, are often called *geometric mean beam lengths*, based on the work by Dunkle [30].

Example 20.2. Determine the mean beam lengths of Example 20.1 for an optically thin gas layer.

Solution
From the last example we have

$$\frac{q_\eta}{E_{b\eta}} = 1 - e^{-\kappa_\eta L_e} = 1 - 2E_3(\kappa_\eta L),$$

which, for $\kappa_\eta L \ll 1$, becomes

$$\frac{q_\eta}{E_{b\eta}} = 1 - 1 + \kappa_\eta L_0 = 1 - 2\left(\tfrac{1}{2} - \kappa_\eta L\right) = 2\kappa_\eta L,$$

or

$$L_0 = 2L.$$

The mean beam length for the entire surface is, of course, again the same. This could also have been found immediately from equation (20.8) as

$$L_0 = 4\frac{V}{A} = 4\frac{A_{\text{plate}} \times L}{2A_{\text{plate}}} = 2L.$$

Equation (20.8) is trivial to evaluate for any geometry, but even equations (20.7) (mean beam length to a part of the bounding surface) and (20.5) (mean beam length to a point on the bounding surface) are readily integrated for many configurations.

The geometric mean beam lengths between a gas volume and a bounding surface for a number of configurations, as collected by Hottel and Sarofim [29], with values for concentric cylinders and spheres added from Andersen and coworkers [31,32], have been summarized in Table 20.1.

Spectrally Averaged Mean Beam Lengths

The spectral heat flux, generated by emission from an isothermal volume, that is absorbed by an element of the black bounding surface (or the average heat flux onto a finite area) is given by equation (20.2) as

$$q_\eta = \epsilon_\eta(L_e)\pi I_{b\eta} = (1 - e^{-\kappa_\eta L_e})\pi I_{b\eta}, \tag{20.9}$$

where the mean beam length L_e depends on the spectral absorption coefficient as well as the geometry of the volume. However, Hottel noticed that the spectral heat flux q_η is not very sensitive to the spectral fluctuations of L_e, and that replacing the spectrally varying L_e by an *average mean beam length* L_m (independent of κ_η) predicts spectral heat fluxes with acceptable accuracy. This fact is demonstrated in Fig. 20-2, which shows the ratio of exact and approximate spectral heat fluxes, that is,

$$\frac{q_\eta\left(\kappa_\eta, L_e = L_e(\kappa_\eta)\right)}{q_\eta(\kappa_\eta, L_e = L_m = \text{const})} = \frac{1 - e^{-\kappa_\eta L_e}}{1 - e^{-\kappa_\eta L_m}}. \tag{20.10}$$

Two different geometries have been considered in Fig. 20-2, namely, an infinite slab radiating to a point on its boundary (or to an entire face), as given by Example 20.1, and a spherical volume radiating to a point on its surface (or to its entire surface). Inspection of Fig. 20-2 shows that the error in the evaluation of the spectral heat flux, if the average mean beam length is used, is never more than ~5% (if a suitable L_m is chosen). This statement may be generalized to other geometries. Values for the average mean beam lengths have also been included in Table 20.1. Inspection of the ratio between average and optically thin mean beam lengths, L_m/L_0, shows that their value is generally in the vicinity of 0.9. Therefore, a value of

$$L_m \simeq 0.9L_0 = 3.6\frac{V}{A} \tag{20.11}$$

TABLE 20.1
Mean beam lengths for radiation from a gas volume to a surface on its boundary.

Geometry of gas volume	Characterizing dimension L	Geometric mean beam length L_0/L	Average mean beam length L_m/L	L_m/L_0
Sphere radiating to its surface	Diameter, $L = D$	0.67	0.65	0.97
Concentric spheres to [32]:	Outer radius,			
inner surface (R_1)	$L = R_2$	$\phi_{s1}(R_1/R_2)$		
outer surface (R_2)	$L = R_2$	$\phi_{s2}(R_1/R_2)$		
Infinite circular cylinder to bounding surface	Diameter, $L = D$	1.00	0.94	0.94
Concentric cylinders to [31]:	Outer radius,			
inner surface (R_1)	$L = R_2$	$\phi_{c1}(R_1/R_2)$		
outer surface (R_2)	$L = R_2$	$\phi_{c2}(R_1/R_2)$		
Semi-infinite circular cylinder to:	Diameter, $L = D$			
Element at center of base		1.00	0.90	0.90
Entire base		0.81	0.65	0.80
Circular cylinder (height/diameter = 1) to:	Diameter, $L = D$			
Element at center of base		0.76	0.71	0.92
Entire surface		0.67	0.60	0.90
Circular cylinder (height/diameter = 2) to:	Diameter, $L = D$			
Plane base		0.73	0.60	0.82
Concave surface		0.82	0.76	0.93
Entire surface		0.80	0.73	0.91
Circular cylinder (height/diameter = 0.5) to:	Diameter, $L = D$			
Plane base		0.48	0.43	0.90
Concave surface		0.53	0.46	0.88
Entire surface		0.50	0.45	0.90
Infinite semicircular cylinder to center of plane rectangular face	Radius, $L = R$		1.26	
Infinite slab to its surface	Slab thickness, L	2.00	1.76	0.88
Cube to a face	Edge, L	0.67	0.6	0.90
Rectangular 1×1×4 parallelepipeds to:	Shortest edge, L			
1×4 face		0.90	0.82	0.91
1×1 face		0.86	0.71	0.83
all faces		0.89	0.81	0.91

$$\phi_{s1}(x) = \frac{2}{3x^2}\left[1 - x^3 - (1-x^2)^{3/2}\right], \quad \phi_{s2}(x) = \tfrac{2}{3}\left[1 - x^3 + (1-x^2)^{3/2}\right]$$

$$\phi_{c1}(x) = 1 - x^2 + \frac{2}{\pi}\left[\cos^{-1} x - x\sqrt{1-x^2}\right], \quad \phi_{c2}(x) = \frac{2}{\pi}\left(\sqrt{1-x^2} + \frac{1}{x}\sin^{-1} x\right) - x$$

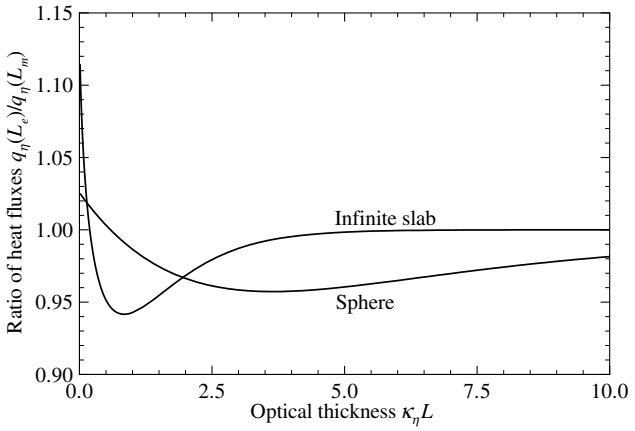

FIGURE 20-2
Ratio of the exact spectral heat flux from an isothermal gas volume to a surface, with that evaluated using the average mean beam length.

is recommended for geometries for which values for L_e are not available.

Besides saving computational effort for the evaluation of L_e, employing an average value L_m has the tremendous advantage that it allows the straightforward spectral integration of equation (20.9), resulting in a total heat flux of

$$q = \int_0^\infty q_\eta \, d\eta = \int_0^\infty \left(1 - e^{-\kappa_\eta L_m}\right) \pi I_{b\eta}(T) \, d\eta = \epsilon(L_m, T) \pi I_b(T) = \epsilon(L_m, T) n^2 \sigma T^4, \tag{20.12}$$

where $\epsilon(L_m, T)$ is the total emissivity of an isothermal gas layer of thickness L_m.

Example 20.3. Combustion products at $p = 5$ bar, $T = 1000$ K, consisting of 70% N_2, 10% CO_2, and 20% H_2O are contained within a spherical container of radius $R = 75$ cm. Assuming that the container wall is cold and black, estimate the radiative heat flux to the wall.

Solution
The radiative heat flux to the container walls is readily found from equation (20.12), once the total emissivity for the gas mixture has been determined for an average mean beam length of $L_m = 0.65D \simeq 100$ cm, as indicated by Table 20.1. Total emissivities for carbon dioxide–steam mixtures have been discussed in Chapter 11, and the total emissivity for this particular gas mixture for a 100 cm thick layer has already been evaluated in Example 11.13 (surprise!) as $\epsilon = 0.593$. Therefore,

$$q = 0.593 \times 5.670 \times 10^{-12} \times 1000^4 \, \text{W/cm}^2 = 3.36 \, \text{W/cm}^2.$$

Example 20.4. A 1 m thick isothermal layer of pure CO_2 at a pressure of 1 bar and a temperature of 1700 K is confined between two parallel, cold, black plates. Estimate the total heat loss from the gas using the mean beam length approach.

Solution
Again, the heat flux to the walls is readily determined from equation (20.12) if the total emissivity for the mean beam length is known, which in this case is $L_m = 1.76L = 176$ cm. The total emissivity for the CO_2 may be determined from Fig. 11-30 or equation (11.177). Using Fig. 11-30, we find ϵ_0 (176 bar cm, 1 bar, 1700 K) $\simeq 0.17$. The correction factor ϵ/ϵ_0 is determined from equation (11.178) with the correlation constants given in Table 11.4, which leads to $\epsilon/\epsilon_0 \simeq 1.00$ and, therefore, $\epsilon \simeq 0.17$. Substituting this value into equation (20.12), we obtain

$$-q(0) = q(L) = 0.17 \times 5.670 \times 10^{-12} \, 1700^4 \, \text{W/cm}^2 = 8.05 \, \text{W/cm}^2,$$

and the total heat lost from both sides is $2 \times 8.05 = 16.1 \, \text{W/cm}^2$. Had we used Leckner's correlation by calling subroutine `totemiss` in Appendix F, this would have returned $\epsilon = 0.153$, for a total heat loss of $2 \times 7.25 = 14.5 \, \text{W/cm}^2$.

20.3 SEMIGRAY APPROXIMATIONS

It is common practice in engineering to treat properties as "constants," that is, as being independent of one or more dependent variables, primarily to linearize the problem. For example, in heat conduction it is generally assumed that the thermal conductivity is independent of temperature. Very accurate results can be obtained with such an analysis if (*i*) the temperature variation of the material's conductivity is not too strong, and (*ii*) an appropriate, constant "effective conductivity" can be found. It is tempting to use such simplifying assumptions in the calculation of radiative heat fluxes, in particular as far as spectral variations are concerned. A number of researchers, such as Viskanta [33], Finkleman and coworkers [34–36], and Traugott [37,38], have introduced several different "effective" absorption coefficients and incorporated them into "semigray" schemes, all with limited success.

Consider the volume of a participating medium at a uniform temperature T. If the medium is optically thin (i.e., it emits but does not absorb any of the emitted radiation), the total heat loss from the volume is, according to equation (10.54),

$$Q = 4V \int_0^\infty \kappa_\eta E_{b\eta}\, d\eta, \tag{20.13}$$

or, with the definition of the Planck-mean absorption coefficient, equation (11.182),

$$Q = 4V\kappa_P n^2 \sigma T^4. \tag{20.14}$$

This expression is equivalent to taking the direction-integrated equation of transfer (or conservation of radiative energy), equation (10.60), and integrating it over the entire volume after dropping the self-absorption term. Therefore, for optically thin media, it is reasonable to set

$$\nabla \cdot \mathbf{q} = \int_0^\infty \kappa_\eta (4\pi I_{b\eta} - G_\eta)\, d\eta \simeq \kappa_P (4\pi I_b - G). \tag{20.15}$$

On the other hand, for optically thick media radiative heat flux obeys the diffusion limit or, from equation (15.19) for an isotropically scattering medium,

$$\mathbf{q}_\eta \simeq -\frac{1}{3\beta_\eta} \nabla E_{b\eta}; \tag{20.16}$$

and, using the definition of the Rosseland-mean extinction coefficient, equation (11.188),

$$\mathbf{q} = -\int_0^\infty \frac{1}{3\beta_\eta} \nabla E_{b\eta}\, d\eta = -\frac{1}{3\beta_R} \nabla E_b. \tag{20.17}$$

Apparently, to make accurate calculations using a gray model, the effective absorption coefficient must be close to the Planck-mean for optically thin situations and close to the Rosseland-mean for optically thick cases. A simple (i.e., not dependent on geometry and, through it, optical thickness) average value should only be expected to give accurate results if the Planck-mean and Rosseland-mean are of similar value (while in real life they frequently are orders of magnitude apart, in particular for molecular gases).

Replacing E_b in equation (20.17) by incident radiation G gives, together with equation (20.15), a semigray P_1-approximation,

$$\nabla \cdot \mathbf{q} = \kappa_P (4\pi I_b - G), \tag{20.18a}$$

$$\nabla G = -3\beta_R \mathbf{q}. \tag{20.18b}$$

Eliminating $\mathbf{q}$ leads to a single equation for G,

$$\nabla^2 G - 3\beta_R \kappa_P (G - 4\pi I_b) = 0, \tag{20.19}$$

where we have assumed κ_P and β_R to be constant (spatially) for simplicity. Thus, comparing equation (20.19) with (16.39) (setting $A_1 = 0$ for isotropic scattering) leads to an effective absorption coefficient of

$$\kappa_{\text{eff}} \simeq \sqrt{\kappa_P \kappa_R}, \tag{20.20}$$

which is quite commonly employed in gray analyses. However, equation (20.20) should only be used with great caution, (*i*) since accurate answers can be expected only if κ_P/κ_R is close to unity, and (*ii*) since use of the Rosseland-mean absorption coefficient is problematic for pure molecular gases. In the second instance the diffusion limit applies only to optically thick situations, while all molecular gases have transparent regions over large parts of the spectrum.

Consider a gas–particulate mixture, whose absorption coefficient may be written as

$$\kappa_\eta = \kappa_{p\eta} + \kappa_{g\eta} = \kappa_{p\eta} + \sum_{n=1}^{N} \kappa_{n\eta}. \tag{20.21}$$

Here $\kappa_{p\eta}$ is the spectral absorption coefficient of the particles and $\kappa_{g\eta}$ that of the gas, which is composed of N individual vibration–rotation bands, each with its own spectral absorption coefficient $\kappa_{n\eta}$. We shall also assume that the bands are relatively narrow, do not overlap, and may be described by the wide band model of Chapter 11. Then the Planck-mean absorption coefficient may be evaluated as

$$\begin{aligned}\kappa_P &= \frac{1}{E_b}\int_0^\infty \kappa_\eta E_{b\eta}\, d\eta = \kappa_{p,P} + \sum_{n=1}^{N} \frac{1}{E_b}\int_{\text{band } n} \kappa_{n\eta} E_{b\eta}\, d\eta \\ &\simeq \kappa_{p,P} + \sum_{n=1}^{N} \frac{E_{b\eta_n}}{E_b}\int_{\text{band } n} \kappa_{n\eta}\, d\eta = \kappa_{p,P} + \sum_{n=1}^{N} \frac{E_{b\eta_n}}{E_b}\alpha_n,\end{aligned} \tag{20.22}$$

where α_n is the band strength parameter and $E_{b\eta_n}$ is the spectral, blackbody emissive power at the band center, both for band n. The Rosseland-mean absorption coefficient may be evaluated similarly as

$$\begin{aligned}\frac{1}{\kappa_R} &= \int_0^\infty \frac{1}{\kappa_\eta}\frac{dE_{b\eta}}{dE_b}\, d\eta = \frac{1}{\kappa_{p,R}} - \int_0^\infty \left(\frac{1}{\kappa_{p\eta}} - \frac{1}{\kappa_\eta}\right)\frac{dE_{b\eta}}{dE_b} d\eta \\ &\simeq \frac{1}{\kappa_{p,R}} - \sum_{n=1}^{N}\left(\frac{dE_{b\eta}}{dE_b}\right)_{\eta_n}\int_{\text{band } n}\left(\frac{1}{\kappa_{p\eta_n}} - \frac{1}{\kappa_{p\eta_n} + \kappa_{n\eta}}\right) d\eta,\end{aligned} \tag{20.23}$$

where $\kappa_{p\eta_n}$ is a constant average value, assuming that $\kappa_{p\eta}$ does not vary greatly across each band. We shall also assume that, inside the integral, $\kappa_{n\eta}$ may be replaced by the narrow band average, $(S/d)_\eta$, for which the wide band model stipulates [cf. equation (11.142)]

$$\left(\frac{S}{d}\right)_\eta \simeq \frac{\alpha_n}{\omega_n}\, e^{-t|\eta - \eta_n|/\omega_n}, \tag{20.24}$$

where ω_n is the band width parameter and $t = 1$ for a band with head, and $t = 2$ for a symmetric band. Substituting this expression into equation (20.23) leads to

$$\begin{aligned}\int_{\text{band } n}\left(\frac{1}{\kappa_{p\eta_n}} - \frac{1}{\kappa_{p\eta_n} + \kappa_{n\eta}}\right) d\eta &= \frac{1}{\kappa_{p\eta_n}}\int_0^\infty \frac{(S/d)_\eta}{\kappa_{p\eta_n} + (S/d)_\eta} d\eta \\ &= \frac{\alpha_n}{\kappa_{p\eta_n}}\int_0^\infty \frac{e^{-x}\, dx}{\kappa_{p\eta_n} + (\alpha_n/\omega_n)\, e^{-x}} = \frac{\omega_n}{\kappa_{p\eta_n}} \ln\left(1 + \frac{\alpha_n}{\omega_n\, \kappa_{p\eta_n}}\right),\end{aligned} \tag{20.25}$$

regardless of the value of t (cf. the development of Example 11.3). Thus,

$$\frac{1}{\kappa_R} = \frac{1}{\kappa_{p,R}} - \sum_{n=1}^{N} \frac{\omega_n}{\kappa_{p\eta_n}}\left(\frac{dE_{b\eta}}{dE_b}\right)_{\eta_n} \ln\left(1 + \frac{\alpha_n}{\omega_n\, \kappa_{p\eta_n}}\right). \tag{20.26}$$

It is evident from equation (20.26) that for a pure molecular gas, $\kappa_R \to 0$. This statement is also true if the assumption of a narrow band is relaxed: It is readily observed that $1/\kappa_{n\eta}$ tends toward infinity faster than $E_{b\eta}$ tends to zero for both $\eta \to 0$ and $\eta \to \infty$. Clearly, for a pure molecular gas $\kappa_P/\kappa_R \to \infty$, so that (*i*) κ_R and equation (20.20) are not suitable for the determination of κ_{eff}, and (*ii*) accurate predictions should not be expected from the semigray approach.

Example 20.5. A molecular gas is confined between two parallel, black plates, spaced 1 m apart, which are kept isothermal at $T_1 = 1200\,\text{K}$ and $T_2 = 800\,\text{K}$, respectively. The (hypothetical) gas has a single vibration–rotation band in the infrared, with an average absorption coefficient of

$$\left(\frac{S}{d}\right)_\eta = \frac{\alpha}{\omega}\, e^{-2|\eta-\eta_0|/\omega}, \quad \eta_0 = 3000\,\text{cm}^{-1}, \quad \omega = 200\,\text{cm}^{-1},$$

and an overlap parameter of β (see the discussion of narrow band and wide band models in Chapter 11). Assuming convection and conduction to be negligible, estimate the radiative heat flux between the two plates using the semigray model. Carry out the analysis for variable values of (α/ω) and β. Repeat the calculations for the same gas mixed with nonscattering particles whose absorption coefficient is $\kappa_p = 0.1\,\text{m}^{-1}$ (gray).

Solution

To make an "equivalent" gray analysis, a suitable gray absorption coefficient must be found. Since for a pure molecular gas the Rosseland-mean is inappropriate, and for want of any better value, we choose the Planck-mean absorption coefficient, which leads to

$$\tau_P = \kappa_P L = \alpha \frac{E_{b\eta_0}}{\sigma T^4} L = \tau_L \frac{\omega E_{b\eta_0}(T)}{\sigma T^4}, \quad \tau_L = \left(\frac{\alpha}{\omega}\right) L.$$

Consequently, τ_P depends on the local temperature of the gas, even if $(\alpha/\omega) = \text{const}$. To simplify the analysis we use a constant Planck-mean absorption coefficient evaluated at some average temperature, say $T_{\text{av}} = 1000\,\text{K}$. Thus, $\eta_0/T_{\text{av}} = 3\,\text{cm}^{-1}/\text{K}$ and, from Appendix C,

$$\tau_P = \frac{200 \times 1.36576 \times 10^{-8}}{5.670 \times 10^{-8} \times 1000} \times \tau_L = 0.0482\,\tau_L.$$

For a gray medium the radiative heat flux between the two plates is determined from Example 15.5 for the P_1-approximation as

$$\Psi_{\text{gray}} = \frac{1}{1 + \frac{3}{4}\tau_P} = \frac{1}{1 + 0.0362\,\tau_L}.$$

If a particle background is present, it is better to utilize κ_{eff} from equation (20.20). Thus, with $\tau_p = \kappa_p L = 0.1 \times 1 = 0.1$,

$$\tau_P = 0.1 + 0.0482\,\tau_L,$$

$$\frac{1}{\tau_R} = \frac{1}{\tau_p} - \frac{1}{\tau_p}\left(\omega \frac{dE_{b\eta}}{dE_b}\right)_{\eta_n} \ln\left(1 + \frac{\tau_L}{\tau_p}\right).$$

From equation (1.14) it follows that

$$\omega \frac{dE_{b\eta}}{dE_b} = \frac{\omega}{4\sigma T^3}\frac{dE_{b\eta}}{dT} = \frac{\omega}{4\sigma T^3}\frac{d}{dT}\left[\frac{C_1\eta^3}{\exp(C_2\eta/T) - 1}\right]$$
$$= \frac{\omega C_1 \eta^3}{4\sigma T^3}\frac{\exp(C_2\eta/T)\, C_2\eta/T^2}{[\exp(C_2\eta/T) - 1]^2} = \frac{1}{4}\frac{\omega E_{b\eta}}{E_b}\frac{(C_2\eta/T)\exp(C_2\eta/T)}{\exp(C_2\eta/T) - 1},$$

$$\left(\omega \frac{dE_{b\eta}}{dE_b}\right)_{\eta_n} = \frac{1}{4} \times 0.0482 \times \frac{4.3164\, e^{4.3164}}{e^{4.3164} - 1} = 0.0527,$$

$$\tau_R = \frac{0.1}{1 - 0.0527\,\ln(1 + 10\,\tau_L)}.$$

τ_P and τ_R may be calculated for any τ_L, and the heat flux becomes

$$\Psi = \frac{1}{1 + \frac{3}{4}\sqrt{\tau_P\,\tau_R}}.$$

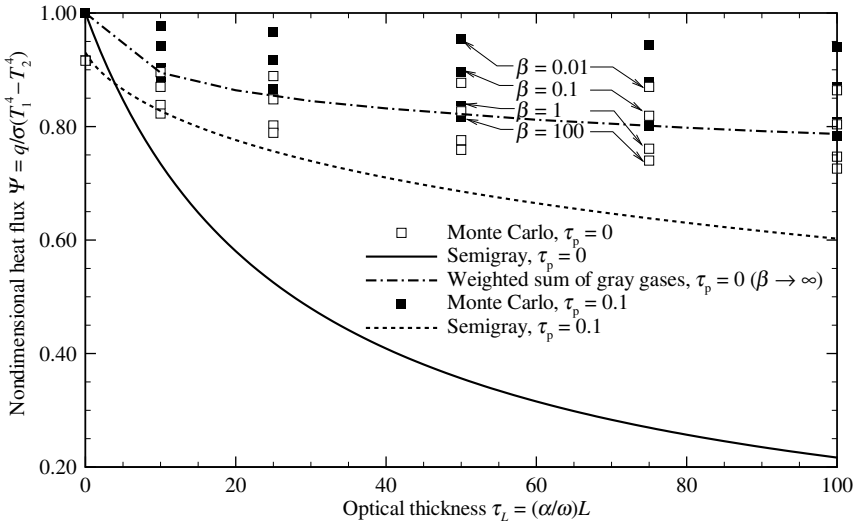

FIGURE 20-3
Nondimensional radiative heat flux for radiative equilibrium across a molecular gas–particulate layer bounded by parallel, black walls, calculated by the semigray method.

Representative results are shown in Fig. 20-3, together with exact results found by the Monte Carlo method [39,40], and results from the weighted-sum-of-gray-gases method (discussed later in this chapter). Clearly, for a pure molecular gas the semigray approximation fails miserably, since the Planck-mean is much too large to be a good effective absorption coefficient for optically thick bands. With a particle background the method performs considerably better, with κ_P/κ_R ranging in value between 1 (for $\tau_L = 0$) and 31 ($\tau_L = 100$). The semigray approach cannot account for spectral windows, nor for line structure (line overlap parameter β): If there is little line overlap (small β) radiation can travel unimpeded through "mini-windows" between strong spectral lines. For a gray gas the heat flux must always tend to zero for optically thick gases.

20.4 THE STEPWISE-GRAY MODEL (BOX MODEL)

Another simple way to incorporate the effects of absorption–emission bands of molecular gases in radiative heat transfer calculations is to approximate the band absorptances through the box model described in Section 11.10. In this model the spectral absorption coefficient for a molecular gas with N vibration–rotation bands is approximated (see Fig. 20-4) as

$$\kappa_\eta \simeq \sum_{n=1}^{N} \kappa_n \left[H(\eta - \eta_n + \tfrac{1}{2}\Delta\eta_n) - H(\eta - \eta_n - \tfrac{1}{2}\Delta\eta_n) \right], \tag{20.27}$$

where η_n is the wavenumber at the band center, $\Delta\eta_n$ is the band width and κ_n is the absorption coefficient of the nth band (assumed constant for each band). Finally, the function $H(x)$ is *Heaviside's unit step function.*[1] If the molecular gas is accompanied by absorbing and/or scattering particles (e.g., soot or ash particles), the absorption coefficient of equation (20.27) must be augmented by the extinction coefficient of the background. If the background material can be approximated as gray, the mixture extinction coefficient may be expressed as

$$\beta_\eta = \beta_p + \sum_{n=1}^{N} \kappa_n \left[H(\eta - \eta_n + \tfrac{1}{2}\Delta\eta_n) - H(\eta - \eta_n - \tfrac{1}{2}\Delta\eta_n) \right]. \tag{20.28}$$

[1]For its definition see equation (11.103) in Section 11.9.

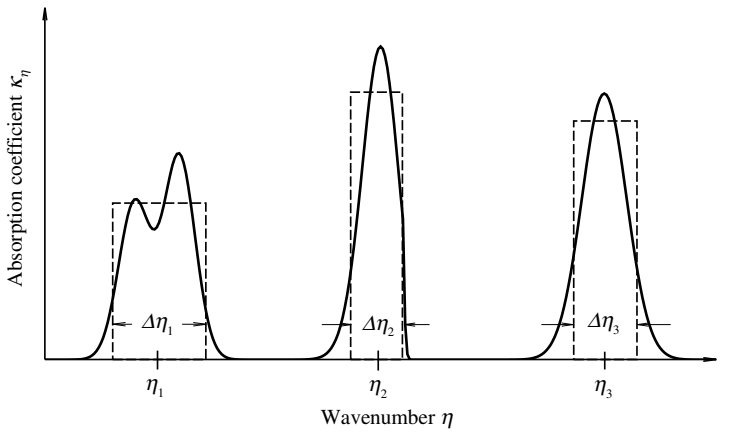

FIGURE 20-4
Box model approximation of molecular gas bands.

A number of researchers have used various forms of the box model to solve nongray radiation problems. Originally proposed by Chandrasekhar [41], the model has primarily been applied to one-dimensional plane media at radiative equilibrium, for example by Siewert and Zweifel [42], Kung and Sibulkin [43], and Reith, Siewert, and Özişik [44]. Greif [45] applied the method to combined conduction/radiation in a plane layer. Modest [46] showed that, for gases with a single band strength, the box model approach can be incorporated into the P_1-approximation, making multidimensional calculations possible. This was extended to the general box model by Modest and Sikka [39], and a consistent method for the determination of box model parameters was given. The combination of box model and P_1-approximation was also used by Thynell [47] to predict radiation in a one-dimensional cylindrical medium with carbon dioxide, water vapor, soot, and larger particles; similarly, Kaminski and coworkers [48,49] investigated laminar cross flow over a cylinder and turbulent flow through a tube, respectively, for mixtures of combustion products. The method was also employed by Mazumder and Modest to determine the importance of interaction between turbulence and radiation in reacting [50] and nonreacting [51] flows.

Comparing the box model with the mean beam length method, we see that the mean beam length method can model the spectral variations of the absorption coefficient very well, but it is limited to isothermal, black-walled enclosures with nonscattering media. The box model, on the other hand, can handle nonisothermal, scattering media bounded by nonblack walls, while its spectral modeling is rather crude.

How well the box model predicts radiative heat fluxes (or their divergence) for nongray media largely depends on how well "optimum" box parameters are determined for a given medium. To find appropriate values for these parameters, one must realize that the exact integral relationships that govern radiative heat transfer in a participating medium [see, for example, equation (10.28)] contain the spectral absorption coefficient in the form of the spectral emissivity (or its derivative)

$$\epsilon_\eta = 1 - e^{-\kappa_\eta X}. \tag{20.29}$$

Here $X = L$ if the linear absorption coefficient is used, or L multiplied by the partial density or pressure of the absorbing gas if either mass or pressure absorption coefficient is used; and L is the geometric path length over which absorption/emission is being considered. Spectrally integrated heat fluxes (or their divergence), therefore, depend strongly on the total band absorptances of the medium,

$$A(X) = \int_{\text{band}} \epsilon_\eta \, d\eta = \int_{\text{band}} (1 - e^{-\kappa_\eta X}) \, d\eta. \tag{20.30}$$

Thus, the aim of the box model must be to approximate the total band absorptance as well as possible for all possible conditions. For a gas without particle background, as shown in Fig. 20-4,

we have for band n,

$$A_n(X) \simeq \Delta\eta_n(1 - e^{-\kappa_n X}), \tag{20.31}$$

where $\Delta\eta_n$ and κ_n are two parameters that may have arbitrary dependence on all gas conditions (pressure, temperature, line overlap, etc.), *except* path length X. Consequently, $A_n(X)$ as calculated by equation (20.31) ranges in value between 0 and $\Delta\eta_n$ and can coincide with the exact value of $A_n(X)$ (as discussed in Chapter 11) for precisely two values of X. It is this restriction that limits the accuracy of the box model, since the "exact" value of the total band absorptance increases as $\ln(\kappa_\eta X)$ for optically thick conditions (cf. Table 11.2). Modest and Sikka [39] found that best results are obtained by choosing $\Delta\eta_n$ and κ_n in such a way that equation (20.31) predicts the correct band absorptance for optically thin situations (X small) and for a characteristic length X_m based on the mean beam length L_m (as listed in Table 20.1). In the optically thin limit we have

$$X \ll X_m: \quad A_n(x) = \int_{\text{band}} \kappa_\eta X \, d\eta = \alpha_n X = \kappa_n \Delta\eta_n X, \tag{20.32}$$

where α_n is the integrated absorption coefficient, or

$$\alpha_n \simeq \kappa_n \Delta\eta_n. \tag{20.33}$$

At the mean beam length we have

$$X = X_m: \quad A_n(X_m) = \Delta\eta_n(1 - e^{-\kappa_n X_m}), \tag{20.34}$$

where $A_n(X_m)$ must be evaluated from any appropriate wide band model. Equations (20.33) and (20.34) constitute a set of two equations for the unknowns κ_n and $\Delta\eta_n$, which are readily solved, especially if $\kappa_n X_m \gg 1$ (which will be the case for most important bands).

As a simple illustration we consider radiative equilibrium in a one-dimensional plane-parallel layer of molecular gases confined between two isothermal, gray-diffuse plates. The medium does not scatter and the absorption coefficient obeys equation (20.27). As a further simplification we assume that all bands are of equal strength, that is,

$$\kappa_1 = \kappa_2 = \cdots = \kappa_N = \overline{\kappa}, \tag{20.35}$$

and that the band width $\Delta\eta_n$ does not vary with location or temperature. For this simple case the spectral values for incident radiation, G_η, and radiative heat flux, q_η, are readily found from equations (14.34) and (14.35) as

$$G_\eta(\tau_\eta) = 2\Big\{J_{1\eta}E_2(\tau_\eta) + J_{2\eta}E_2(\tau_{L\eta} - \tau_\eta) + \int_0^{\tau_L} E_{b\eta}(\tau_\eta')E_1(|\tau_\eta - \tau_\eta'|)\, d\tau_\eta'\Big\}, \tag{20.36}$$

$$\begin{aligned} q_\eta(\tau_\eta) = 2\Big\{&J_{1\eta}E_3(\tau_\eta) - J_{2\eta}E_3(\tau_{L\eta} - \tau_\eta) \\ &+ \int_0^{\tau_\eta} E_{b\eta}(\tau_\eta')E_2(\tau_\eta - \tau_\eta')\, d\tau_\eta' - \int_{\tau_\eta}^{\tau_{L\eta}} E_{b\eta}(\tau_\eta')E_2(\tau_\eta' - \tau_\eta)\, d\tau_\eta'\Big\}, \end{aligned} \tag{20.37}$$

where

$$\begin{aligned} \tau_\eta &= \int_0^z \overline{\kappa}\, dz \sum_{n=1}^{N} \Big[H(\eta - \eta_n + \tfrac{1}{2}\Delta\eta_n) - H(\eta - \eta_n - \tfrac{1}{2}\Delta\eta_n)\Big] \\ &= \begin{cases} \overline{\tau}, & \text{within bands,} \\ 0, & \text{across windows.} \end{cases} \end{aligned} \tag{20.38}$$

Integrating equations (20.36) and (20.37) over all *bands* (excluding windows) results in

$$G_B(\overline{\tau}) = 2\Big\{J_{B1}E_2(\overline{\tau}) + J_{B2}E_2(\overline{\tau}_L - \overline{\tau}) + \int_0^{\overline{\tau}_L} E_B(\overline{\tau}')E_1(|\overline{\tau} - \overline{\tau}'|)\, d\overline{\tau}'\Big\}, \tag{20.39}$$

$$q_B(\overline{\tau}) = 2\Big\{J_{B1}E_3(\overline{\tau}) - J_{B2}E_3(\overline{\tau}_L - \overline{\tau}) + \int_0^{\overline{\tau}} E_B(\overline{\tau}')E_2(\overline{\tau} - \overline{\tau}')\, d\overline{\tau}' - \int_{\overline{\tau}}^{\overline{\tau}_L} E_B(\overline{\tau}')E_2(\overline{\tau}' - \overline{\tau})\, d\overline{\tau}'\Big\}, \tag{20.40}$$

where the subscript B denotes a quantity integrated over all bands, for example,

$$G_B = \sum_{n=1}^{N} \int_{\eta_n - \frac{1}{2}\Delta\eta_n}^{\eta + \frac{1}{2}\Delta\eta_n} G_\eta \, d\eta. \tag{20.41}$$

On the other hand, integrating the equation of transfer over the *entire spectrum* (including windows) gives, from equation (10.60),

$$\nabla \cdot \mathbf{q} = \frac{dq}{dz} = \int_0^\infty \kappa_\eta (4E_{b\eta} - G_\eta) \, d\eta = \overline{\kappa}(4E_B - G_B) = 0, \tag{20.42}$$

where the zero is due to the fact that radiative equilibrium prevails. Since integrating the equation of transfer over the bands only (excluding windows) would have resulted in the identical right-hand side, we conclude that $dq_B/dz = 0$ or $q_B = \text{const}$, and $G_B = 4E_B$. Thus, equations (20.39) and (20.40) are identical to the gray case, equations (14.34) and (14.35), after replacing total values by band-integrated values, or

$$\Phi_B = \frac{E_B(\overline{\tau}) - J_{B2}}{J_{B1} - J_{B2}} = \frac{1}{2}\left[E_2(\overline{\tau}) + \int_0^{\overline{\tau}_L} \Phi_B(\overline{\tau}') E_1(|\overline{\tau} - \overline{\tau}'|) \, d\overline{\tau}'\right], \tag{20.43}$$

$$\Psi_B = \frac{q_B}{J_{B1} - J_{B2}} = 1 - 2\int_0^{\overline{\tau}_L} \Phi_B(\overline{\tau}') E_2(\overline{\tau}') \, d\overline{\tau}'. \tag{20.44}$$

The total heat flux between the plates is then determined by adding to this the heat flux over the spectral windows

$$q_W = \int_{\text{windows}} (J_{1\eta} - J_{2\eta}) \, d\eta = J_1 - J_2 - (J_{B1} - J_{B2}), \tag{20.45}$$

or

$$\Psi = \frac{q}{J_1 - J_2} = \frac{q_W + q_B}{J_1 - J_2} = 1 - \frac{J_{B1} - J_{B2}}{J_1 - J_2}(1 - \Psi_B). \tag{20.46}$$

We note that, for a gray medium, Ψ varies between 1 (vacuum) and 0 (opaque medium), while the minimum heat flux for a nongray medium is

$$\Psi_{\min} = 1 - \frac{J_{B1} - J_{B2}}{J_1 - J_2}, \tag{20.47}$$

since radiation will travel unimpeded from surface to surface over spectral windows, even if the bands are opaque.

Example 20.6. Pure CO_2 at 1 bar = 100 kPa pressure is confined between two parallel, black plates, spaced 1 m apart, which are kept isothermal at $T_1 = 1000$ K and $T_2 = 2000$ K, respectively. Assuming conduction and convection to be negligible, estimate the radiative heat flux between the two plates.

Solution

From Table 11.3 we find that carbon dioxide has three important bands in the infrared: at 3660 cm^{-1} (2.7 μm), 2410 cm^{-1} (4.3 μm), and 667 cm^{-1} (15 μm). Since the walls are at 1000 and 2000 K, respectively, the most important wavelength regime will be between approximately 1 μm and 4 μm (Wien's displacement law, Chapter 1). At first glance it would appear that the 2.7 μm band is the most important. However, the 4.3 μm band is approximately 20 times stronger and, therefore, should be modeled most accurately. Before we can employ the box model we must find suitable box parameters for these bands. We shall do this by comparing the band absorptances of the box model with those of the (more accurate) exponential wide band model [39], by applying equations (20.33) and (20.34). Since we should like to use a single $\overline{\kappa}$ for all bands we cannot use all of these conditions, and shall apply equation (20.34) only for the (most important) 4.3 μm band. Thus,

$$\overline{\kappa}\Delta\eta_i = \alpha_i, \quad \text{for all three bands,}$$

$$\Delta\eta_{4.3} = A_{4.3}(X_m), \quad \text{for the } 4.3\,\mu\text{m band.}$$

In the last relation we have assumed $\overline{\kappa}X_m \gg 1$, which needs to be verified.

To simplify the analysis further we shall calculate the box model parameters at a single temperature, say $T_{\text{av}}^4 = (T_1^4 + T_2^4)/2$ or $T_{\text{av}} \simeq 1700\,\text{K}$. With a gas constant of $R = 0.18892\,\text{kJ/kg K}$ for CO_2 [52] and the data in Table 11.3, and Fig. 11-24 we get

$$\rho_{CO_2} = p/RT = 100\,\text{kPa}/(0.18892\times1700\,\text{kJ/kg}) = 311.4\,\text{g/m}^3,$$

2.7 μm band:
$$\alpha\rho_{CO_2} = \alpha_0(\alpha/\alpha_0)\rho = 4.0\times1.61\times311.4 = 2005\,\text{cm}^{-1}/\text{m},$$
$$\omega = 23.5\times\sqrt{17} = 96.9\,\text{cm}^{-1},$$

4.3 μm band:
$$\alpha\rho_{CO_2} = 110.0\times1\times311.4 = 34{,}254\,\text{cm}^{-1}/\text{m},$$
$$\omega = 11.2\times\sqrt{17} = 46.2\,\text{cm}^{-1},$$
$$\gamma = \gamma_0(\gamma/\gamma_0) = 0.247\times24.8 = 6.12,$$
$$P_e = 1.3^{0.8} = 1.234,\ \beta = 6.12\times1.234 = 7.55,$$

15 μm band:
$$\alpha\rho_{CO_2} = 19.0\times1\times311.4 = 5917\,\text{cm}^{-1}/\text{m},$$
$$\omega = 12.7\times\sqrt{17} = 52.4\,\text{cm}^{-1}.$$

With an average mean beam length of $L_m = 1.76\times1\,\text{m} = 1.76\,\text{m}$, we obtain for the important 4.3 μm band from Table 11.3

$$\Delta\eta_{4.3} = A_{4.3} = \omega_{4.3}\left[\ln\frac{\alpha_{4.3}\rho_{CO_2}L_m}{\omega_{4.3}} + 1\right]$$
$$= 46.2\,\text{cm}^{-1}\left[\ln\frac{34{,}254\times1.76}{46.2} + 1\right] = 377.6\,\text{cm}^{-1},$$

and

$$\overline{\kappa} = \left(\alpha\rho_{CO_2}/\Delta\eta\right)_{4.3} = 34{,}254/377.6 = 90.7\,\text{m}^{-1} = 0.907\,\text{cm}^{-1}.$$

Noting that $\overline{\kappa}$ is a *linear* absorption coefficient, and multiplying with L_m, we find $\overline{\kappa}L_m = 0.907\times176 = 160 \gg 1$, so neglecting the exponential in equation (20.34) was indeed justified.

The widths of the other two bands follow from the same relationship as

$$\Delta\eta_{2.7} = \alpha_{2.7}\rho_{CO_2}/\overline{\kappa} = 2005/90.7 = 22.1\,\text{cm}^{-1},$$
$$\Delta\eta_{15} = \alpha_{15}\rho_{CO_2}/\overline{\kappa} = 5917/90.7 = 65.2\,\text{cm}^{-1}.$$

We are now in a position to calculate the nondimensional heat flux between the plates from equation (20.46) with $\overline{\tau} = \overline{\kappa}L = 90.7$. $\Psi_B(\overline{\tau})$ obeys the same equation as $\Psi_b(\tau)$ in Chapter 14 and, thus, may be evaluated from Table 14.1. Since the bands are essentially opaque we find $\Psi_B = 0.015 \ll 1$, and

$$\Psi = 1 - 0.985\frac{E_{B1} - E_{B2}}{E_{b1} - E_{b2}} \simeq 1 - \frac{0.985}{E_{b1} - E_{b2}}\sum_{n=1}^{3}(E_{b\eta_n,1} - E_{b\eta_n,2})\Delta\eta_n,$$

where radiosity is replaced by emissive power for the black-walled enclosure, and we assume that the bands are narrow (to justify evaluation of E_B as the value at band center × band width). To look up values for spectral emissive power in Appendix C, we write with $\eta_{2.7} = 3660\,\text{cm}^{-1}$, $\eta_{4.3} \simeq 10^4/4.3 = 2326\,\text{cm}^{-1}$ (since the 4.3 μm band is a band with head, it is better to evaluate $E_{b\eta}$ near the center of the band), and $\eta_{15} = 667\,\text{cm}^{-1}$,

$$\Psi = 1 - \frac{0.985}{\sigma(T_1^4 - T_2^4)}\sum_{n=1}^{3}\left[\frac{E_{b\eta}(\eta_n/T_1)}{T_1^3}T_1^3 - \frac{E_{b\eta}(\eta_n/T_2)}{T_2^3}T_2^3\right]\Delta\eta_n$$
$$= 1 - \frac{0.985}{5.670\times10^{-8}(1000^4 - 2000^4)}\times\Big[\left(0.9523\times10^{-8+9} - 1.7747\times2^3\times10\right)\times22.1$$
$$+ \left(1.7157\times10 - 1.3589\times2^3\times10\right)\times377.6 + \left(0.6885\times10 - 0.2251\times2^3\times10\right)\times65.2\Big]$$
$$= 0.956.$$

Thus, the heat flux is reduced only by 4.7%, as compared with the no-gas case, to

$$q = 0.956 \times 5.670 \times 10^{-8}(2000^4 - 1000^4) = 813{,}000\,\mathrm{W/m^2} = 81.3\,\mathrm{W/cm^2}.$$

Note that, since all bands are essentially opaque, the (somewhat arbitrary) choice for band widths is of extreme importance in this model.

The P_1-Approximation for Radiative Equilibrium in a Gas with Single Band Strength

The method discussed in the previous section enables us to calculate heat transfer rates for a nongray medium at radiative equilibrium in a simple way. Unfortunately, the method is limited to one-dimensional plane-parallel media. Following the treatment of Modest [46], we shall now show that the same box-model absorption coefficient may also be applied to the P_1 or differential approximation, making solutions for arbitrary multidimensional geometries possible.

The governing equations for the P_1-approximation, on a spectral basis and for a nonscattering medium, are, from Section 16.5

$$\nabla \cdot \mathbf{q}_\eta = \kappa_\eta (4E_{b\eta} - G_\eta), \tag{20.48}$$

$$\nabla G_\eta = -3\kappa_\eta \mathbf{q}_\eta, \tag{20.49}$$

subject to the boundary condition

$$2\mathbf{q}_\eta \cdot \hat{\mathbf{n}} = 4J_{w\eta} - G_\eta. \tag{20.50}$$

Assuming again that the absorption coefficient may be approximated by equation (20.35), we integrate equation (20.48) over the entire spectrum, and over all bands only, resulting in

$$\nabla \cdot \mathbf{q} = \nabla \cdot \mathbf{q}_B = \overline{\kappa}(4E_B - G_B) = 0, \tag{20.51}$$

where the zero is again due to the fact that radiative equilibrium is assumed. Now, integrating equations (20.49) and (20.50) over all bands gives

$$\nabla G_B = -3\overline{\kappa}\mathbf{q}_B, \tag{20.52}$$

$$2\mathbf{q}_B \cdot \hat{\mathbf{n}} = 4J_{Bw} - G_B. \tag{20.53}$$

The heat flux may be eliminated from these equations, leading to a single elliptic equation in G_B as

$$\nabla^2_{\overline{\tau}} G_B = 0, \tag{20.54}$$

with boundary condition

$$-\tfrac{2}{3}\hat{\mathbf{n}} \cdot \nabla_{\overline{\tau}} G_B + G_B = 4J_{Bw}, \tag{20.55}$$

where the subscript $\overline{\tau}$ indicates that the gradients are with respect to optical coordinates $d\overline{\tau} = \overline{\kappa}\, ds$. Once the band-integrated incident radiation, G_B, has been determined, the heat flux for the gas bands follows as

$$\mathbf{q}_B = -\frac{1}{3}\nabla_{\overline{\tau}} G_B. \tag{20.56}$$

Finally, to calculate total heat transfer rates, the heat fluxes through the optical windows, $\mathbf{q}_W$, must be determined independently through standard methods (Chapters 5 and 6), as indicated in the previous section for one-dimensional, plane-parallel media, equation (20.45).

Example 20.7. Repeat Example 20.6 using the differential approximation.

Solution

Since we use the same box model as in the previous example to approximate the absorption coefficient, we shall again use $\overline{\kappa} = 0.907\,\text{cm}^{-1}$, $\Delta\eta_{2.7} = 22.1\,\text{cm}^{-1}$, $\Delta\eta_{4.3} = 377.6\,\text{cm}^{-1}$, and $\Delta\eta_{15} = 65.2\,\text{cm}^{-1}$. Equations (20.51) through (20.53) or equations (20.54) and (20.55) are identical to the general P_1-approximation for gray media (except for the added subscript B). Thus, for radiative equilibrium in a one-dimensional plane-parallel medium

$$\Psi_B = \frac{1}{1 + \frac{3}{4}\overline{\tau}} = 0.015.$$

The heat flux over the spectral windows is, of course, the same as calculated for the previous example, as is the expression for total heat flux, equation (20.46). We conclude that the heat flux evaluation using the P_1-approximation gives the identical result as the exact [2] method.

Both the exact method for one-dimensional plane-parallel media and the P_1-approximation for general geometries are readily extended to the general box model in which the extinction coefficient is approximated by equation (20.28), including nongray backgrounds, as developed by Modest and Sikka [39].

20.5 GENERAL BAND MODEL FORMULATION

While the stepwise-gray model is very convenient, it is unfortunately not necessarily very accurate. We have already seen that the rather arbitrary choice for the band width can introduce serious errors. In addition, there are situations in which even the most careful choice for the band width leads to unacceptable results. Consider, for example, flow of an absorbing/emitting gas inside a tube. Let the gas temperature be equal to the surface temperature at the wall (no slip) and hotter inside. The gas will emit and absorb radiation over the spectral regions of its vibration–rotation bands, and there will be no net radiative heat flux over the spectral regions of the windows. If the radius of the tube is sufficiently large and the box model is employed, such that $\overline{\kappa}R \gg 1$, then the spectral heat flux for the bands will also vanish as a result of the diffusion limit (since there is no temperature discontinuity). Thus, the stepwise-gray model predicts a zero total radiative heat flux for this case, which is clearly not realistic. The reason for this error is that the box model cannot take into account the effects of the exponentially decaying band wings of a vibration–rotation band: No matter how optically thick the band center is, there will always be a portion of the band wings that has an intermediate optical thickness and, thus, contributes strongly to the radiative heat flux.

In this section we will use the band models of Chapter 11 (narrow band models, wide band models, and the resulting emissivities) to formulate the solutions for spectrally integrated intensities, incident radiation, and radiative heat fluxes for an absorbing/emitting medium; the absorption coefficient of the medium may have arbitrary functional form (although we shall look also at the important special cases of molecular gases and particulate suspensions), and the geometry may be arbitrary and multidimensional. The development will be limited to nonscattering media confined between black walls because of the limitations inherent to the band models. While these formulations are not as general as one would like, they do have a number of important applications, most notably heat transfer within combustion chambers, where the medium consists of combustion gases and (nonscattering) soot, and where the walls are soot covered (and nearly black).

The equation of transfer for the radiative intensity at a wavenumber η and along a path s is, for a nonscattering medium, from equation (10.21),

$$\frac{dI_\eta}{ds} = \kappa_\eta (I_{b\eta} - I_\eta), \tag{20.57}$$

[2] Exact calculation of radiative heat flux based on very approximate expressions for the spectral variation of the absorption coefficient.

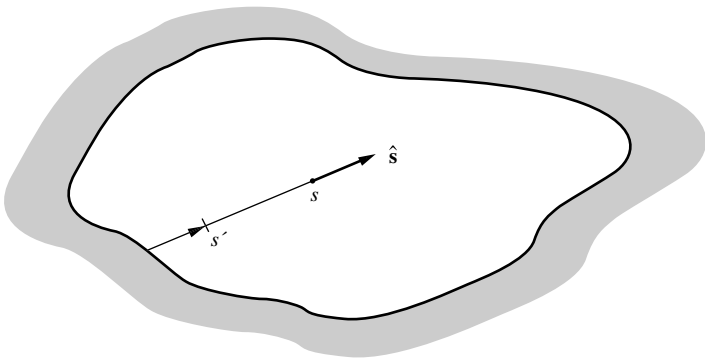

FIGURE 20-5
Spectral intensity within an arbitrary black-walled enclosure.

with the formal solution, equation (10.29),

$$I_\eta(s) = I_{bw\eta}\,\exp\left(-\int_0^s \kappa_\eta\,ds'\right) + \int_0^s I_{b\eta}(s')\,\exp\left(-\int_{s'}^s \kappa_\eta\,ds''\right)\kappa_\eta(s')\,ds', \tag{20.58}$$

where $I_{bw\eta} = I_{b\eta}(T_w)$ is the intensity emitted into the medium from the (black) wall at $s = 0$, as shown in Fig. 20-5. Integrating this expression over the entire spectrum, we obtain the total intensity as

$$I(s) = \int_0^\infty I_\eta\,d\eta = \int_0^\infty I_{bw\eta}\,\exp\left(-\int_0^s \kappa_\eta\,ds'\right)d\eta + \int_0^s \int_0^\infty I_{b\eta}(s')\,\exp\left(-\int_{s'}^s \kappa_\eta\,ds''\right)\kappa_\eta(s')\,d\eta\,ds'. \tag{20.59}$$

In Sections 10.2 and 10.3 we defined the spectral absorptivity and emissivity of a participating medium as

$$\alpha_\eta(0\to s) = \epsilon_\eta(0\to s) = 1 - \exp\left(-\int_0^s \kappa_\eta\,ds'\right). \tag{20.60}$$

For a constant absorption coefficient the absorptivity depends on the thickness of the gas layer as well as the (constant) absorption coefficient. If κ_η is not constant but varies spatially and/or with temperature, the absorptivity depends on the variation of κ_η along the entire path, here denoted by the argument $0\to s$. Substituting equation (20.60) into (20.59), and using

$$\frac{\partial \alpha_\eta}{\partial s'}(s'\to s) = \frac{\partial}{\partial s'}\left[1 - \exp\left(-\int_{s'}^s \kappa_\eta\,ds''\right)\right] = -\kappa_\eta(s')\,\exp\left(-\int_{s'}^s \kappa_\eta\,ds''\right) \tag{20.61}$$

where Leibniz's rule was used for the differentiation of an integral,[3] we get

$$I(s) = \int_0^\infty I_{bw\eta}\left[1-\alpha_\eta(0\to s)\right]d\eta - \int_0^s \int_0^\infty I_{b\eta}(s')\frac{\partial \alpha_\eta}{\partial s'}(s'\to s)\,d\eta\,ds'. \tag{20.62}$$

Physically, the first term represents transmitted radiation from the wall, and the second term augmentation due to emission along the path s.[4] With the definition of the *total absorptivity* as

$$\begin{aligned}\alpha(T, s'\to s) &= \frac{1}{I_b(T)}\int_0^\infty \alpha_\eta(s'\to s)\,I_{b\eta}(T)\,d\eta \\ &= \frac{1}{I_b(T)}\int_0^\infty \left[1 - \exp\left(-\int_{s'}^s \kappa_\eta\,ds''\right)\right]I_{b\eta}(T)\,d\eta,\end{aligned} \tag{20.63}$$

[3]Leibniz's rule was first introduced in Chapter 3, equation (3.106).

[4]Thus, use of transmissivity $\tau = 1 - \alpha$ would be more appropriate; we use absorptivity here primarily to avoid confusion with "optical path length," for which we also use the symbol τ.

we may consolidate equation (20.62) as[5]

$$I(s) = [1 - \alpha(T_w,\, 0 \to s)]\, I_{bw} - \int_0^s \frac{\partial \alpha}{\partial s'}[T(s'),\, s' \to s]\, I_b(s')\, ds'. \tag{20.64}$$

To determine total heat flux, the total intensity must be integrated over all directions, after multiplication with the unit vector $\hat{\mathbf{s}}$, or

$$\mathbf{q} = \int_0^\infty \mathbf{q}_\eta\, d\eta = \int_{4\pi} I\, \hat{\mathbf{s}}\, d\Omega. \tag{20.65}$$

To evaluate the divergence of the radiative heat flux (for a known temperature field) or the temperature field (for radiative equilibrium), the equation governing conservation of radiative energy must be integrated over all wavenumbers or, from equation (10.60),

$$\begin{aligned} \nabla \cdot \mathbf{q} = \nabla \cdot \int_0^\infty \mathbf{q}_\eta\, d\eta &= \int_0^\infty \kappa_\eta \left(4\pi I_{b\eta} - \int_{4\pi} I_\eta\, d\Omega\right) d\eta \\ &= 4\pi \kappa_p I_b - \int_{4\pi} \left(\int_0^\infty \kappa_\eta I_\eta\, d\eta\right) d\Omega, \end{aligned} \tag{20.66}$$

where κ_p is the Planck-mean absorption coefficient first defined in equation (11.182). Thus, multiplying equation (20.58) by $\kappa_\eta(s)$ and integrating, we get

$$\begin{aligned} \int_0^\infty \kappa_\eta(s) I_\eta(s)\, d\eta = \int_0^\infty I_{bw\eta} \kappa_\eta(s)\, \exp\left(-\textstyle\int_0^s \kappa_\eta\, ds''\right) d\eta \\ + \int_0^s \int_0^\infty I_{b\eta}(s')\, \exp\left(-\textstyle\int_{s'}^s \kappa_\eta\, ds''\right) \kappa_\eta(s') \kappa_\eta(s)\, d\eta\, ds'. \end{aligned} \tag{20.67}$$

Differentiating equation (20.61) with respect to s, again using Leibniz's rule, leads to

$$\frac{\partial^2 \alpha_\eta}{\partial s \partial s'}(s' \to s) = \kappa_\eta(s') \kappa_\eta(s) \exp\left(-\textstyle\int_{s'}^s \kappa_\eta\, ds''\right). \tag{20.68}$$

Therefore,

$$\begin{aligned} \int_0^\infty \kappa_\eta I_\eta\, d\eta &= \int_0^\infty I_{bw\eta} \frac{\partial \alpha_\eta}{\partial s}(0 \to s)\, d\eta + \int_0^s \int_0^\infty I_{b\eta}(s') \frac{\partial^2 \alpha_\eta}{\partial s \partial s'}(s' \to s)\, d\eta\, ds' \\ &= \frac{\partial \alpha}{\partial s}(T_w, 0 \to s) I_{bw} + \int_0^s \frac{\partial^2 \alpha}{\partial s \partial s'}[T(s'), s' \to s]\, I_b(s')\, ds'. \end{aligned} \tag{20.69}$$

The functional form of $\alpha(T, s' \to s)$ depends, of course, on the local properties of the participating medium. We shall briefly discuss the special cases of pure gas and gas–particulate mixtures.

Pure Molecular Gas

For a pure gas the total absorptivity needed in equations (20.65) and (20.66) can be calculated from a narrow band model, a wide band model, or from a total absorptivity correlation. Narrow band calculations are potentially the most accurate, provided an accurate database is used, such as the RADCAL [53, 54] (based on experimental data) and EM2C [55] (calculated from high-resolution data) databases. However, they require a few hundred to thousands of spectral evaluations. Some results for one-dimensional slabs were obtained by Menart and colleagues [56–58], the latter two papers overcoming the black-wall limitation of the narrow band

[5]Note that, in concurrence with the definition of total absorptivity, the derivative in $\partial\alpha/\partial s'$ is only with respect to the path $s' \to s$, and *not* with respect to the s' in the temperature $T(s')$.

model, by expanding wall radiosities into infinite series (for multiple reflections). Cherkaoui and coworkers [59] used an approach similar to [57] to determine direct exchange factors (for use with the zonal method of Chapter 18) in a one-dimensional slab with reflecting walls. Multidimensional calculations were primarily carried out by the group around Liu [60–62] for various combustion scenarios. All of the here-cited works used the Malkmus model together with the EM2C database and its predecessors.

If the wide band model is to be used for a gas with N vibration–rotation bands, the absorption coefficient may be stated as

$$\kappa_\eta = \sum_{n=1}^{N} \kappa_{n\eta}. \tag{20.70}$$

To allow the use of wide band correlations it is also assumed that each band is fairly narrow, i.e., that the blackbody intensity does not vary appreciably over each band, and that the bands do not overlap.[6] Then the total absorptivity may be evaluated as

$$\alpha(T, s' \to s) \simeq \sum_{n=1}^{N} \frac{\omega_n I_{b\eta_n}}{I_b}(T) \frac{1}{\omega_n} \int_0^\infty \left[1 - \exp\left(-\int_{s'}^{s} \kappa_{n\eta}\, ds''\right)\right] d\eta = \sum_{n=1}^{N} \frac{\omega_n I_{b\eta_n}}{I_b}(T)\, A_n^*(s' \to s), \tag{20.71}$$

where $I_{b\eta_n}$ is the Planck function at the center of band n, ω_n is the band width parameter, and A_n^* is the nondimensional band absorptance, as discussed in detail in Chapter 11.

Molecular Gas with Suspended Particles

If the molecular gas contains a suspension of nonscattering particles, the absorption coefficient may be written as

$$\kappa_\eta = \kappa_{p\eta} + \kappa_{g\eta} = \kappa_{p\eta} + \sum_{n=1}^{N} \kappa_{n\eta}. \tag{20.72}$$

We shall now assume that, not only are the gas bands narrow and nonoverlapping, but also that the absorption coefficient of the particles, $\kappa_{p\eta}$, does not vary appreciably over each band. Then

$$\begin{aligned}
\alpha(T, s' \to s) &= \frac{1}{I_b(T)} \int_0^\infty \left[1 - \exp\left(-\int_{s'}^{s} \kappa_{p\eta}\, ds''\right) \exp\left(-\int_{s'}^{s} \kappa_{g\eta}\, ds''\right)\right] I_{b\eta}(T)\, d\eta \\
&= \frac{1}{I_b(T)} \int_0^\infty \left[1 - \exp\left(-\int_{s'}^{s} \kappa_{p\eta}\, ds''\right)\right] I_{b\eta}(T)\, d\eta \\
&\quad + \frac{1}{I_b(T)} \int_0^\infty \exp\left(-\int_{s'}^{s} \kappa_{p\eta}\, ds''\right)\left[1 - \exp\left(-\int_{s'}^{s} \kappa_{g\eta}\, ds''\right)\right] I_{b\eta}(T)\, d\eta.
\end{aligned} \tag{20.73}$$

The first term in equation (20.73) is simply the absorptivity for the particle background (without molecular gas). In the second spectral integral we note that the integrand is nonzero only when $\kappa_{g\eta}$ is nonzero, i.e., over the vibration–rotation bands of the gas. Since we assume the gas bands to be spectrally narrow, the particle attenuation term may be evaluated at the band center and taken outside the spectral integral. Then

$$\alpha(T, s' \to s) \simeq \alpha_p(T, s' \to s) + \sum_{n=1}^{N} \frac{\omega_n I_{b\eta_n}}{I_b}(T)\, \exp\left(-\int_{s'}^{s} \kappa_{p\eta_n}\, ds''\right) A_n^*(s' \to s). \tag{20.74}$$

[6] These assumptions are usually very good except in the limit of extreme optical thickness, which tends to widen bands. Even at lesser optical thickness some bands of important gases overlap, most notably the 2.7 μm bands of CO_2 and H_2O (see Chapter 11).

Radiative Equilibrium

In the case of radiative equilibrium equation (20.69) is used to determine the temperature field. Substituting the result into equation (20.66), with $\nabla \cdot \mathbf{q} = 0$, yields

$$4\pi\kappa_P I_b = \int_{4\pi} \left[\frac{\partial \alpha}{\partial s}(T_w, 0 \to s) I_{bw} + \int_0^s \frac{\partial^2 \alpha}{\partial s \partial s'} [T(s'), s' \to s] I_b(s')\, ds' \right] d\Omega. \tag{20.75}$$

This is a single (but rather complicated) integral equation for the unknown temperature. Once the temperature field is known, the heat flux follows from equations (20.65) and (20.64) as

$$\mathbf{q} = \int_{4\pi} \left[[1 - \alpha(T_w, 0 \to s)] I_{bw} - \int_0^s \frac{\partial \alpha}{\partial s'} [T(s'), s' \to s]\, I_b(s')\, ds' \right] \hat{\mathbf{s}}\, d\Omega. \tag{20.76}$$

In equations (20.75) and (20.76) the absorptivities and their derivatives are obtained from equation (20.71) (pure molecular gas) or (20.74) (gas–particulate mixture).

Medium with Known Temperature Field

If the temperature field is known, the local heat flux may be determined from equation (20.76), while the divergence of the heat flux follows from equations (20.66) and (20.69) as

$$\nabla \cdot \mathbf{q} = 4\pi\kappa_P I_b - \int_{4\pi} \left[\frac{\partial \alpha}{\partial s}(T_w, 0 \to s) I_{bw} + \int_0^s \frac{\partial^2 \alpha}{\partial s \partial s'} [T(s'), s' \to s] I_b(s')\, ds' \right] d\Omega. \tag{20.77}$$

Again, the absorptivities and their derivatives are obtained from equations (20.71) (pure molecular gas) or (20.74) (gas–particulate mixture).

The general relationships developed in this section will be employed over the following two sections to carry out heat transfer calculations. First we shall look in some detail at radiative transfer within an isothermal, one-dimensional nongray medium. Then follows a section describing how the concept of a weighted-sum-of-gray-gases can be applied to the general nongray medium problem.

The Wide Band Model for Isothermal Media

For an isothermal medium, we assume that the absorption coefficient is a function of temperature only (and is, therefore, constant throughout the medium). The definition of the total absorptivity, equation (20.63), keeping in mind that the absorption coefficient depends on T_m, while the Planck function may be evaluated at medium or wall temperature, then simplifies to

$$\alpha(T, T_m, s) = \frac{1}{I_b(T)} \int_0^\infty \left(1 - e^{-\kappa_\eta(T_m)s}\right) I_{b\eta}(T)\, d\eta, \tag{20.78}$$

that is, the total absorptivity no longer depends on the entire path, but only on the path length itself. If $T = T_w$, equation (20.78) gives the absorption of wall emission along the path s, while for $T = T_m$ equation (20.78) represents the total emissivity

$$\epsilon(T_m, s) = \frac{1}{I_b(T_m)} \int_0^\infty \left(1 - e^{-\kappa_\eta(T_m)s}\right) I_{b\eta}(T_m)\, d\eta. \tag{20.79}$$

Similarly, the nondimensional band absorptance of molecular gases now depends only on the optical path length (as well as a line overlap parameter), as discussed in Chapter 11, or

$$A_n^*(s' \to s) = A^*[\kappa_n(s - s'), \beta_n], \tag{20.80}$$

where $\kappa_n = \rho_a \alpha_n / \omega_n$ is the gas absorption coefficient at the band center or band head,[7] and β_n is the overlap parameter, all evaluated at T_m. Equation (20.64) then reduces for an isothermal medium to

$$I(s) = [1 - \alpha(T_w, T_m, s)] I_{bw} + \epsilon(T_m, s) I_{bm}, \tag{20.81}$$

where $I_{bm} = I_b(T_m)$ and T_m is the (constant) temperature of the medium.

Example 20.8. Consider a 1 m thick isothermal layer of pure CO_2 at a pressure of 100 kPa and a temperature of 1700 K. The gas is confined between two parallel, cold, black plates. Calculate the radiative transfer from the gas to the walls using the exponential wide band model.

Solution

For a slab $0 < z < L$ the intensity as given by equation (20.81) may emanate from either of the two bounding surfaces. Splitting intensity into I^+ and I^- ("positive" and "negative" directions), as was done in Section 14.2, leads to $s = z/\mu$ for "positive" directions ($0 < \mu < 1$) and to $s = -(L-z)/\mu$ for "negative" directions ($-1 < \mu < 0$), as shown in Fig. 14-1. Substituting into equation (20.81) results in

$$I^+(z) = \Big[1 - \alpha(T_w, T_m, z/\mu)\Big] I_{bw} + \epsilon(T_m, z/\mu) I_{bm}, \qquad 0 < \mu < 1,$$

$$I^-(z) = \Big[1 - \alpha\Big(T_w, T_m, -(L-z)/\mu\Big)\Big] I_{bw} + \epsilon\Big(T_m, -(L-z)/\mu\Big) I_{bm}, \qquad -1 < \mu < 0.$$

The local heat flux is then determined from

$$\begin{aligned} q(z) &= 2\pi \left[\int_{-1}^{0} I^- \mu \, d\mu + \int_{0}^{+1} I^+ \mu \, d\mu \right] \\ &= 2\pi \left\{ \int_0^1 \left[\epsilon\left(T_m, \frac{z}{\mu}\right) - \epsilon\left(T_m, \frac{L-z}{\mu}\right) \right] \mu \, d\mu \, I_b(T_m) \right. \\ &\quad \left. - \int_0^1 \left[\alpha\left(T_w, T_m, \frac{z}{\mu}\right) - \alpha\left(T_w, T_m, \frac{L-z}{\mu}\right) \right] \mu \, d\mu \, I_b(T_w) \right\}. \end{aligned}$$

If the medium is a molecular gas, equation (20.71) is substituted into this expression. Using emissive powers in favor of intensities, $E_{b\eta} = \pi I_{b\eta}$, then leads to

$$q(z) = \sum_{n=1}^{N} \omega_n \Big[E_{b\eta_n}(T_m) - E_{b\eta_n}(T_w) \Big] \big[A_s(\kappa_n z, \beta_n) - A_s(\kappa_n (L-z), \beta_n) \big],$$

where A_s, termed *slab band absorptance* by Edwards and Balakrishnan [63], is defined as

$$A_s(\tau, \beta) = 2 \int_0^1 A^*\left(\frac{\tau}{\mu}, \beta\right) \mu \, d\mu. \tag{20.82}$$

The slab band absorptance may be evaluated explicitly for a number of band absorptance correlations, such as the Edwards and Menard correlation of Table 11.2 and the high-pressure limit given by equation (11.155), and must be evaluated numerically for more involved correlations such as the ones by Felske and Tien, equation (11.156), and Wang, equation (11.158). The line overlap parameter β was already calculated for the most important 4.3μm band in Example 20.6 ($\beta_{4.3} = 7.55$), and is substantially larger than unity for all bands. Thus, the high-pressure limit may be used, and we shall only consider the high-pressure limit ($\beta \to \infty$) here,

$$A^*(\tau, \infty) = E_1(\tau) + \ln \tau + \gamma_E,$$

or

$$A_s(\tau, \infty) = 2 \int_0^1 \left[E_1\left(\frac{\tau}{\mu}\right) + \ln \frac{\tau}{\mu} + \gamma_E \right] \mu \, d\mu.$$

Integrating by parts we obtain, with $E_1'(x) = -E_0(x) = e^{-x}/x$,

$$A_s(\tau, \infty) = \mu^2 \left[E_1\left(\frac{\tau}{\mu}\right) + \ln \frac{\tau}{\mu} + \gamma_E \right]_0^1 - \int_0^1 \mu^2 \left(\frac{\tau}{\mu^2} \frac{e^{-\tau/\mu}}{\tau/\mu} - \frac{1}{\mu} \right) d\mu,$$

[7] Note that, in wide band correlations, the band strength parameter α is usually based on a mass absorption coefficient and must, therefore, be corrected by multiplying with the partial density of the absorbing gas, ρ_a.

or

$$A_s(\tau,\infty) = E_1(\tau) + \ln\tau + \gamma_E + \tfrac{1}{2} - E_3(\tau). \tag{20.83}$$

Calculating q at $z = L$ for the three important CO_2 bands, we obtain [with $T_w = 0$ and $A_s(0,\beta) = 0$]

$$q_n(L) = \omega_n E_{b\eta_n}(T_m) A_s\left(\frac{\alpha_n \rho_{CO_2}}{\omega_n} L, \beta\right).$$

All required terms have already been calculated in the previous example, and we find the following:[8]

2.7 μm band:
$$\alpha_{2.7}\rho_{CO_2}L/\omega_{2.7} = 2005 \times 1/96.9 = 20.69$$
$$A_{S2.7}(20.69,\infty) = E_1(20.69) + \ln 20.69 + 0.5772 + 0.5 - E_3(20.69) = 4.107$$
$$q_{2.7}(L) = 1.7649 \times 10^{-8} \times 1700^3 \times 96.9 \times 4.107 = 34{,}508\,\mathrm{W/m^2};$$

4.3 μm band:
$$\alpha_{4.3}\rho_{CO_2}L/\omega_{4.3} = 34{,}254 \times 1/46.2 = 741.43$$
$$A_{S4.3}(741.43,\infty) = E_1(741.43) + \ln 741.43 + 0.5772 + 0.5 - E_3(741.43) = 7.686$$
$$q_{4.3}(L) = 1.5548 \times 10^{-8} \times 1700^3 \times 46.2 \times 7.686 = 27{,}125\,\mathrm{W/m^2};$$

15 μm band:
$$\alpha_{15}\rho_{CO_2}L/\omega_{15} = 5917 \times 1/52.4 = 112.92$$
$$A_{S15}(112.92,\infty) = E_1(112.92) + \ln 112.92 + 0.5772 + 0.5 - E_3(112.92) = 5.804$$
$$q_{15}(L) = 0.2979 \times 10^{-8} \times 1700^3 \times 52.4 \times 5.804 = 4805\,\mathrm{W/m^2}.$$

Finally, the total heat loss from the gas is

$$q = 2 \times [34{,}508 + 27{,}125 + 4805] = 13.29\,\mathrm{W/cm^2}.$$

Comparison with Example 20.2 shows that the present results agree excellently with those of the mean beam length method.

A number of investigators have obtained exact wide band model solutions to the relatively simple problems of one-dimensional isothermal media. Edwards and Balakrishnan [63] found expressions for the heat flux in an isothermal gas slab and gave results for the high-pressure limit (strong spectral line overlap). Edwards [64] gave an expression for the heat loss from an isothermal gas sphere, while heat loss from an isothermal gas cylinder was discussed by Wassel and Edwards [65]. More recent wide band calculations have been done by Kim and coworkers [56] for a one-dimensional slab containing water vapor (to compare with their narrow band calculations). The wide band approach was also used by Hutchison and Richards [66] investigating combined conduction and radiation in a layer containing CO_2, again treating reflecting walls by expanding radiosities into infinite series. Calculations for gases with suspended particles have been carried out by Modest [67] (general wide band formulation with nongray particles), Cumber and coworkers [68] (applying the Goody model together with the RADCAL database to a jet flame with water vapor, CO_2, and soot), Liu and colleagues [69] (three-dimensional mixtures of water vapor, CO_2, and alumina particles, using the EM2C database), and Maruyama and Guo [70] (three-dimensional furnace with water vapor, CO_2, and carbon particles, using a spectral version of the wide band model combined with the Elsasser narrow band model). The latter two papers attempt to overcome the no-scattering limitation of the band models.

20.6 THE WEIGHTED-SUM-OF-GRAY-GASES (WSGG) MODEL

The concept of a weighted-sum-of-gray-gases approach was first presented by Hottel [29] within the framework of the zonal method, which is described in detail in Chapter 18. Modest [40] has demonstrated that this approach can be applied to the directional equation of transfer,

[8] Note that all three bands are optically so thick that the exponential integrals essentially vanish.

equation (20.57), and, therefore, to any solution method for the equation of transfer (exact, P_N-approximation, discrete ordinates method, etc.), provided all boundaries are black and the medium is nonscattering. In this method the nongray gas is replaced by a number of gray gases, for which the heat transfer rates are calculated independently. The total heat flux is then found by adding the heat fluxes of the gray gases after multiplication with certain weight factors.

As a starting point consider equation (20.64). For mathematical simplicity we shall limit ourselves here to a spatially constant (or averaged) absorption coefficient, which may, however, vary across the spectrum. Such an absorption coefficient no longer depends on the local temperature, although the choice for an appropriate constant value will be based on the overall temperature field in the medium. Thus, we have for the spectrally-integrated intensity

$$I(s) = [1 - \alpha(T_w, s)]I_{bw} - \int_0^\infty \frac{\partial \epsilon}{\partial s'} [T(s'), s-s'] \, I_b(s') \, ds', \tag{20.84}$$

where the expressions for total absorptivity and emissivity are similar to the ones developed for an isothermal medium, equation (20.78),

$$\epsilon(T, s) = \frac{1}{I_b(T)} \int_0^\infty (1 - e^{-\kappa_\eta s}) \, I_{b\eta}(T) \, d\eta, \quad \alpha(T_w, s) = \epsilon(T_w, s). \tag{20.85}$$

Since the absorption coefficient is assumed spatially constant, the total absorptivity no longer depends on the medium's temperature. It follows that, for a gray medium with $\kappa_\eta = \kappa = \text{const}$,

$$\epsilon(T, s) = \alpha(T, s) = 1 - e^{-\kappa s}. \tag{20.86}$$

We shall now assume that the emissivity and absorptivity of equation (20.85) may be approximated by a *weighted sum of gray gases*, or

$$\epsilon(T, s) = \alpha(T, s) \simeq \sum_{k=0}^{K} a_k(T) \, (1 - e^{-\kappa_k s}) \, . \tag{20.87}$$

Consistent with equations (20.84) and (20.85) we have chosen the gray-gas absorption coefficients κ_k to be constants, while the weight factors a_k may be functions of source temperature [wall temperature for the absorptivity and local medium temperature for emissivity, as required in equation (20.84)]. Neither a_k nor κ_k are allowed to depend on path length s. Depending on the material, the quality of the fit, and the accuracy desired, a K of 2 or 3 usually gives results of satisfactory accuracy [29]. Since, for an infinitely thick medium, the absorptivity approaches unity, we find

$$\sum_{k=0}^{K} a_k(T) = 1. \tag{20.88}$$

Still, for a pure molecular gas with its "spectral windows" it would take very large path lengths indeed for the absorptivity to be close to unity. For this reason equation (20.88) starts with $k = 0$ (with an implied $\kappa_0 = 0$), to allow for spectral windows. If the medium contains particles, such that $\kappa_\eta > 0$ always, the $k = 0$ term is simply dropped, i.e., $a_0 = 0$.

Substituting equation (20.87) into equation (20.84) and using

$$1 - \alpha(T_w, s) = \sum_{k=0}^{K} a_k(T_w) \, e^{-\kappa_k s},$$

$$\frac{\partial \epsilon}{\partial s'} (T, s - s') = \frac{\partial}{\partial s'} \sum_{k=0}^{K} a_k(T) \left[1 - e^{-\kappa_k (s-s')}\right] = - \sum_{k=0}^{K} a_k(T) \, \kappa_k \, e^{-\kappa_k (s-s')},$$

leads to

$$I(s) = \sum_{k=0}^{K} a_k(T_w)\, e^{-\kappa_k s} I_{bw} + \int_0^s \sum_{k=0}^{K} a_k[T(s')]\kappa_k\, e^{-\kappa_k(s-s')} I_b(s')\, ds'$$

$$= \sum_{k=0}^{K} \left\{ [a_k I_b](T_w)\, e^{-\kappa_k s} + \int_0^s [a_k I_b](s')\, e^{-\kappa_k(s-s')} \kappa_k\, ds' \right\}. \tag{20.89}$$

Setting

$$I(s) = \sum_{k=0}^{K} I_k(s), \tag{20.90}$$

and comparing equations (20.89) and (20.58) we find that I_k satisfies the equation of transfer

$$\frac{dI_k}{ds} = \kappa_k([a_k I_b] - I_k), \tag{20.91}$$

subject to the boundary condition

$$s = 0: \qquad I_k = [a_k I_b](T_w). \tag{20.92}$$

This expression is, of course, the equation of transfer for a gray gas with constant absorption coefficient κ_k, but with blackbody intensity I_b (for medium as well as surfaces) replaced by a weighted intensity $a_k I_b$. Thus, if the temperature field is known (or assumed), the intensity field (or simply the heat fluxes) must be determined for $k = 0, 1, \ldots, K$, using any standard solution method. The results are then added to give the total intensity (or radiative heat flux). Note that, as for the stepwise-gray approximation, it will always be necessary to know or assume a temperature profile: For radiative equilibrium the condition $\nabla \cdot \mathbf{q} = 0$ applies to the total heat flux only and, in general, $\nabla \cdot \mathbf{q}_k \neq 0$.

The curve fit of the total absorptivity of the medium, equation (20.87), should be tailored to the medium at hand, depending on composition, pressure levels, temperature levels, number of molecular gas bands, and so on. Only if the fit is optimized will one be able to achieve acceptable accuracy with a weighted sum of two or three gray gases. Unfortunately, the curve fit is a nonlinear one, and is further complicated by the fact that the a_k may be functions of temperature, pressure, composition, and so forth. As a result of these difficulties the curve fitting effort may become more involved than the heat transfer calculations themselves! Some weighted-gray-gas absorptivity fits for important gases have been reported in the literature for use with the zonal method (Chapter 18), e.g., by Smith and coworkers [71] for water vapor–carbon dioxide mixtures, and by Farag and Allam [72] for carbon dioxide. A "cookbook" formula for any gas, for which wide band data are available, has been given by Modest [40], and has been used to obtain the WSGG results included in Fig. 20-3. A collection of WSGG parameters for varying mixtures of water vapor, carbon dioxide, and soot has been given by Truelove [73]. His correlation for the common case of $p_{H_2O} = 2p_{CO_2}$ (e.g., resulting from complete combustion of methane) is reproduced in Table 20.2, with equation (20.87) slightly altered to

$$\epsilon\,(T, s) = \alpha(T, s) = \sum_{k=0}^{K} \sum_{l=1}^{L} a_{kl}(T) \left(1 - e^{-[\kappa_{gk}(p_{H_2O} + p_{CO_2}) + \kappa_{pl}\rho_p f_v]s}\right), \tag{20.93}$$

where ρ_p is the density of the soot and f_v is its volume fraction. Another, similar set of WSGG parameters has been generated by Taylor and Foster [74].

Recently, to address global warming issues, oxy-fuel combustion systems have garnered a lot of attention, where oxygen (rather than air) is used to burn coal, producing an exhaust gas consisting primarily of H_2O and CO_2. The H_2O can be condensed leaving a highly concentrated CO_2 stream, which can be sequestered. Temperature control is achieved by returning part of the CO_2. This leads to much higher levels of H_2O and CO_2, promoting radiative heat transfer

TABLE 20.2
Weighted-sum-of-gray-gases absorption coefficients and weight factors for a mixture of water vapor, carbon dioxide, and soot, for a fixed ratio of partial pressures $p_{H_2O} = 2p_{CO_2}$, $a_{kl} = a^0_{kl} + a^1_{kl}T$, from Truelove [73].

k	l	a^0_{kl}	$a^1_{kl} \times 10^3$	$\kappa_{g,k}$ (m^{-1} atm^{-1})	$\kappa_{p,l}$ (m^2 kg^{-1})
0	1	0.588	−0.2401	0.0	541
0	2	−0.165	0.2834	0.0	2749
1	1	0.412	−0.1665	0.89	541
1	2	−0.127	0.2178	0.89	2749
2	1	0.2375	−0.0941	15.5	541
2	2	−0.0105	0.0265	15.5	2749
3	1	0.0585	−0.0243	239.0	541
3	2	0.0065	−0.0027	239.0	2749

and requiring different sets of WSGG parameters. Yin [75] and coworkers used the wide band model data of Table 11.3 to find a set of four gray gas parameters for ten different p_{H_2O}/p_{CO_2} ratios of relevance in oxy-fuel combustion. A similar set was generated by Johansson *et al.* [76] for two p_{H_2O}/p_{CO_2} ratios (1/8 and 1), employing the EM2C narrow band database [55].

Example 20.9. Consider an isothermal slab at temperature $T = 1000$ K, and a total pressure of $p = 1$ atm. The slab consists of a mixture of 70% N_2, 20% H_2O, and 10% CO_2 (by volume), and is bordered by cold, black walls. Determine the heat loss from this slab as a function of slab thickness L, using the WSGG method with Truelove's parameters. In addition, determine the heat lost from the layer if the gas is mixed with soot ($\rho_p = 2{,}000\,kg/m^3$, $f_v = 5 \times 10^{-6}$).

Solution
If no soot is present, the summation over l in equation (20.93) can be carried out immediately, and with $a_0 = (0.588 - 0.2401) + (-0.165 + 0.2834) = 0.466$, etc., and also using $\kappa_k = \kappa_{g,k}(0.2 + 0.1)$ atm, we obtain

$$\begin{array}{llll} a_0 = 0.466, & a_1 = 0.337, & a_2 = 0.159, & a_3 = 0.038; \\ \kappa_0 = 0, & \kappa_1 = 0.267\,m^{-1}, & \kappa_2 = 4.65\,m^{-1}, & \kappa_3 = 71.7\,m^{-1}. \end{array}$$

If we use the exact solution to the (spectral) equation of transfer, the answer was found in Example (14.1) for a gray medium as

$$q = \sigma T^4 [1 - 2E_3(\kappa L)] \tag{20.94}$$

(where we have set $T_w = 0$, $\epsilon_w = 1$, and $\tau_L = \kappa L$). Therefore, if we use the WSGG method, this leads to (in nondimensional form)

$$\Psi = \frac{q}{\sigma T^4} = \sum_{k=0}^{3} a_k [1 - 2E_3(\kappa_k L)]. \tag{20.95}$$

A plot of this result is given in Fig. 20-6, together with line-by-line (LBL) results obtained from the HITEMP 1995 database [17]. The WSGG method is seen to give results of very respectable accuracy, except for extremely long path lengths, for which the method underpredicts the gas emissivity somewhat.

If soot is added to the gas mixture, the number of terms is doubled. With $\rho_p f_v = 10^{-2}\,kg/m^3$, we obtain

$$\begin{array}{llll} a_{01} = 0.348, & a_{02} = 0.118; & a_{11} = 0.246, & a_{12} = 0.091; \\ a_{21} = 0.143, & a_{22} = 0.016; & a_{31} = 0.034, & a_{32} = 0.004. \end{array}$$

Similarly, with $\kappa_{p1}\rho_p f_v = 541 \times 10^{-2} = 5.41\,m^{-1}$ and $\kappa_{p2}\rho_p f_v = 27.49\,m^{-1}$, the corresponding gray-gas absorption coefficients become

$$\begin{array}{llll} \kappa_{01} = 5.41\,m^{-1}, & \kappa_{02} = 27.49\,m^{-1}; & \kappa_{11} = 5.68\,m^{-1}, & \kappa_{12} = 27.76\,m^{-1}; \\ \kappa_{21} = 10.05\,m^{-1}, & \kappa_{22} = 32.14\,m^{-1}; & \kappa_{31} = 77.11\,m^{-1}, & \kappa_{32} = 99.19\,m^{-1}; \end{array}$$

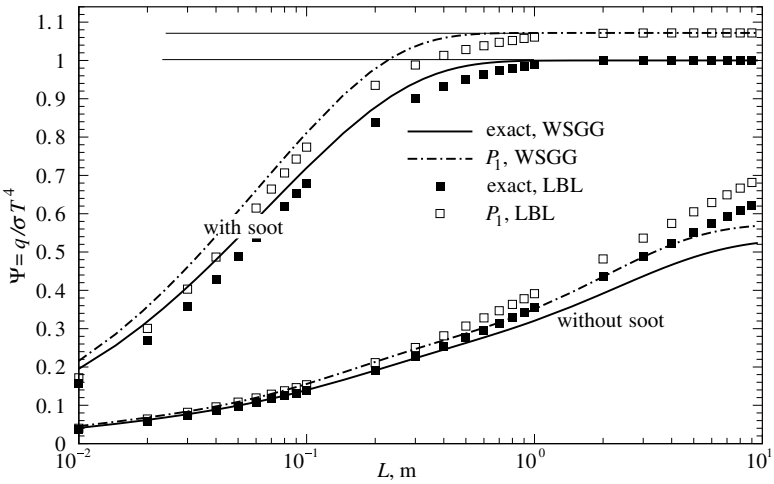

FIGURE 20-6
Nondimensional heat loss from an isothermal N_2, H_2O, CO_2 mixture with and without soot.

and the nondimensional heat flux is evaluated from

$$\Psi = \frac{q}{\sigma T^4} = \sum_{k=0}^{3} \sum_{l=1}^{2} a_{kl}[1 - 2E_3(\kappa_{kl} L)], \tag{20.96}$$

which is also plotted in Fig. 20-6 together with LBL results for a soot absorption coefficient that varies linearly with wavenumber, and that has $C_0 = 5.71$ [obtained from equation (12.123), using the Chang and Charalampopoulos refractive index of $m = 1.89 - 0.92i$ of Example 12.4]. For such soot the WSGG model overpredicts emission by about 20% for small slab thicknesses, and the error gradually diminishes with increasing L. Choosing $C_0 = 7$, or $m = 1.38 - 0.69i$, would result in almost perfect agreement. Truelove's report [73] admits to great uncertainty for the values of the $\kappa_{p,l}$, and the values reported in Table 20.2 represent compromise values chosen by Bressloff [77]. Also, equation (20.93) requires the density of the soot, while equation (12.123) does not. There is additional uncertainty attached to the soot's density, which was here arbitrarily set to $\rho_p = 2{,}000\,\text{kg/m}^3$ (approximating the density of pyrolytic graphite) and, finally, there are great variations possible in the index of refraction, as shown in Fig. 12-20. Therefore, considering the substantial uncertainties surrounding soot generation and properties, the agreement may be considered good; differences can be attributed to the soot model rather than the WSGG approximation.

Example 20.10. Reconsider the isothermal medium of Example 20.9 (with and without particles). Assuming the medium is confined between two parallel, cold and black plates a distance L apart, calculate the radiative heat flux within the slab, using the weighted-sum-of-gray-gases approach together with the P_1-approximation.

Solution
The P_1-approximation for an isothermal medium with absorption coefficient κ_k and a Planck function of $[a_k I_b]$, bounded by cold and black plates, is

$$\begin{aligned}
\frac{dq_k}{dz} &= \kappa_k(4\pi[a_k I_b] - G_k), \\
\frac{dG_k}{dz} &= -3\kappa_k q_k, \\
z = 0: &\quad 2q_k + G_k = 0, \\
z = L: &\quad -2q_k + G_k = 0.
\end{aligned}$$

The answer to this simple set of equations follows immediately, as a special case of Example 16.2, as

$$q_k(z) = a_k E_b \frac{2\sinh\sqrt{3}\kappa_k(z - L/2)}{\sinh\frac{1}{2}\sqrt{3}\kappa_k L + \frac{1}{2}\sqrt{3}\cosh\frac{1}{2}\sqrt{3}\kappa_k L}.$$

Since the medium is identical to the one of Example 20.9, their total absorptivities and, thus, the values for the correlation coefficients a_k and κ_k are identical as well. The total nondimensional heat flux follows as

$$\Psi = \frac{q}{\sigma T^4} = \frac{\sum_{k=0}^{L} q_k}{\sigma T^4} = \sum_{k=0}^{L} \frac{2a_k \sinh \sqrt{3}\kappa_k (z - L/2)}{\sinh \frac{1}{2}\sqrt{3}\kappa_k L + \frac{1}{2}\sqrt{3} \cosh \frac{1}{2}\sqrt{3}\kappa_k L}.$$

Results from the P_1-approximation for $z = L$ are also included in Fig. 20-6, together with their LBL results. The trends are the same as for the previous example, with the P_1-approximation always slightly overpredicting emission rates. The error is largest for large optical thicknesses, which is due to the cold boundary as was discussed in Example 16.2.

At first glance, the weighted-sum-of-gases method appears to be a rather crude, approximate tool to estimate radiative heat fluxes from extremely complicated participating media. And, when the method was first developed before the advent of powerful computers and accurate, high-resolution databases, it was just that. Still, even in its crudest form, the method has enjoyed great popularity, since it is easy to apply and since more accurate calculations were difficult, if not impossible, to obtain (in part due to a lack of accurate high-temperature spectral property data). For example, Ramamurthy and coworkers [78] applied the method together with an S_4 discrete ordinates approach to reacting flow in radiant tubes. Mesyngier and Farouk [79] investigated turbulent free convection in a square enclosure containing mixtures with water vapor and/or carbon dioxide, Liu and coworkers [80] looked at natural gas-fired furnaces, and Baek *et al.* [81] studied single droplet combustion, all using the WSGG scheme together with the discrete ordinates method. Kühlert and Renz [82] considered a pulverized coal flame, and Bressloff [77] compared the accuracy of the WSGG model with results obtained from narrow band calculations, as did Pierrot and coworkers [7] (also using several other spectral methods). Yu and colleagues [83] investigated various isothermal, one-dimensional H_2O–CO_2–soot mixtures, and Omori *et al.* [84] used the method together with a commercial flow solver to study an industrial furnace.

Today we know that the method can also be applied to reflecting (albeit gray) walls, to variable absorption coefficients as long as they obey the scaling approximation [see equation (11.130) in Section 11.9], and that accurate gray-gas coefficients can be obtained from high-resolution databases, mostly through the extensions to the WSGG method made by Denison and Webb [3,5,85–87]. Noting that the WSGG method can be seen as a box model of Section 20.4 with thousands of boxes across the spectrum (but relatively few different box heights κ_k), the weight factors a_k are simply the sum of the $(E_{b\eta}\Delta\eta)_i$ for all "boxes" with height κ_k, and normalized by E_b; i.e., the a_k are the fraction of the emissive power spectrum, where the absorption coefficient equals κ_k. This approach, which they call Spectral-Line-Based Weighted-Sum-of-Gray-Gases, or SLW, can finite-difference the spectral line structure of molecular gases to any desired accuracy. Their calculations show that extremely accurate results (compared to LBL benchmarks) can be obtained for homogeneous gas mixtures, using only three or four spectral calculations and—to a lesser extent—also in mixtures with varying temperature and concentrations. Additional SLW parameters were found by Solovjov and Webb [18], who also investigated schemes to treat overlapping gas bands in mixtures [12], including soot [88]. A very similar method, the Absorption Distribution Function (ADF) model, was developed by Rivière and coworkers [6–8] and applied to one-dimensional mixtures of water vapor and carbon dioxide with various temperature and concentration profiles. In [8] the approach is extended to include fictitious gases, as was done for the narrow band k-distribution in equation (11.138).

20.7 k-DISTRIBUTION MODELS

When the band models were developed in Chapter 11 we noted that results were obtained in terms of spectrally averaged transmissivities or emissivities (narrow band models), total band absorptances (wide band models), or total emissivities and absorptivities (full spectrum

or "global" models), *not* in terms of a smoothened absorption coefficient. For that reason band models are limited to line-of-sight calculations, i.e., they cannot be used in media with reflecting walls and/or scattering particles, or at least only with great difficulty. While *k*-distributions share some of the weaknesses of the band models (such as difficulty to apply the method to nonhomogeneous media), they result in a reordered, rather than smoothened, absorption coefficient and can, therefore, be applied to arbitrary enclosures (including reflecting walls and scattering), using arbitrary RTE solution methods (including the stochastic Monte Carlo method discussed in Chapter 21. However, *k*-distributions tend to be cumbersome to assemble and must be generated individually for every cell in the computational domain, generally from high-resolution databases, such as HITRAN 2008 [1] and HITEMP 2010 [2], with their millions (and even hundreds of millions) of spectral lines. Thus, the rapid assembly of *k*-distributions is of utmost importance, either through correlations or using a precalculated *k*-distribution database.

Like traditional band models, *k*-distributions come in narrow band, wide band, and full spectrum or global versions.

Narrow Band *k*-Distribution Calculations In traditional band models "narrow band" implies a spectral range over which the applied statistics are valid (such as the Malkmus model), limiting a narrow band to $\Delta\eta \simeq 4$ to $10\,\mathrm{cm}^{-1}$ for high accuracy calculations, to an absolute maximum of perhaps $25\,\mathrm{cm}^{-1}$. For *k*-distributions "narrow band" implies a spectral range across which the Planck function $I_{b\eta}$ can be assumed to remain constant, i.e., perhaps 25 to $100\,\mathrm{cm}^{-1}$ for high accuracy, and up to several $100\,\mathrm{cm}^{-1}$ for fair accuracy. However, *k*-distributions require approximately 10 spectral calculations for each $\Delta\eta$ range, making the numerical effort roughly equivalent for both types of narrow band calculations. Most narrow band *k*-distribution calculations to date have employed the *k*-distribution database of Soufiani and Taine [55] (based on HITRAN96 plus proprietary high-temperature extrapolations). Marin and Buckius [11] applied the method to a one-dimensional slab containing water vapor or carbon dioxide (but not both) with fixed concentrations and varying temperatures (steps and parabolic profiles). Using wavenumber ranges of up to $\Delta\eta = 1000\,\mathrm{cm}^{-1}$ they noted that little loss of accuracy occurred for $\Delta\eta \leq 500\,\mathrm{cm}^{-1}$. Dembele and coworkers used the method to determine radiation from fires with water spray curtains, using the discrete ordinates method and Mie scattering for the water droplets [89], and also to predict intensities exiting from a natural gas flame [90]. Tang and Brewster [20] also studied a one-dimensional slab containing CO_2, but included anisotropic scattering. Pierrot and colleagues [7, 8] considered one-dimensional slabs containing H_2O and CO_2, as well, comparing various spectral solution methods. Liu *et al.* [91] tested different quadrature schemes for narrow band *k*-distribution calculations, and used the method for a three-dimensional geometry, to verify an approximate formulation of the statistical narrow band model applied to scattering media [91]. The method was further optimized and applied to several two-dimensional flames [92], using the EM2C database [55] to generate *k*-distributions from equation (11.108). Finally, Tessé [93] applied the method for the evaluation of turbulence–radiation interactions in turbulent flames.

Wide Band *k*-Distribution Calculations In traditional band models "wide band" implies the spectral range covered by an entire vibration–rotation band, and it is assumed (somewhat tenuously) that the Planck function is constant across the band. The same definition is generally used for *k*-distributions, making the distinction between narrow band and wide band *k*-distributions a judgement call. A number of approximate wide band *k*-distributions have been generated to facilitate their use, which distinguishes them from narrow band distributions. In one approach [94–98] experimentally determined wide band parameters were reformulated, to allow their use in arbitrary RTE solvers, as described in Section 11.10. These exponential wide band based *k*-distributions have been tested by their authors on various one-dimensional isothermal gas mixtures contained between parallel plates. In the other approach [99–102] *k*-distributions for various vibration–rotation bands of CO_2 and H_2O were obtained from the HITRAN92 database [103], and relatively easy-to-use approximate correlations were formulated.

Full Spectrum *k*-Distributions and Related Methods Narrow band and wide band *k*-distributions rely on the fact that the Planck function is relatively constant across a band. Modest and Zhang [104] have extended the *k*-distribution concept to the full spectrum by incorporating the spectrally varying blackbody intensity, and showed that the WSGG method, as applied in the SLW and ADF forms, is just a crude implementation of the Full Spectrum *k*-Distribution (FSK) method and, as such, can also be used in media with (gray) scattering particles. Because of the close relationship between the models, the SLW method will be described as a special case of the full spectrum *k*-distribution approach.

20.8 THE FULL SPECTRUM *k*-DISTRIBUTION (FSK) METHOD FOR HOMOGENEOUS MEDIA

Like the WSGG method the Full Spectrum *k*-Distribution (FSK) method demands that, except for the absorption coefficient, no other radiative property varies across the spectrum, and then attempts to integrate the radiative transfer equation across the entire spectrum *before* solving it. And, like the narrow band *k*-distribution of Section 11.9, this is achieved by reordering the absorption coefficient into a monotonically increasing function. However, in the full spectrum case allowance must be made for a blackbody intensity (or Planck function) varying across the spectrum. The FSK method can be developed very much like a narrow band *k*-distribution via a gas column transmissivity (or absorptivity), clearly showing its close relationship with the WSGG approach. This has been described in the original paper by Modest and Zhang [104]. The FSK method can also be applied directly to the RTE, resulting in a more powerful derivation, because it shows that the approach is also valid for arbitrarily scattering media and for arbitrarily reflecting surfaces, as long as the absorption coefficient remains the only spectrally varying radiative property [104, 105]. We will describe here only the latter approach.

In this section we will first consider the simple case of a homogeneous medium, i.e., a medium with uniform temperature, pressure, and mixture mole fraction throughout. Such a mixture has an absorption coefficient that, while varying across the spectrum, is spatially constant. The radiative transfer equation for such a medium is, from equation (10.21),

$$\frac{dI_\eta}{ds} = \kappa_\eta I_{b\eta} - (\kappa_\eta + \sigma_s) I_\eta + \frac{\sigma_s}{4\pi} \int_{4\pi} I_\eta(\hat{\mathbf{s}}')\, \Phi(\hat{\mathbf{s}}, \hat{\mathbf{s}}')\, d\Omega', \tag{20.97}$$

where—in order to establish a global model—scattering coefficient and phase function are assumed to be independent of wavenumber (gray). Let equation (20.97) be subject to the boundary conditions at a wall

$$I_\eta = I_{w\eta} = \epsilon_w I_{bw\eta} + (1 - \epsilon_w) \frac{1}{\pi} \int_{\hat{\mathbf{n}}\cdot\hat{\mathbf{s}}<0} I_\eta\, |\hat{\mathbf{n}} \cdot \hat{\mathbf{s}}|\, d\Omega, \tag{20.98}$$

where $I_{w\eta}$ is the spectral intensity leaving the enclosure wall, due to (diffuse gray) emission and/or (diffuse gray) reflection (and extension to more general boundary conditions is straightforward, provided the surface properties remain gray).

A full spectrum *k*-distribution is defined, in accordance with equation (11.98) for a narrow band, as[9]

$$f(T, k) = \frac{1}{I_b} \int_0^\infty I_{b\eta}(T)\, \delta(k - \kappa_\eta)\, d\eta. \tag{20.99}$$

The $f(T, k)$ in equation (20.99) is a *Planck-function-weighted k-distribution* and is a function of temperature through the blackbody intensity. A reordered RTE is obtained by multiplying

[9]For a definition of the Dirac-delta function see Section 11.9, equation (11.99).

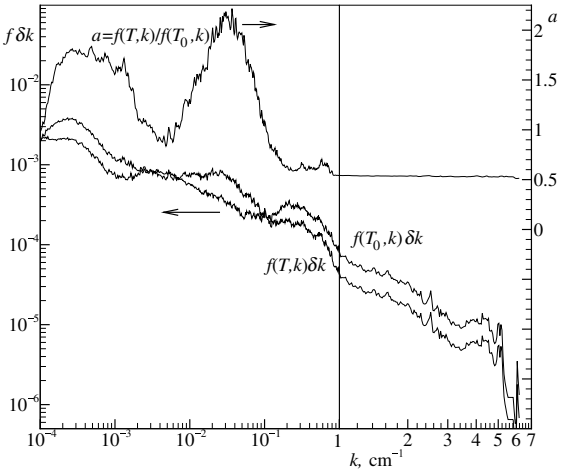

FIGURE 20-7
Planck-function-weighted k-distributions for 10% CO_2 in nitrogen for Planck function temperatures of $T = 1000\,\text{K}$ and $T_w = 500\,\text{K}$.

equations (20.97) and (20.98) by the Dirac-delta function $\delta(k - \kappa_\eta)$, followed by integration over the entire spectrum. This leads to

$$\frac{dI_k}{ds} = kf(T,k)I_b - (k + \sigma_s)I_k + \frac{\sigma_s}{4\pi}\int_{4\pi} I_k(\hat{\mathbf{s}}')\,\Phi(\hat{\mathbf{s}},\hat{\mathbf{s}}')\,d\Omega' \tag{20.100}$$

with boundary condition

$$I_k = I_{wk} = \epsilon_w f(T_w,k)I_{bw} + (1-\epsilon_w)\frac{1}{\pi}\int_{\hat{\mathbf{n}}\cdot\hat{\mathbf{s}}<0} I_k\,|\hat{\mathbf{n}}\cdot\hat{\mathbf{s}}|\,d\Omega, \tag{20.101}$$

where

$$I_k = \int_0^\infty I_\eta\,\delta(k-k_\eta)\,d\eta \tag{20.102}$$

is the intensity I_η collected over all spectral locations where $k_\eta = k$ (per dk). Thus, once I_k has been found from equation (20.100), the total intensity can be determined from

$$I = \int_0^\infty I_\eta\,d\eta = \int_0^\infty I_k\,dk. \tag{20.103}$$

Note that two Planck-function-weighted k-distributions are required: one at the temperature of the homogeneous medium, $f(T,k)$, and one evaluated at the wall temperature, $f(T_w,k)$, but both using the absorption coefficient evaluated at the conditions of the medium. Two typical Planck-function-weighted k-distributions are shown in Fig. 20-7 for a medium at $T = 1000\,\text{K}$ and a wall temperature $T_w = 500\,\text{K}$, for a mixture of 10% CO_2 in nitrogen at 1000 K, 1 bar, as evaluated from the HITEMP 1995 database [17]. Unfortunately, full spectrum k-distributions vary significantly with their method of evaluation, span across many orders of magnitude (partially suppressed in Fig. 20-7 by plotting $f\,\delta k$ instead of f itself), and may be quite ill-behaved, much like their narrow band counterparts (cf. Fig. 11-15). Also, k-distributions at different Planck function temperatures are seen to be quite different: different Planck function temperatures emphasize different parts of the spectrum and, therefore, different spectral lines. However, as noted in Section 11.9, the sharp peaks in $f(T,k)$ are due to maxima and minima of κ_η, which remain the same for all Planck function temperatures. Consequently, the ratio of any two full spectrum k-distributions evaluated at different Planck function temperatures should produce a much smoother function, in particular if the temperatures are close together. This is indeed the case and is also indicated in Fig. 20-7 through the function $a(T,k)$, although some remnant noise remains, in particular for (fortunately fairly unimportant) small values of k and low temperatures, as shown here. In Fig. 20-7 the smoothing effect is most obvious

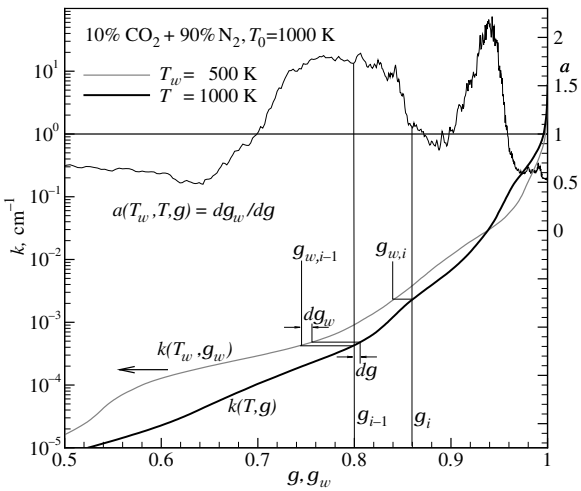

FIGURE 20-8
Planck-function-weighted cumulative k-distributions for 10% CO_2 in nitrogen for Planck function temperatures of 1000 K and 500 K.

for large values of k, reducing noise by a factor of more than 100. For T_w approaching T, the a-function approaches $a \to 1$ in a smooth manner, and is generally well-behaved for high temperatures (for both T and T_w). The reason for this behavior is that, for low temperatures, the Planck function is essentially negligible across some important vibration–rotation bands while, at high temperatures, all bands contribute regardless of their position in the spectrum. Based on this discussion, to facilitate integration of equation (20.103), equations (20.100) and (20.101) are divided by the k-distribution evaluated at the temperature of the medium. This leads to a reordered RTE in smoothly-varying g-space, where the cumulative k-distribution g is a nondimensional, Planck-function-weighted, reordered wavenumber. This is termed the *Full Spectrum k-Distribution (FSK) method*:

$$\frac{dI_g}{ds} = k\Big(I_b(T) - I_g\Big) - \sigma_s\left(I_g - \frac{1}{4\pi}\int_{4\pi} I_g(\hat{s}')\,\Phi(\hat{s},\hat{s}')\,d\Omega'\right), \tag{20.104}$$

with the boundary conditions

$$I_g = I_{wg} = \epsilon_w a(T_w,T,g) I_{bw} + (1-\epsilon_w)\frac{1}{\pi}\int_{\hat{\mathbf{n}}\cdot\hat{\mathbf{s}}<0} I_g\,|\hat{\mathbf{n}}\cdot\hat{\mathbf{s}}|\,d\Omega, \tag{20.105}$$

where

$$I_g = I_k/f(T,k) = \int_0^\infty I_\eta\,\delta\Big(k-\kappa_\eta\Big)\,d\eta\Big/ f(T,k), \tag{20.106}$$

$$g(T,k) = \int_0^k f(T,k)\,dk, \tag{20.107}$$

$$a(T_w,T,g) = \frac{f(T_w,k)}{f(T,k)} = \frac{dg_w(T_w,k)}{dg(T,k)}. \tag{20.108}$$

Physically, g is the Planck-function-weighted fraction of the spectrum with absorption coefficient $\kappa_\eta < k$. Thus, the total intensity is evaluated from

$$I = \int_0^\infty I_\eta\,d\eta = \int_0^\infty I_k\,dk = \int_0^1 I_g\,dg. \tag{20.109}$$

In equation (20.108) numerator and denominator are both evaluated at identical values of k, which in turn is related to g through equation (20.107).

The cumulative k-distributions for the CO_2-distributions of Fig. 20-7 are shown in Fig. 20-8, and are seen to be smooth, monotonically increasing functions of nondimensional "wavenumber" g. Both k-distributions, $k(T, g)$ and $k(T_w, g_w)$, have the same range of k-values (the absorption coefficient of CO_2 at $T = 1000$ K), but different g-values, and the function a is the stretching factor dg_w/dg between the two distributions, evaluated at identical k-values (horizontal lines in Fig. 20-8): Wherever the slope of $k(T_w, g_w)$ is less than that of $k(T, g)$ (for the same value of k) $a(T_w, T, g) > 1$ and vice versa. While $k(T, g)$ is a monotonically increasing function (with tiny steps wherever κ_η has a maximum or a minimum), $a(T_w, T, g)$ is not. Mathematically, wherever κ_η has a maximum or a minimum $f(T_w, k)$ and $f(T, k)$ both tend toward infinity, leading to a zero-divided-by-zero situation. Taking the limits, $a(T_w, T, g)$ *should* be a smooth function but, in reality, this depends on the fidelity with which the k-distributions are evaluated. It is, in general, better to evaluate the $a(T_w, T, g)$ employing the slopes of $g(k)$ as opposed to using the f themselves, as indicated in equation (20.108), perhaps even only after slight smoothing of the $g(k)$.

It is important to understand that the FSK method given by equations (20.104) through (20.108) is an *exact* method (subject to the restrictions of a homogeneous medium). In fact, the method is also exact for nonhomogeneous media, provided the absorption coefficient is spatially invariant (e.g., evaluated at a reference condition and then applied to the entire medium). Within these restrictions the FSK results are equivalent to LBL calculations, the former requiring roughly 10 spectral evaluations *vs.* about 1,000,000 for LBL.

20.9 THE SPECTRAL-LINE-BASED WEIGHTED SUM OF GRAY GASES (SLW)

It is also of interest to note what happens if equations (20.104) through (20.109) are applied to a nonscattering medium bounded by black walls, and are integrated using a crude trapezoidal scheme, i.e., the variable absorption coefficient $k(T, g)$ is replaced by a single, constant value $\widetilde{k}_i(T)$ for the ith finite range of g spanning across $g_{i-1} < g \le g_i$. Integrating equation (20.104), and omitting the scattering terms, then reduces it to

$$\frac{dI_i}{ds} = \widetilde{k}_i(T)\Big(\bar{a}_i(T)I_b(T) - I_i\Big), \quad i = 1, \ldots, N, \tag{20.110}$$

for the N gray gases, subject to the boundary condition

$$I_{wi} = \bar{a}_i(T_w)I_b(T_w), \tag{20.111}$$

where

$$I_i = I_g(\widetilde{k}_i)(g_i - g_{i-1}). \tag{20.112}$$

The weight function $\bar{a}_i$ in equation (20.110) is

$$\bar{a}_i(T) = g_i - g_{i-1}, \tag{20.113}$$

while for the boundary condition $\bar{a}_i$ is evaluated from equation (20.108) as

$$\bar{a}_i(T_w) = \int_{g_{i-1}}^{g_i} a(T_w, T, g)\, dg(T) = \int_{g_{w,i-1}}^{g_{w,i}} dg_w(T_w) = g_{w,i} - g_{w,i-1}. \tag{20.114}$$

Thus, $\bar{a}_i$ is the ith finite range of the cumulative k-distribution evaluated at the *local* Planck function temperature (T or T_w). This is also indicated in Fig. 20-8. The $\widetilde{k}_i$ is an average value of $k(T, g)$ over the range $g_{i-1} < g \le g_i$. This is the SLW method as developed by Denison and Webb [3, 5, 86], who suggest evaluating $\widetilde{k}_i$ from a square-root average, i.e.,

$$\widetilde{k}_i(T) = \sqrt{k(T, g_{i-1})k(T, g_i)}. \tag{20.115}$$

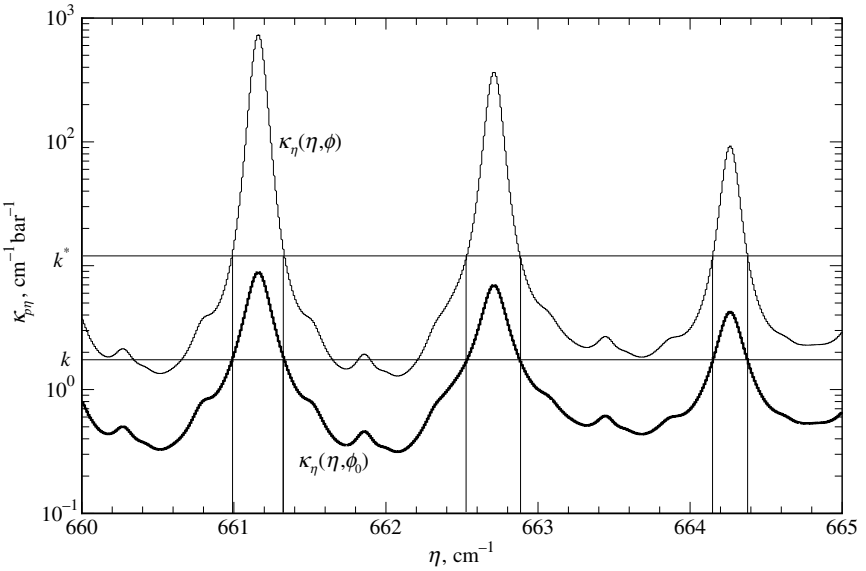

FIGURE 20-9
Extraction of k-distributions from spectral absorption coefficient data (thick line is for CO_2 in nitrogen, across a small portion of the 15 μm band, $p = 1.0$ bar, $T = 296$ K; thin line is an artificially created correlated absorption coefficient).

Inspection of equations (20.91) and (20.92) shows that the SLW scheme is simply the weighted-sum-of-gray-gases method, with absorption coefficients k_i and weights a_i evaluated from a line-by-line database. While in the development of the SLW method scattering was not considered, we may conclude that (*a*) the WSGG method may be applied to gray scattering media as well as to gray reflecting walls, and (*b*) the SLW method—or the WSGG method with its parameters based on a spectral line database—is nothing but the crudest possible implementation of the FSK method. Recently, Solovjov and coworkers [106] introduced the SLW-1 model for quick calculations with a single gray gas, which is essentially the box model of equation (20.4), but offering several ways of determining the $\widetilde{k}_1(T)$.

20.10 THE FSK METHOD FOR NONHOMOGENEOUS MEDIA

It was already noted in Section 11.9 that, like conventional band models, it is not possible to develop exact k-distributions for arbitrary absorption coefficients in nonhomogeneous media. Thus, to develop a full spectrum k-distribution method for nonhomogeneous media we will, as for narrow band k-distributions, assume that the spectral absorption coefficient is correlated or even obeys the scaling approximation. Defining a vector $\boldsymbol{\phi}$ that contains the composition variables that affect the absorption coefficient, i.e., temperature T, pressure p, and mole fractions of gases (or the volume fraction of small particles, if present) $\mathbf{x}$, the absorption coefficient may be written as

$$\kappa_\eta(\eta,\boldsymbol{\phi}) = \begin{cases} k^*_\eta(\boldsymbol{\phi}, k_\eta), & \text{correlated,} \\ k_\eta(\eta)\, u(\boldsymbol{\phi},\boldsymbol{\phi}_0), & \text{scaled,} \end{cases} \tag{20.116}$$

where $k_\eta(\eta) = \kappa_\eta(\eta,\boldsymbol{\phi}_0)$ is the absorption coefficient at a reference state $\boldsymbol{\phi}_0 = (T_0, p_0, \mathbf{x}_0)$. If the absorption coefficient is *correlated* then, at every wavenumber where $\kappa_\eta(\eta,\boldsymbol{\phi}_0)$ has one and the same value k, $\kappa_\eta(\eta,\boldsymbol{\phi})$ always also has one unique value $k^*(\boldsymbol{\phi}, k)$, as illustrated in Fig. 20-9 for a small part of a CO_2 band. If the ratio k^*_η/k_η is constant (not a function of k_η) then the absorption coefficient is *scaled*, and $u(\boldsymbol{\phi},\boldsymbol{\phi}_0)$ is called the scaling function.

For such an absorption coefficient the general radiative transfer equation (10.21) becomes

$$\frac{dI_\eta}{ds} = k_\eta^*(\boldsymbol{\phi}, k_\eta) I_{b\eta} - \left(k_\eta^*(\boldsymbol{\phi}, k_\eta) + \sigma_s\right) I_\eta + \frac{\sigma_s}{4\pi} \int_{4\pi} I_\eta(\hat{\mathbf{s}}') \, \Phi(\hat{\mathbf{s}}, \hat{\mathbf{s}}') \, d\Omega', \tag{20.117}$$

subject to the boundary condition (20.98).

Extension of the FSK method to nonhomogeneous media with correlated absorption coefficients will require k-distributions evaluated for different absorption coefficient states $\boldsymbol{\phi}$ as well as different Planck function temperatures T. It is, therefore, important to understand the relationships between these k-distributions, as reported by Modest [105].

Correlated Full Spectrum k-Distributions

For a nonhomogeneous medium a generalized full spectrum k-distribution is defined as

$$f(T, \boldsymbol{\phi}, k) = \frac{1}{I_b} \int_0^\infty I_{b\eta}(T) \, \delta\Big(k - \kappa_\eta(\eta, \boldsymbol{\phi})\Big) d\eta, \tag{20.118}$$

which is a function of temperature through the Planck function, and also of $\boldsymbol{\phi}$ through the state at which the absorption coefficient κ_η is evaluated. Similar to narrow band k-distributions Planck-function weighted k-distributions are evaluated as

$$f(T, \boldsymbol{\phi}_0, k) = \frac{1}{I_b} \int_0^\infty I_{b\eta}(T) \, \delta\left(k - \kappa_\eta(\eta, \boldsymbol{\phi}_0)\right) \frac{d\eta}{d\kappa_\eta} \, d\kappa_\eta = \frac{1}{I_b(T)} \sum_i I_{b\eta i}(T) \left| \frac{d\eta}{d\kappa_\eta} \right|_{\kappa_\eta(\eta_i, \boldsymbol{\phi}_0) = k}. \tag{20.119}$$

In this relation the summation is over all occurrences where $\kappa_\eta(\eta, \boldsymbol{\phi}_0) = k$, as illustrated in Fig. 20-9 (the absolute value signs stem from the fact that, if $d\eta/d\kappa_\eta < 0$, then also $d\kappa_\eta < 0$). Similarly, one can obtain the k-distribution for the local state $\boldsymbol{\phi}$, or

$$f(T, \boldsymbol{\phi}, k^*) = \frac{1}{I_b(T)} \sum_i I_{b\eta i}(T) \left| \frac{d\eta}{d\kappa_\eta} \right|_{\kappa_\eta(\eta_i, \boldsymbol{\phi}) = k^*}, \tag{20.120}$$

which has identical k^*–κ_η–intersection wavenumbers η_i, as also indicated in Fig. 20-9. From equation (20.116) we have

$$\left| \frac{d\kappa_\eta}{d\eta} \right|_{\kappa_\eta(\eta_i, \boldsymbol{\phi}) = k^*} = \left| \frac{dk_\eta^*}{d\eta} \right|_{k_\eta^* = k^*} = \left| \frac{dk_\eta^*}{dk_\eta} \right| \left| \frac{dk_\eta}{d\eta} \right|_{k_\eta = k} = \left| \frac{d\kappa_\eta}{d\eta} \right|_{\kappa_\eta(\eta_i, \boldsymbol{\phi}_0) = k} \frac{dk^*}{dk} \tag{20.121}$$

and, therefore,

$$f(T, \boldsymbol{\phi}, k^*) \, dk^* = f(T, \boldsymbol{\phi}_0, k) \, dk. \tag{20.122}$$

The cumulative k-distribution g is then identical for both cases, i.e.,

$$g(T, \boldsymbol{\phi}_0, k) = \int_0^k f(T, \boldsymbol{\phi}_0, k) \, dk = \int_0^{k^*} f(T, \boldsymbol{\phi}, k^*) \, dk^* = g(T, \boldsymbol{\phi}, k^*). \tag{20.123}$$

Equation (20.123) may be inverted for both k and k^*, with both being a function of the same cumulative k-distribution g. This is the definition of *correlated k-distributions*.

We will now compare correlated k-distributions evaluated for the same absorption coefficient (say, at the reference state $\boldsymbol{\phi}_0$), but for different Planck function temperatures (say, local temperature T and reference state temperature T_0). Using equation (20.123) this will result in two different cumulative k-distributions g (for medium temperature T) and g_0 (for reference state temperature T_0). Since $k(T, \boldsymbol{\phi}_0, g)$ and $k(T_0, \boldsymbol{\phi}_0, g_0)$ are both reordering the same absorption coefficient (but using different weight functions), $k(T_0, \boldsymbol{\phi}_0, g_0)$ is simply stretched in g-space, as

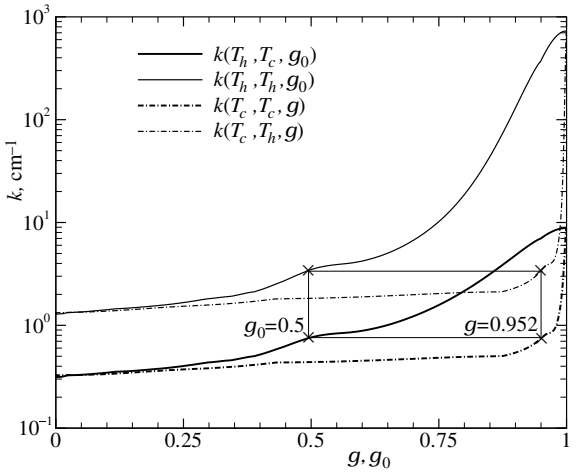

FIGURE 20-10
k-distribution equivalence of correlated absorption coefficients for varying Planck function temperatures.

shown in Fig. 20-10 (the four k-distributions in Fig. 20-10 were obtained from the two absorption coefficient distributions of Fig. 20-9, after spreading their spectral range across the entire spectrum, for Planck function temperatures of 300 K and 1000 K). The two thick lines, $k(T_h, T_c, g_0)$ and $k(T_c, T_c, g)$, are both based on the thick line in Fig. 20-9, i.e., the absorption coefficient evaluated at $T = T_c = 300$ K (second argument for k). The thick, solid line shows $k(T_h, T_c, g_0)$, implying that the Planck function is evaluated at the reference temperature, here set to $T_0 = T_h = 1000$ K (first argument for k), resulting in the reference cumulative k-distribution g_0. The thick, dash-dot line is the k-distribution for the same absorption coefficient, but evaluated at $T = T_c = 300$ K resulting in the cumulative k-distribution g. Both k-distributions have identical k-values, but different g-distributions. The thin lines in Fig. 20-10 show the equivalent two k-distributions, with the (artificial) absorption coefficient evaluated at $T_0 = T_h = 1000$ K (thin line in Fig. 20-9). Since the absorption coefficients in Fig. 20-9 are truly correlated, and since equation (20.123) can be applied at any temperature, including $T = T_0$, it is clear that $k^*(T_0, \boldsymbol{\phi}, g_0)$ is stretched in exactly the same way, or

$$k^*(\boldsymbol{\phi}, k) = k^*(T, \boldsymbol{\phi}, g) = k^*(T_0, \boldsymbol{\phi}, g_0). \tag{20.124}$$

Note that equation (20.124) is exact only for a truly correlated absorption coefficient: Fig. 20-11 shows the equivalent four k-distributions for a 10% CO_2–20% H_2O–70% N_2 mixture evaluated from the HITEMP 1995 database [17]: if the k-distributions $k(T_0 = 1000\,\text{K}, T = 300\,\text{K}, g_0)$ (Planck function evaluated at the reference temperature of 1000 K, absorption coefficient at 300 K) and $k(T_0 = 1000\,\text{K}, T_0 = 1000\,\text{K}, g_0)$ (Planck function at 1000 K, κ_η at 1000 K) were correlated, then, from equation (20.123), they should also be correlated for a Planck function evaluated at 300 K. This implies that for any value of g (here shown for $g = 0.3$) the two k-values at one Planck function temperature (here 300 K) should map to identical g_0-values at any other Planck function temperature (here $T_0 = 1000$ K). This is clearly not the case for the given carbon dioxide–water vapor mixture. On the other hand, a graph such as Fig. 20-11 can be employed to investigate how close to correlatedness an absorption coefficient actually is.

The Full Spectrum Correlated-k (FSCK) Method

A reordered RTE is obtained by multiplying equation (20.117) and boundary condition (20.98) by the Dirac-delta function $\delta(k - k_\eta)$, i.e., using the absorption coefficient at a representative reference state $\boldsymbol{\phi}_0$ introduced in equation (20.116). This is then followed by integration over the entire spectrum. Noting that

$$\int_0^\infty k_\eta^*(\boldsymbol{\phi}, k_\eta) I_{b\eta}(T)\, \delta(k - k_\eta)\, d\eta = k^*(\boldsymbol{\phi}, k) \int_0^\infty I_{b\eta}(T)\, \delta(k - k_\eta)\, d\eta,$$

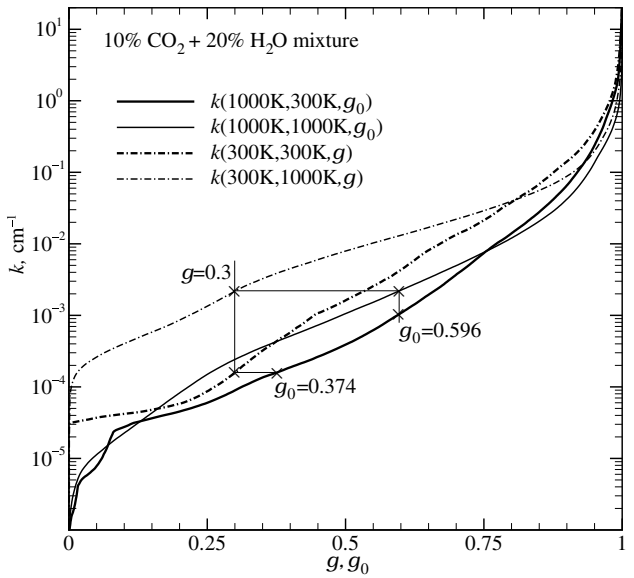

FIGURE 20-11
(Lack of) k-distribution equivalence for varying Planck function temperatures for real gas mixtures (CO_2–H_2O–N_2 mixture at different temperatures using HITEMP 1995: T_{hot} = 1000 K, T_{cold} = 300 K, uniform p = 1 bar, $x_{CO_2} = 0.1$, $x_{H_2O} = 0.2$).

because $\delta(k - k_\eta)$ is nonzero only wherever $k_\eta = k$, this leads to

$$\frac{dI_k}{ds} = k^*(\boldsymbol{\phi}, k) f(T, \boldsymbol{\phi}_0, k) I_b - \left(k^*(\boldsymbol{\phi}, k) + \sigma_s\right) I_k + \frac{\sigma_s}{4\pi} \int_{4\pi} I_k(\hat{\mathbf{s}}')\, \Phi(\hat{\mathbf{s}}, \hat{\mathbf{s}}')\, d\Omega' \tag{20.125}$$

with boundary condition

$$I_k = I_{wk} = \epsilon_w f(T_w, \boldsymbol{\phi}_0, k) I_{bw} + (1 - \epsilon_w) \frac{1}{\pi} \int_{\hat{\mathbf{n}}\cdot\hat{\mathbf{s}}<0} I_k\, |\hat{\mathbf{n}} \cdot \hat{\mathbf{s}}|\, d\Omega, \tag{20.126}$$

and

$$I_k = \int_0^\infty I_\eta\, \delta(k - k_\eta)\, d\eta. \tag{20.127}$$

Again, to facilitate integration, equations (20.125) and (20.126) are divided by a k-distribution. To allow such a division, this k-distribution must be evaluated at a constant but arbitrary Planck function reference temperature T_0 [generally chosen to be identical to the one used for the absorption coefficient in equation (20.116)]. This leads to a reordered RTE in smoothly-varying g_0-space, and is called the *Full Spectrum Correlated-k (FSCK) method*:

$$\frac{dI_g}{ds} = k^*(T_0, \boldsymbol{\phi}, g_0) \left[a(T, T_0, g_0) I_b(T) - I_g\right] - \sigma_s \left(I_g - \frac{1}{4\pi} \int_{4\pi} I_g(\hat{s}')\, \Phi(\hat{s}, \hat{s}')\, d\Omega'\right), \tag{20.128}$$

subject to the boundary condition

$$I_g = I_{wg} = \epsilon_w a(T_w, T_0, g_0) I_{bw} + (1 - \epsilon_w) \frac{1}{\pi} \int_{\hat{\mathbf{n}}\cdot\hat{\mathbf{s}}<0} I_g\, |\hat{\mathbf{n}} \cdot \hat{\mathbf{s}}|\, d\Omega. \tag{20.129}$$

Here

$$I_g = I_k / f(T_0, \boldsymbol{\phi}_0, k) = \int_0^\infty I_\eta\, \delta\left(k - \kappa_\eta(\eta, \boldsymbol{\phi}_0)\right) d\eta \Big/ f(T_0, \boldsymbol{\phi}_0, k), \tag{20.130}$$

$$g_0(T_0, \boldsymbol{\phi}_0, k) = \int_0^k f(T_0, \boldsymbol{\phi}_0, k)\, dk, \tag{20.131}$$

$$a(T, T_0, g_0) = \frac{f(T, \boldsymbol{\phi}_0, k)}{f(T_0, \boldsymbol{\phi}_0, k)} = \frac{dg(T, \boldsymbol{\phi}_0, k)}{dg_0(T_0, \boldsymbol{\phi}_0, k)}, \tag{20.132}$$

and the total intensity is evaluated from

$$I = \int_0^\infty I_\eta \, d\eta = \int_0^\infty I_k \, dk = \int_0^1 I_g \, dg_0. \tag{20.133}$$

As for a homogeneous medium, numerator and denominator in equation (20.132) are both evaluated at identical values of k, which in turn are related to g_0 through equation (20.131). It turns out that the weight function $a(T, T_0, g_0)$ is actually independent of $\boldsymbol{\phi}_0$ for a truly correlated absorption coefficient [as a consequence of equation (20.122)]. In equation (20.128) the $k^*(\boldsymbol{\phi}, k)$ of equation (20.125) has been replaced by $k^*(T_0, \boldsymbol{\phi}, g_0)$, using equation (20.124), i.e., k^* is the $k(g)$ value obtained from the k-distribution obtained for the *absorption coefficient at local conditions* and the *Planck function at reference temperature*.

The Full Spectrum Scaled-k (FSSK) Method

As for narrow band k-distributions the problem is reduced to a single k-distribution if a scaled absorption coefficient is employed. Then the k^*-term in equation (20.128) is replaced by

$$k^*(T, \boldsymbol{\phi}, g) = k(T, \boldsymbol{\phi}_0, g) u(\boldsymbol{\phi}, \boldsymbol{\phi}_0) = k^*(T_0, \boldsymbol{\phi}, g_0) = k(T_0, \boldsymbol{\phi}_0, g_0) u(\boldsymbol{\phi}, \boldsymbol{\phi}_0). \tag{20.134}$$

This then becomes the *Full Spectrum Scaled-k (FSSK) method*:

$$\frac{dI_g}{ds} = k(T_0, \boldsymbol{\phi}_0, g_0) u(\boldsymbol{\phi}, \boldsymbol{\phi}_0) \left[a(T, T_0, g_0) I_b(T) - I_g \right] - \sigma_s \left(I_g - \frac{1}{4\pi} \int_{4\pi} I_g(\hat{s}') \, \Phi(\hat{s}, \hat{s}') \, d\Omega' \right), \tag{20.135}$$

with the same boundary condition (20.129) as for the FSCK method. How to determine the scaling function for a given medium will be discussed below together with the determination of a proper reference state.

Both methods given by equations (20.128) through (20.135) are "exact" like equations (20.104) through (20.108), but are now subject to the somewhat less severe restriction of an absorption coefficient that is correlated or scaled.

The SLW Method for Nonhomogeneous Media

The SLW method of Denison and Webb can also be applied to nonhomogeneous media, including scattering media and reflecting walls. Again, integrating equation (20.128) over the ith g-range, across which $\widetilde{k}_i$ is assumed constant, this leads to

$$\frac{dI_i}{ds} = \widetilde{k}_i(T_0, \boldsymbol{\phi}) \left(\bar{a}_i(T, T_0) I_b(T) - I_i \right) - \sigma_s \left(I_i - \frac{1}{4\pi} \int_{4\pi} I_i(\hat{s}') \, \Phi(\hat{s}, \hat{s}') \, d\Omega' \right), \quad i = 1, \ldots, N, \tag{20.136}$$

subject to the boundary condition

$$I_{wi} = \epsilon_w \bar{a}_i(T_w, T_0) I_b(T_w) + (1 - \epsilon_w) \frac{1}{\pi} \int_{\hat{\mathbf{n}} \cdot \hat{\mathbf{s}} < 0} I_i \, |\hat{\mathbf{n}} \cdot \hat{\mathbf{s}}| \, d\Omega, \tag{20.137}$$

where

$$I_i = I_g(\widetilde{k}_i)(g_{0,i} - g_{0,i-1}). \tag{20.138}$$

The weight function $\bar{a}_i$ is evaluated from equation (20.132) as

$$\begin{aligned} \bar{a}_i(T, \boldsymbol{\phi}_0) &= \int_{g_{0,i-1}}^{g_{0,i}} a(T, T_0, g_0) \, dg_0(T_0, \boldsymbol{\phi}_0) \\ &= \int_{g_{i-1}}^{g_i} dg(T, \boldsymbol{\phi}_0) = g_i(T, \boldsymbol{\phi}_0) - g_{i-1}(T, \boldsymbol{\phi}_0). \end{aligned} \tag{20.139}$$

Thus, $\bar{a}_i$ is the ith finite range of the cumulative k-distribution evaluated at the *local* Planck function temperature. This transformation from reference state g_0 to local state g is indicated in Figs. 20-10 and 20-11 for a single value of g by the lower thin horizontal line. The $\widetilde{k}_i$ is an average value of $k^*(T_0, \boldsymbol{\phi}, g_0)$ over the range $g_{0,i-1} < g_0 \leq g_{0,i}$ (i.e., the value from the k-distribution evaluated from the *local* absorption coefficient and the Planck function evaluated at the *reference* temperature), and is calculated as [3,5,86]

$$\widetilde{k}_i(T_0, \boldsymbol{\phi}) = \sqrt{k_{i-1}(T_0, \boldsymbol{\phi}) k_i(T_0, \boldsymbol{\phi})}. \tag{20.140}$$

Again values of $k_i(T_0, \boldsymbol{\phi})$ are indicated for a single value of g_0 in Figs. 20-10 and 20-11, this time as points on the thin vertical line going through g_0; the top intersection for the case of $\boldsymbol{\phi} = T_h$, the lower for $\boldsymbol{\phi} = T_c$. These rather complicated relationships for $\bar{a}$ and k^* were correctly deduced by Denison and Webb [5,86], well before a solid theoretical foundation describing the interrelationships between k-distributions was developed by Modest [105].

Cumulative Wavenumber Solovjov and Webb [107–109] also introduced the concept of *cumulative wavenumber*, defined as

$$w(\boldsymbol{\phi}; k, \eta) = \int_0^{\eta} H(k - \kappa_\eta)\, d\eta, \tag{20.141}$$

where $H(k)$ is again Heaviside's unit step function, and applied it on a narrow band basis to the SLW method. Comparison with equation (11.102) shows that this is the narrow band k-distribution approach together with the N distinct gray gases of the SLW method. While Solovjov and Webb report some promising results for nonhomogeneous examples, the method is mathematically unclear and is expensive, requiring $N_{\text{nb}} \times N$ RTE evaluations, where N_{nb} is the number of narrow bands employed.

Reference State and Scaling Function

The only errors in the FSK methods for nonhomogeneous media arise from the fact that absorption coefficients of actual gases or, even more so, gas mixtures are not truly correlated. The strength of individual lines is given by equation (11.32), and is seen to be linearly proportional to the (partial) pressure of the absorbing gas, while temperature dependence consists of three parts: the rovibrational partition function, the stimulated emission term, and the influence of the lower energy state E_l. Pressure dependence and rovibrational partition function are the same for all lines and are, therefore, easily separated from spectral dependence. The stimulated emission term varies only gradually with wavenumber, causing little problem. It is the sharp growth of "hot lines" (lines with large E_l), which essentially do not contribute at moderate temperatures, that decorrelate the absorption coefficient and make scaling difficult under extreme conditions. Line broadening is also affected by pressure and temperature, but this dependence again is fairly similar for all lines. In a mixture of gases each species has its own partial pressure and its own temperature dependence, causing further degradation of the absorption coefficient's level of correlation.

Whether the assumption of a correlated absorption coefficient is to be used (FSCK), or whether the absorption coefficient is to be scaled (FSSK), the exact k *vs.* g behavior can be employed only for a single reference state $\boldsymbol{\phi}_0$. Therefore, the choice of $\boldsymbol{\phi}_0$ is very important and should be optimized for any given problem (on the other hand, the reference Planck function temperature is only a mathematical convenience, and its choice does not affect the accuracy of calculations). Modest and Zhang [104] suggest, for a medium at constant total pressure p,

$$\mathbf{x}_0 = \frac{1}{V} \int_V \mathbf{x}\, dV, \tag{20.142}$$

$$\kappa_P(T_0, \mathbf{x}_0) I_b(T_0) = \frac{1}{V} \int_V \kappa_P(T, \mathbf{x}) I_b(T)\, dV, \tag{20.143}$$

i.e., volume-averaged mole fraction and a Planck-mean temperature based on average emission from the volume.

In the correlated-k method, the $k(T, \boldsymbol{\phi}_0, g)$ are then determined, followed by evaluation of $k^* = k(T_0, \boldsymbol{\phi}, g_0)$ making the assumption of corresponding g-values (and its resulting errors). If a scaled absorption coefficient is to be used, scaling functions must be found, and Modest and Zhang [104] suggest the implicit relation

$$\int_0^\infty I_{b\eta}(T_0) \exp\left[-\kappa_\eta(\eta, \boldsymbol{\phi}) L_m\right] d\eta = \int_0^\infty I_{b\eta}(T_0) \exp\left[-\kappa_\eta(\eta, \boldsymbol{\phi}_0) u(\boldsymbol{\phi}, \boldsymbol{\phi}_0) L_m\right] d\eta, \tag{20.144}$$

i.e., forcing correct evaluation of radiation leaving from a homogeneous slab equal in width to the mean beam length, L_m. Using k-distributions this becomes

$$\int_0^1 \exp\left[-k^*(T_0, \boldsymbol{\phi}, g) L_m\right] dg = \int_0^1 \exp\left[-k(T_0, \boldsymbol{\phi}_0, g_0) u(\boldsymbol{\phi}, \boldsymbol{\phi}_0) L_m\right] dg_0. \tag{20.145}$$

Both methods are about equally efficient numerically: besides the evaluation of $k(T, \boldsymbol{\phi}_0, g)$ [needed for both methods to evaluate $k(g_0)$ and the weight function a], for a correlated absorption coefficient k-distributions must be evaluated for all states $\boldsymbol{\phi}$ (with a Planck function based on the reference temperature). For a scaled absorption coefficient, the same k-distributions are needed, but here for the evaluation of the scaling functions u. However, the scaled-k method holds two advantages over its correlated cousin: *(i)* for a poorly correlated absorption coefficient the scaling function from equation (20.145) can partially correct for this lack of correlation, and *(ii)* alternatively, a simplified scaling function can be chosen without the use of equation (20.145), thus reducing the number of cumbersome k-distribution evaluations.

Example 20.11. Consider a mixture of 10% CO_2–20% H_2O–70% N_2 (by volume) confined between two cold, black plates. The mixture is at a total pressure of 1 bar and consists of a hot, isothermal layer of fixed width $L_h = 50$ cm and a temperature of $T_h = 1000$ K, and a cold, isothermal layer ($T_c = 300$ K) of variable width L_c. Determine the radiative heat flux leaving from the cold layer using the FSCK and FSSK methods.

Solution

On a spectral basis the desired heat loss can be determined immediately from equation (14.54) as

$$q_\eta(\tau_L) = 2\pi \int_0^{\tau_L} I_{b\eta}(\tau) E_2(\tau_L - \tau)\, d\tau, \tag{20.146}$$

where we have set $J_1 = J_2 = 0$ (cold, black boundaries) and $S(\tau) = I_{b\eta}(\tau)$ (no scattering). The optical coordinate for a medium with a step in temperature is

$$\tau = \int_0^x \kappa_\eta\, dx = \begin{cases} \kappa_\eta(T_h) x, & x \le L_h, \\ \kappa_\eta(T_h) L_h + \kappa_\eta(T_c)(x - L_h), & x \ge L_h, \end{cases}$$

and $\tau_L = \tau_h + \tau_c = \kappa_\eta(T_h) L_h + \kappa_\eta(T_c) L_c$. Since $I_{b\eta}$ is constant across each layer, equation (20.146) is easily integrated to yield

$$\begin{aligned} q_\eta(\tau_L) &= 2\pi I_{b\eta}(T_h) \int_0^{\tau_h} E_2(\tau_L - \tau)\, d\tau + 2\pi I_{b\eta}(T_c) \int_{\tau_h}^{\tau_L} E_2(\tau_L - \tau)\, d\tau \\ &= 2\pi I_{b\eta}(T_h) E_3(\tau_L - \tau)\Big|_0^{\tau_h} + 2\pi I_{b\eta}(T_c) E_3(\tau_L - \tau)\Big|_{\tau_h}^{\tau_L} \\ &= 2\pi I_{b\eta}(T_h) \left[E_3(\tau_c) - E_3(\tau_c + \tau_h)\right] + \pi I_{b\eta}(T_c) \left[1 - 2E_3(\tau_c)\right]. \end{aligned}$$

If the FSK method is used to calculate the "spectral" flux q_g, the Planck function $I_{b\eta}$ must be replaced by a weighted value aI_b, and the absorption coefficient κ_η by a reordered k. Thus,

$$q_g(\tau_L) = 2a(T_h, T_0, g_0)\sigma T_h^4 \left[E_3(\tau_c) - E_3(\tau_c + \tau_h)\right] + a(T_c, T_0, g_0)\sigma T_c^4 \left[1 - 2E_3(\tau_c)\right],$$

with

$$\text{for FSCK:} \quad \tau_i = k^*(T_0, T_i, g_0)L_i, \qquad i = c \text{ or } h, \quad \text{from equation (20.128),}$$

$$\text{for FSSK:} \quad \tau_i = k(T_0, T_0, g_0)u(T_i, T_0)L_i, \quad i = c \text{ or } h, \quad \text{from equation (20.135).}$$

Before these relations can be applied, a reference temperature must be found from equation (20.143), leading to an implicit relation for T_0

$$\kappa_P(T_0)T_0^4 = \frac{L_h}{L_h + L_c}\kappa_P(T_h)T_h^4 + \frac{L_c}{L_h + L_c}\kappa_P(T_c)T_c^4,$$

which must be solved iteratively. From Fig. 11-31 we find

$$\kappa_P(1000\,\text{K}) = 0.1\,\text{bar} \times 0.231\,\text{cm}^{-1}\,\text{bar}^{-1} + 0.2\,\text{bar} \times 0.051\,\text{cm}^{-1}\,\text{bar}^{-1} = 0.033\,\text{cm}^{-1},$$

$$\kappa_P(300\,\text{K}) = 0.1\,\text{bar} \times 0.259\,\text{cm}^{-1}\ \text{bar}^{-1} + 0.2\,\text{bar} \times 0.516\,\text{cm}^{-1}\text{bar}^{-1} = 0.129\,\text{cm}^{-1};$$

for example, for $L_c = 0\,\text{cm}$ this leads to $T_0 = 1000\,\text{K}$, for $L_c = L_h = 50\,\text{cm}$ to $T_0 = 780\,\text{K}$, etc. Five k-distributions need to be determined: three of these are needed for the weight functions a, all with the absorption coefficient evaluated at T_0, but for the three Planck function temperatures T_c, T_0, and T_h. In addition, $k^*(T_0, T_h, g_0)$ and $k^*(T_0, T_c, g_0)$ are needed for the evaluation of τ_h and τ_c (FSCK) or the scaling function $u(T, T_0)$ (FSSK). For the special case of $T_0 = T_h$ ($L_c \simeq 0$), all the necessary k-distributions are shown in Fig. 20-11. For example, for $a(T_c, T_0)$ we evaluate the k-distributions $k(T_c, T_0, g)$ and $k(T_0, T_0, g_0)$, or rather $g(T_c, T_0, k)$ and $g_0(T_0, T_0, k)$ from equation (20.148). The weight function then follows as

$$a(T_c, T_0, g_0) = \frac{dg(T_c, T_0, k)}{dg_0(T_0, T_0, k)} \simeq \frac{\Delta g}{\Delta g_0}.$$

For $T_0 = 1000\,\text{K}$, this is the ratio of the slopes in Fig. 20-11 of the thin dash-dot line at $g = 0.3$ to that of the thin solid line at $g_0 = 0.596$. The equivalent value for $k^*(T_0, T_c, g_0)$ is the intersection of the thick solid line at $g_0 = 0.596$. If the FSSK method is employed, scaling functions must be evaluated from equation (20.145),

$$\int_0^1 \exp\left[-k^*(T_0, T_i, g)L_m\right] dg = \int_0^1 \exp\left[-k(T_0, T_0, g_0)u(T_i, T_0)L_m\right] dg_0, \quad i = c \text{ or } h,$$

where $L_m = 1.76(L_c + L_h)$ is the mean beam length of the layer (from Table 20.2). This implicit relation is readily solved with a Newton–Raphson technique, starting with a first guess of $u = 1$ (the correct value for $T_i = T_0$), and requiring very few iterations. After determining the two weight functions a, and the two k-distributions $k^*(T_0, T_i, g_0)$ (FSCK) or scaling functions $u(T_i, T_0)$ (FSSK), the "spectral" flux q_g can be integrated over the g-spectrum, or

$$\Psi = \frac{q(L)}{\sigma T_h^4} = \frac{1}{\sigma T_h^4}\int_0^1 q_g(\tau_L)\, dg \simeq \sum_{n=1}^{N} w_n \frac{q_g(g_n)}{\sigma T_h^4},$$

using the same quadrature as in Example 20.10. Results are shown in Fig. 20-12, and are compared with LBL values, using the HITEMP 1995 database [17] for all the calculations. It is observed that both FSCK and FSSK results coincide with LBL data for $L_c = 0$, since the methods become exact. For $L_c > 0$ the FSCK method consistently underpredicts the heat loss, with a maximum error of about 25% at intermediate L_c. The reason is that the FSCK method assumes the absorption coefficient to be correlated, i.e., that large κ_η in the hot layer (emission) line up with large κ_η in the cold layer (absorption). Since this is not the case (in particular in the presence of "hot lines"), absorption in the cold layer is overpredicted. The FSCK method can partially compensate for this lack of correlation, with a maximum error of only about 10% at intermediate L_c.

For comparison, the case of $T_h = 2000\,\text{K}$ is also included in Fig. 20-12 (T_c remains at 300 K), making hot lines much more important and, thus, further decorrelating the absorption coefficients. Maximum relative errors are seen to increase slightly to about 30% (FSCK) and 15% (FSSK).

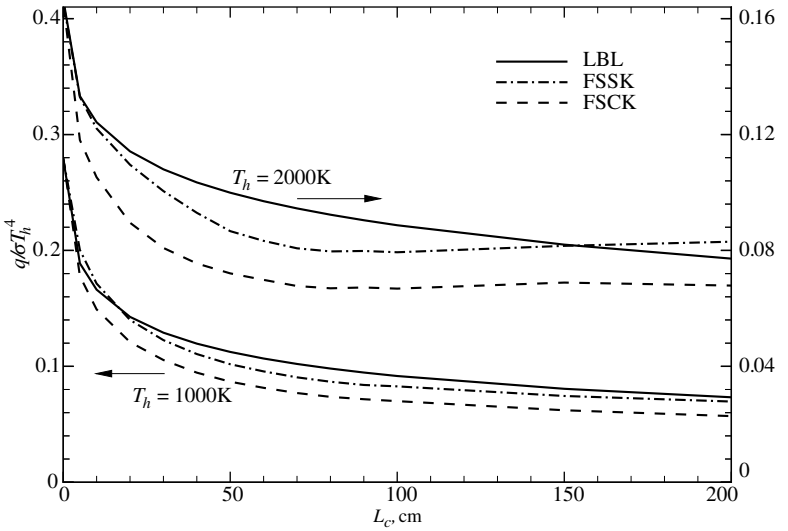

FIGURE 20-12
Heat loss from the cold column of a two-column 10% CO_2–20% H_2O–70% N_2 mixture at different temperatures (T_h = 1000 K and 2000 K, L_h = 50 cm; T_c = 300 K, L_c variable; uniform p = 1 bar, cold and black walls), from LBL, FSSK and FSCK models, all using the HITEMP 1995 database.

Note that the weight function $a(T, T_0)$ is always accompanied by the emissive power σT^4: a is, effectively, a scaling factor attached to the absorption coefficient for emission. In cold regions emission can be neglected, and the a does not need to be calculated (in the present example, cold region emission contributes < 1% to Ψ for T_h = 1000 K, and < 0.1% for 2000 K).

Note also that the present example constitutes an "acid test" for the FSK models: the step in temperature makes the gas extremely uncorrelated. More realistic situations, such as encountered in actual combustion systems, incur much smaller errors.

A realistic example was given in Section 16.9, where a scaled-up version of the much studied (but very small and, therefore, only weakly radiating) Sandia Flame D [110] was considered in the context of the spherical harmonics RTE solution methods. Figure 16-13 shows temperature and mass fraction distributions as well as the resulting radiative source term for one axial location. Comparing Monte Carlo results using LBL and FSCK spectral models (see Section 21.4) shows the FSCK approach to have excellent accuracy (in fact, the error across the entire computational domain rarely exceeds 3% of maximum $\nabla \cdot \mathbf{q}$), if only water vapor and carbon dioxide are allowed to radiate. If methane is included in the calculations, the gas mixture becomes very uncorrelated and small (methane) pockets with large errors are found (up to 40%); such errors can be avoided with higher order methods discussed later in this chapter.

20.11 EVALUATION OF *k*-DISTRIBUTIONS

The full spectrum k-distribution $f(T, k)$ and the cumulative k-distribution $g(T, k)$ are evaluated exactly as outlined in Section 11.9, except that $\delta\eta/\Delta\eta$ is replaced by $I_{b\eta}\,\delta\eta/I_b$, or

$$f(T, k_j)\,\delta k_j \simeq \sum_i \frac{I_{b\eta i}(T)}{I_b(T)} \left|\frac{\delta\eta}{\delta\kappa_\eta}\right|_i [H(k_j + \delta k_j - \kappa_\eta) - H(k_j - \kappa_\eta)]. \tag{20.147}$$

If the simple method described in Section 11.9 is used, the k-distributions can be found simultaneously for any number of temperatures T_i ($i = 1, 2, ..., I$): The relevant (i.e., contributing) part of the total spectrum is broken up into N equal subintervals $\delta\eta$, the absorption coefficient κ_η is evaluated at the center of each interval and, if $k_j \le \kappa_\eta \le k_{j+1}$, the value of each $f(T_i, k_j)\,\delta k_j$ is incremented by $I_{b\eta}(T_i, \eta_n)\,\delta\eta/I_b(T_i)$. At the end, the cumulative function $g(T, k)$ is again calculated

from equation (11.105), or

$$g(T_i, k_{j+1}) = \sum_{j'=1}^{j} f(T_i, k_{j'})\,\delta k_{j'} = g(k_j) + f(T_i, k_j)\,\delta k_j. \tag{20.148}$$

`fskdist` is the corresponding Fortran program in Appendix F that evaluates the $f(T_i, k_j)$ and $g(T_i, k_j)$ for a set of temperatures T_i and absorption coefficients k_j, as well as the $a(T_i, k_j)$. Figure 20-7 shows the full spectrum k-distributions for 10% CO_2 in nitrogen for two temperatures. For efficient integration of equation (20.109) it is desirable to have the function $a(T, g)$ as smooth as possible, which—in turn—depends on the accuracy with which the $f(T, k)$ are evaluated. Different smoothing schemes have been discussed in the original paper by Modest and Zhang [104].

As indicated earlier, assembling narrow band or full spectrum k-distributions from high-resolution databases is a very time-consuming task. First, the absorption coefficient must be calculated at fine spectral resolution for all relevant temperatures, pressures, and concentrations. This was apparently first done by Rivière and coworkers [111] for various gases, using the HITRAN 1992 database together with some proprietary French high-temperature extensions. For repeated calculations absorption coefficients may be precalculated and placed into an absorption coefficient database, such as the one by Wang and Modest [112], which is based on HITEMP 1995 [17] (H_2O and CO), and CDSD-1000 [113] for CO_2. Wang and Modest's database includes 23 temperatures (300–2500 K), 24 pressures (0.1–30 bar), and 5 concentrations, requiring about 225 GB of storage. (In its present version the database also includes several hydrocarbon species and has been updated to HITRAN 2008 and HITEMP 2010). Next, in the case of gas mixtures, the absorption coefficients of individual species are added; then the k-distribution is found from equations (20.147) and (20.148). This should be done for closely spaced δk_j. Finally, the resulting function is inverted to determine the relevant k for desired quadrature points g. Clearly, this process of assembling k-distributions is too involved to make it part of an overall heat transfer analysis, or even a pure radiation calculation. Rather, they must be available from simple correlations or from databases.

Full Spectrum *k*-Distribution Correlations

Denison and Webb [3, 86, 114] have calculated large numbers of k-distributions for water vapor and carbon dioxide, using the HITRAN92 database [103] together with the high-temperature extrapolation scheme of Hartmann and coworkers [115]. The resulting cumulative k-distributions were then presented in the form of relatively straightforward correlations for engineering use. The correlations were subsequently updated by Modest and coworkers using the then-new HITEMP 1995 database [116, 117], and one more time for CO_2 using CDSD-1000 [118], after it was recognized that HITEMP 1995 is seriously in error for CO_2 above 1000 K. The latest correlations (for atmospheric total pressure) have been reproduced in Table 20.3 (water vapor) and Table 20.4 (carbon dioxide). The cumulative k-distributions for a Planck function temperature T_P, and the absorption coefficient evaluated at gas temperature T_g, pressure $p = 1$ bar, and mole fraction x, are calculated from With $k_0 = k$ equations (20.150) and (20.151) give the cumulative k-distribution for air broadening, i.e., for small amounts of absorbing gas in air ($x \simeq 0$, accounting for collision broadening due to collisions with air molecules; see Section 11.4). If the mole fraction of the absorbing gas is substantial, self-broadening must be accounted for (collisions between two molecules of the absorbing species), resulting in a shift in g. For CO_2 this shift is negligible (since CO_2 and air molecules have roughly the same size), and $k_0 = k$. However, for water vapor the effect is quite substantial (since H_2O molecules are much smaller than air molecules), and must be accounted for. Modest and Singh [117] give a correlation for $k_0(T_g, k, x)$

TABLE 20.3
Coefficients for the full spectrum *k*-distribution of water vapor, from [117].

	l	$m \backslash n$	0	1	2	3
a_{lmn}	0	0	1.172739	–0.792337	0.45678	–6.7356E-02
		1	0.88261	3.3022	–2.048	0.394137
		2	–0.28465	1.6339	1.09924	–0.20874
		3	5.2641E-02	0.26822	–0.18706	3.5073E-02
	1	0	0.27995	0.527055	–0.43156	0.13503
		1	1.31104	–1.3535E-02	2.39465E-02	–3.7574E-02
		2	–0.61658	–8.1576E-02	0.15935	–2.2954E-02
		3	0.10234	1.70129E-02	–3.84058E-02	6.51758E-03
	2	0	8.6277E-02	0.34948	–0.20189	5.5391E-02
		1	0.31365	–1.06025	0.857	–0.17833
		2	–0.136779	0.5768	–0.48058	9.1345E-02
		3	2.007E-02	–9.727E-02	8.1344E-02	–1.14502E-02
	3	0	5.5203E-02	–9.0309E-02	0.22803	–5.04129E-02
		1	–2.64678E-02	–6.3565E-02	–0.13107	3.717E-02
		2	1.333E-02	6.7414E-02	2.5817E-02	–1.325E-02
		3	–2.5024E-03	–1.3749E-02	–1.4234E-03	1.9916E-03
b_{lmn}	0	0	–0.89871	0.539		
		1	1.0116	–0.58957		
		2	–0.48279	0.2747		
	1	0	1.0985	–5.829E-02		
		1	–1.0454	0.11542		
		2	0.4717	–5.623E-02		
	2	0	–0.22529	–6.06033E-03		
		1	0.18432	–1.6727E-02		
		2	–7.69132E-02	1.035E-02		

as

$$\log_{10}\left(\frac{k_0}{k_{\text{ref}}}\right) = \log_{10}\left(\frac{k}{k_{\text{ref}}}\right) + \sum_{l=0}^{2}\sum_{m=0}^{2}\sum_{n=0}^{1} b_{lmn}\left[\log_{10}\left(\frac{k}{k_{\text{ref}}}\right)\right]^n [x]^{m+1}\left[\frac{T_g}{T_{\text{ref}}}\right]^l. \tag{20.149}$$

$$g(T_P, T_g, x; k) = \frac{1}{2}\left[1 + \tanh\left(P(T_P, T_g, x; k)\right)\right], \tag{20.150}$$

with the function P given as

$$P(T_P, T_g, x; k) = \sum_{l=0}^{3}\sum_{m=0}^{3}\sum_{n=0}^{3} a_{lmn}\left[\frac{T_g}{T_{\text{ref}}}\right]^n \left[\frac{T_P}{T_{\text{ref}}}\right]^m \left[\log_{10}\left(\frac{k_0(T_g, k, x)}{k_{\text{ref}}}\right)\right]^l,$$
$$(T_{\text{ref}} = 1000\,\text{K}, \quad k_{\text{ref}} = 1\,\text{cm}^{-1}\text{bar}^{-1}). \tag{20.151}$$

The values for the b_{lmn} are also included in Table 20.3. As an example, results of the correlational fit (20.150) (based on the CDSD-1000 database), for a 10% CO_2–N_2 mixture at 1000 K are compared in Fig. 20-13 with the one calculated from the new HITEMP 2010 (which is based on a CDSD-1000 version), both directly or assembled from the NBKDIR database described in the following section. It is observed that the fit is generally very good for large values of k ($> 10^{-3}$ cm^{-1}, the range over which most of the heat transfer takes place in common applications). Extensive tests have shown that Planck-mean absorption coefficients and slab emissivities determined with this correlation are never in error by more than 10% for CO_2 and 8% for H_2O, respectively.

For the convenience of the reader several Fortran routines are included in Appendix F for the evaluation of equations (20.150) through (20.149). `fskdh2o` and `fskdco2` are for the correlations given by Tables 20.3 and 20.4, while `fskdh2odw` and `fskdco2dw` for the older Dennison and Webb correlations are also included in Appendix F.

TABLE 20.4
Coefficients for the full spectrum *k*-distribution of carbon dioxide, from [118].

	l	$m \backslash n$	0	1	2	3
a_{lmn}	0	0	1.85071	0.33373	0.62660	–0.12890
		1	–0.20643	–2.57690	0.30090	–0.14090
		2	0.27664	1.81420	–0.24728	0.10052
		3	–0.37435E-01	–0.37762	0.53014E-01	–0.20836E-01
	1	0	0.67523	1.25760	0.67523E-01	–0.39669E-01
		1	–0.70897	–3.07080	1.71150	–0.57694
		2	0.48493	2.04603	–1.20220	0.40510
		3	–0.98138E-01	–0.41928	0.24956	–0.84109E-01
	2	0	0.20690	0.28500	–0.48324E-01	0.15174E-01
		1	–0.39473	–0.42333	0.54095	–0.23469
		2	0.29020	0.21882	–0.34748	0.15857
		3	–0.61998E-01	–0.38629E-01	0.68728E-01	–0.32314E-01
	3	0	0.38488E-01	0.18292E-01	–0.18958E-01	0.61307E-02
		1	–0.41013E-01	–0.59115E-02	0.47118E-01	–0.23229E-01
		2	0.37740E-01	–0.30114E-01	–0.11303E-01	0.12140E-01
		3	–0.87906E-02	0.98357E-02	–0.53884E-04	–0.20604E-02

k-Distribution Databases

k-distributions may be databased in narrow band form, which can then be collected into full spectrum versions, or they may be stored directly in full spectrum form. Narrow band *k*-distributions depend only on the local gas state, i.e., $\boldsymbol{\phi} = (T, p, \mathbf{x})$, and — assuming a fixed constant pressure — can be obtained by double interpolation in temperature and mole fraction (albeit for many narrow bands). They have the additional advantage that they lend themselves better to mixing of species (as shown later in this section). Full spectrum *k*-distributions, on the other hand, also depend on the Planck function temperature, i.e., a triple interpolation is required.

As already indicated in Chapter 11, Soufiani and Taine [55] have assembled a narrow band database for H_2O and CO_2, using the HITRAN 1992 database together with some proprietary French high-temperature extensions, which includes narrow band *k*-distributions for atmospheric pressure and 16 temperatures (EM2C database). There are 17 narrow bands for CO_2 (ranging in width from 100–300 cm^{-1}), and 44 for H_2O (50–500 cm^{-1} widths), each containing 7 Gauss-Lobatto quadrature points. A more voluminous high-accuracy narrow band database was generated by Wang and Modest [112], using the absorption coefficients described earlier in this section. They broke up the spectrum into 248 narrow bands (10–250 cm^{-1} widths), common to all species, *(i)* to ensure that taking a constant Planck function across each band causes < 0.5% error, and *(ii)* to allow for accurate mixing of the species. The database covers 23 temperatures (300–2500 K) and 24 pressures (0.1–30 bar), and each *k*-distributions is given for nth order nested quadrature schemes: the (variable) nth order guarantees 0.5% accuracy, but the nesting allows the use of lower orders (with fewer quadrature points). The latest version of this database, extended to five species ($CO_2, H_2O, CO, CH_4, C_2H_4$), and higher temperatures and pressures, and updated to HITEMP 2010, is contained in the NBKDIR database. Both the EM2C and NBKDIR databases are included in Appendix F.

Full spectrum *k*-distributions from narrow band data are assembled from narrow band data using the definition of the cumulative *k*-distribution,

$$g(T_P, \boldsymbol{\phi}_0, k) = \int_0^k f(T_P, \boldsymbol{\phi}_0, k)\, dk = \frac{1}{I_b} \int_0^\infty I_{b\eta}(T_P) H\left(k - \kappa_\eta(\boldsymbol{\phi}_0)\right) d\eta$$
$$= \sum_{j \in [\text{all NB's}]} \frac{I_{bj}}{I_b} g_j(\boldsymbol{\phi}_0, k), \tag{20.152}$$

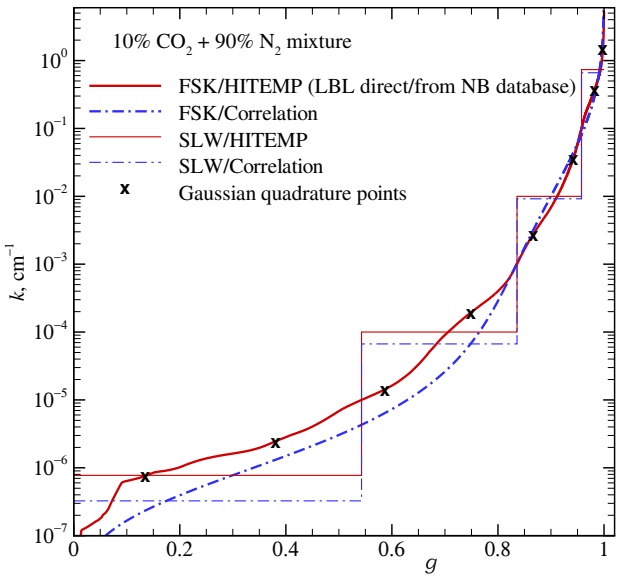

FIGURE 20-13
Planck-function-weighted cumulative k-distributions for 10% CO_2 in nitrogen for gas and Planck function temperatures of 1000 K, as evaluated from the HITEMP database and the correlation by Modest and Mehta.

where H is the Heaviside step function, and I_{bj} is the Planck function integrated over the narrow band:

$$I_{bj} = \int_{\Delta\eta_j} I_{b\eta}\, d\eta. \tag{20.153}$$

A collection of full spectrum k-distributions is included in the spectral module of Pal *et al.* [119]. This database covers the same temperature and pressure ranges as the Wang and Modest narrow band database, as well as their nested quadrature scheme.

Example 20.12. Reconsider Example 20.9, i.e., the heat loss from an isothermal slab at $T = 1000$ K, but here consisting of a 90% N_2–10% CO_2 (by volume) binary gas mixture. Calculate the heat loss from this slab using the FSK and SLW methods, employing both the HITEMP database and the correlation of Modest and Mehta [118].

Solution
For a homogeneous medium without scattering the FSK's radiative transfer equation, equation (20.104), reduces to

$$\frac{dI_g}{ds} = k(I_b - I_g), \tag{20.154}$$

subject to the cold-wall boundary condition of $I_g = 0$ at both walls. Since the walls are cold no a-function is needed and only one k-distribution must be obtained, either *(i)* directly from the HITEMP 2010 database using the Fortran program `fskdist` from Appendix F, *(ii)* assembling it from a narrow band database, such as the EM2C database [55] or the one by Wang and Modest [112] (the latter employed here), or *(iii)* from the Modest and Mehta correlation using subroutine `fskdco2`. All three distributions are shown in Fig. 20-13, with the k-distribution obtained from the narrow band database being indistinguishable from the exact direct calculation. The solution to the spectral equation (20.154) is, as in Example 20.9

$$q_g(L) = \sigma T^4 \left[1 - 2E_3(kL)\right],$$

and the total, nondimensional heat flux becomes,

$$\Psi = \frac{q}{\sigma T^4} = \int_0^1 \left[1 - 2E_3(kL)\right] dg \simeq \sum_{n=1}^{N} w_n \left[1 - 2E_3\Big(k(g_n)L\Big)\right],$$

where the integral is evaluated through an N-point numerical quadrature (with quadrature points g_n and weights w_n). Usually $N \simeq 10$ gives accuracies better than 1% if the quadrature scheme is chosen

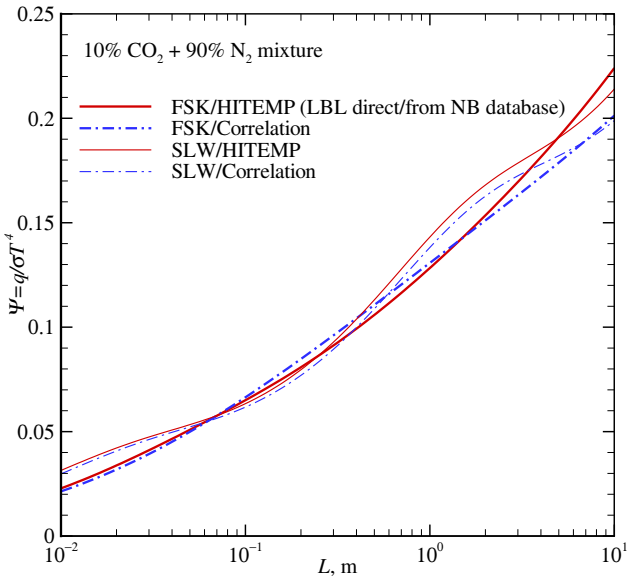

FIGURE 20-14
Heat loss from an isothermal slab of 10% CO_2 in nitrogen at $T = 1000$ K, as evaluated from the LBL, FSK, and SLW models.

wisely. Since k-values generally vary over several orders of magnitude, and since the larger k-values tend to have a larger impact on the solution, quadrature points should move closer together for larger values of k and g. The Gauss–Lobatto quadrature scheme [120] has probably been the most popular for this purpose. Another scheme, the mth order Gaussian quadrature of moments [120], is somewhat more flexible, because, depending on the order m, the spacing of quadrature points can be controlled. We will here use an eight-point, third order Gaussian quadrature of moments, whose quadrature points have been obtained from a Numerical Recipes [121] routine and are included in Fig. 20-13. Results are shown in Fig. 20-14 and are seen to virtually coincide with line-by-line results: for a homogeneous medium the FSK methods are exact and any discrepancies are due to quadrature errors (for the LBL as well as the FSK quadratures). Using the k-distribution correlation of Modest and Mehta gives very respectable results, slightly overpredicting the LBL data for intermediate L, with a maximum error of about 5% in that range. For large L the correlation would be expected to underpredict the heat loss, since the fit underpredicts small k-values (see Fig. 20-13); indeed, Fig. 20-14 shows the correlation to be about 10% in error for $L = 10$ m.

For the SLW approach four g-ranges have been chosen, namely ranges (based on the LBL k-distribution) with $k < 10^{-5}\,\text{cm}^{-1}$ (and a lower limit taken as k at $g = 0.01$), $10^{-5}\,\text{cm}^{-1} < k < 10^{-3}\,\text{cm}^{-1}$, $10^{-3}\,\text{cm}^{-1} < k < 10^{-1}\,\text{cm}^{-1}$, and $k > 10^{-1}\,\text{cm}^{-1}$ (and the actual maximum k as the upper limit), and the same g-values are employed for the k-distribution correlation. The $\widetilde{k}$-values are then calculated from equation (20.115), resulting in almost identical values for the HITEMP and correlation distributions for large g (where the correlation is very accurate), and $k_{\text{HITEMP}} > k_{\text{correlation}}$ for $g < 0.8$ (where the correlation underpredicts actual k-values); see Fig. 20-13. Consequently, both SLW simulations yield similar results for small L (where large k dominate), with increasing underprediction by the correlation as L increases. The SLW results oscillate slightly around the LBL data, indicating that the accuracy of the SLW method depends mostly on a wise choice of g-ranges (with different optima for different slab widths L).

Full Spectrum *k*-Distributions for Mixtures

Similar to narrow band k-distributions, variable mixtures of different absorbing gases, and perhaps the addition of nonscattering particles, such as soot, pose no additional difficulty, in principle, because the absorption coefficient of all species can simply be added up. In practice, however, because of the considerable effort involved, one would like to precalculate and database all necessary k-distributions, before embarking on detailed heat transfer calculations. Because of the infinite number of possible mixture concentrations this would quickly become a Herculean task. Therefore, it would be highly desirable to build full spectrum k-distributions

for arbitrary gas mixtures from relatively few distributions databased for individual species. Exact construction of such k-distributions is possible as long as the absorption coefficient of each species is unaffected by the other species (i.e., collisions with varying amounts of other species have no impact on line broadening), but the integral in equation (20.109) or (20.133) becomes a multiple integral (one for each species) [6, 8, 12]. Numerical effort would increase from N RTE evaluations (number of quadrature points), to N^M RTE evaluations in a mixture of M absorbing species, quickly eliminating the advantages of the FSK methods. Mixing full spectrum k-distributions is essentially identical to the narrow band mixing case described in Section 11.9, equations (11.111) through (11.126) and, therefore, the discussion here will be very brief.

Variable Mole Fraction of a Single Absorbing Gas As in equation (11.111) we consider an absorption coefficient that is linearly dependent on its partial pressure, i.e., a gas whose line broadening is unaffected by its own partial pressure, or

$$\kappa_{x\eta}(T, p, x; \eta) = x\kappa_\eta(T, p; \eta). \tag{20.155}$$

Going through the identical steps as for narrow bands, we obtain

$$f_x(T_P, T_g, p, x; k_x) = \frac{1}{x} f(T_P, T_g, p; k_x/x), \tag{20.156}$$

and

$$g(T_P, T_g, p; k) = g_x(T_P, T_g, p, x; k_x), \tag{20.157}$$

where the arguments, from the definition of full spectrum k-distributions, now include a Planck function temperature T_P. As before, the k *vs.* g behavior is independent of mole fraction, with k_x smaller than $k(g)$ by the multiplicative factor x for any value of g. Equation (20.156) also implies that the nongray stretching function a remains unaffected if the mole fraction is changed [see equations (20.108) and (20.132)].

Single Absorbing Gas Mixed with Gray Medium Identical to its narrow band equivalent, if

$$\kappa_{p\eta}(T, p, \kappa_p; \eta) = \kappa_\eta(T, p, \eta) + \kappa_p, \tag{20.158}$$

it follows that

$$f_p(T_P, T_g, p, \kappa_p; k_p) = f(T_P, T_g, p; k = k_p - \kappa_p) \tag{20.159}$$

$$g(T_P, T_g, p; k) = g_p(T_P, T_g, p, \kappa_p; k_p = k + \kappa_p). \tag{20.160}$$

As for narrow bands, for the same g the k-values are displaced by a constant additive factor κ_p and, as for the variable mole fraction case, equation (20.159) implies that the weight factor a remains unaffected.

Superposition of *k*-Distributions Under certain conditions it may be acceptable to neglect overlap of spectral lines from different species. For example, Bansal and coworkers [122] have shown that radiation in air plasma is dominated by few widely spaced electronic excitation lines of monatomic N and O. Thus, if we consider a mixture of M different absorbing gases, whose absorption coefficients do not overlap each other anywhere across the entire spectrum, then the k-distributions of the individual species are unaffected by the others, i.e., the spectral locations where $k = \kappa_{m\eta}$ for the mth species remain unaffected by the other gases, and

$$f_{\text{mix}}(T_P, T_g, p; k) = \sum_{m=1}^{M} f_m(T_P, T_g, p; k), \tag{20.161}$$

where the f_m are the k-distributions of the individual species. Keeping in mind that, for nonoverlapping absorption coefficients, each species must have large parts of the spectrum with $\kappa_{m\eta} \equiv 0$,

we integrate equation (20.161) as

$$1 - g_{\text{mix}}(T_P, T_g, p; k) = \int_k^\infty f(T_P, T_g, p; k)\, dk = \sum_{m=1}^{M} \int_k^\infty f_m(T_P, T_g, p; k)\, dk = \sum_{m=1}^{M} \Big(1 - g_m(T_P, T_g, p; k)\Big)$$

or

$$g_{\text{mix}}(T_P, T_g, p; k) = \sum_{m=1}^{M} g_m(T_P, T_g, p; k) - M + 1. \tag{20.162}$$

Therefore, the cumulative k-distribution for a nonoverlapping mixture is constructed by simply adding up the individual components. Note that $1 - g_m$ is the (Planck function weighted) part of the spectrum where $\kappa_{m\eta} > 0$ and, thus, their sum can never exceed unity.

***k*-Distributions for Random Overlap** As pointed out by Taine and Soufiani [123], there is no physical reason why there should be any significant correlation between the spectral variation of absorption coefficients of different gas species. If one treats the absorption coefficients of the M species as statistically independent random variables of wavenumber, the k-distributions are said to be *statistically uncorrelated*. Using such an argument, Solovjov and Webb [12] postulated that the cumulative k-distributions are multiplicative, or

$$g_{\text{mix}}(T_P, T_g, p; k) = g_1(T_P, T_g, p; k) \times g_2(T_P, T_g, p; k) \times \ldots = \prod_{m=1}^{M} g_m(T_P, T_g, p; k). \tag{20.163}$$

Statistically Uncorrelated Gas Mixtures Taine and Soufiani [123] argued that, if the M species in a gas mixture are statistically uncorrelated, then their transmissivities should be multiplicative, i.e.,

$$\overline{\tau}_{\text{mix}} = \prod_{m=1}^{M} \overline{\tau}_{\eta,m}, \tag{20.164}$$

and this was shown to be true on a narrow band basis by comparison with LBL calculations (see [123] as well as Fig. 11-18). Based on equation (20.164) Modest and Riazzi [124] developed the narrow band mixing scheme in Section 11.9, equations (11.121) through (11.126). The same argument can also be made at the full spectrum level. Defining a full spectrum transmissivity as

$$\overline{\tau}(T, L) = \frac{1}{I_b} \int_0^\infty I_{b\eta}(T) e^{-\kappa_\eta L}\, d\eta, \tag{20.165}$$

we can manipulate this expression, using the definition of the Dirac-delta function given by equation (11.99), to obtain

$$\begin{aligned}
\overline{\tau}(T, L) &= \frac{1}{I_b} \int_{\eta=0}^\infty I_{b\eta}(T) e^{-\kappa_\eta L} \int_{k=0}^\infty \delta(k - \kappa_\eta)\, dk\, d\eta \\
&= \int_{k=0}^\infty e^{-kL} \frac{1}{I_b} \int_{\eta=0}^\infty I_{b\eta}(T) \delta(k - \kappa_\eta)\, d\eta\, dk \\
&= \int_{k=0}^\infty e^{-kL} f(T, k)\, dk = \int_{g=0}^1 e^{-kL} dg,
\end{aligned} \tag{20.166}$$

which is identical to equation (11.122). Assuming equation (20.164) to hold, the analysis is identical to the narrow band case, leading to

$$g_{\text{mix}}(T, k_{\text{mix}}) = \int_{g_1=0}^1 \int_{g_2=0}^1 H[k_{\text{mix}} - (k_1 + k_2)] dg_2\, dg_1 = \int_{g_1=0}^1 g_2(k_{\text{mix}} - k_1)\, dg_1 \tag{20.167}$$

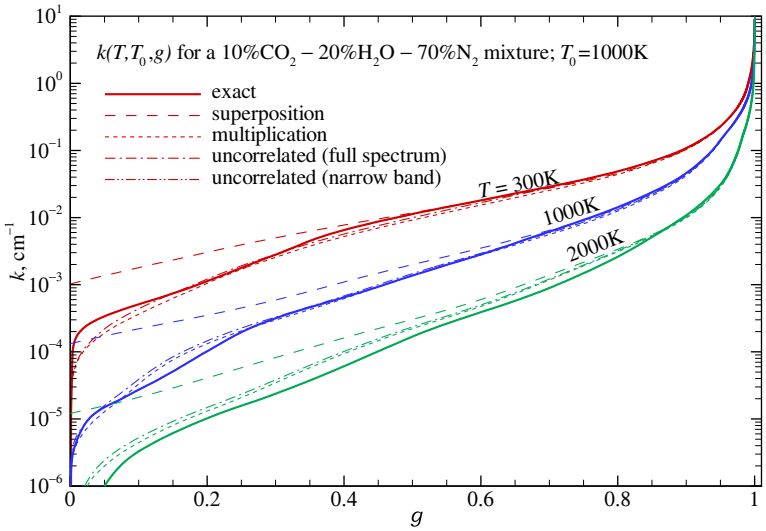

FIGURE 20-15
Full-spectrum k-distributions for a 10% CO_2–20% H_2O–70% N_2 mixture without soot, for various Planck function temperatures (absorption coefficient evaluated at 1000 K).

for a two-component mixture, and

$$g_{\text{mix}}(T, k_{\text{mix}}) = \int_{g_1=0}^{1} .... \int_{g_M=0}^{1} H[k_{\text{mix}} - (k_1 + ... + k_M)]dg_M....dg_1 \tag{20.168}$$

for a mixture of M species, but now using full spectrum k-distributions.

Mixtures of Gases and Particles If the particles are assumed to be gray, equation (20.160) applies directly, i.e., the full spectrum k-distribution is found for the gas mixture as $g(T_P, T_g, p; k)$. The mixture's k-distribution is then determined by simply adding the particles' constant absorption coefficient κ_p for every value of g. If the particles' absorption coefficient is nongray, mixing *must* be performed at the narrow band level, assuming that $\kappa_{p\eta} = \kappa_{p,j}$ is constant across narrow band range j. Any of the narrow band schemes described in Section 11.9 may be employed. For example, with the Modest and Riazzi [124] model, equation (11.126), for each narrow band:

$$g_{\text{mix},j}(\boldsymbol{\phi}_0, k) = \int_{g_1=0}^{1} .... \int_{g_M=0}^{1} H[k_{\text{mix}} - (k_1 + ... + k_M + \kappa_{p,j})]dg_M....dg_1, \tag{20.169}$$

where $\boldsymbol{\phi}_0$ is the (reference) state at which the absorption coefficients of the gas are evaluated, and $\kappa_{p,j}$ has been added to the argument inside the Heaviside function according to equation (11.119). The full spectrum k-distribution is then determined from

$$g(T_P, \boldsymbol{\phi}_0, k) = \sum_{j\in[\text{all NB's}]} \frac{I_{bj}}{I_b}(T)\, g_{\text{mix},j}(\boldsymbol{\phi}_0, k). \tag{20.170}$$

Test Calculations A real gas mixture will, of course, always have some spectral overlap, and the absorption coefficient will never be quite statistically uncorrelated. Figure 20-15 shows the case of a 10% CO_2–20% H_2O–70% N_2 mixture, with the absorption coefficient evaluated at a reference temperature of $T_0 = 1000$ K. Full-spectrum k-distributions were evaluated for a number of Planck function temperatures by five methods: *(i)* the exact k-distribution for the mixture was found from the HITEMP database [2], *(ii)* individual k-distributions were found for CO_2 and H_2O, and a mixture distribution was found from equation (20.162) (superposition, neglecting overlap), *(iii)* similarly a mixture distribution was determined from equation (20.163) (random overlap), and *(iv)* the Modest and Riazzi full spectrum mixing of equation (20.167) was

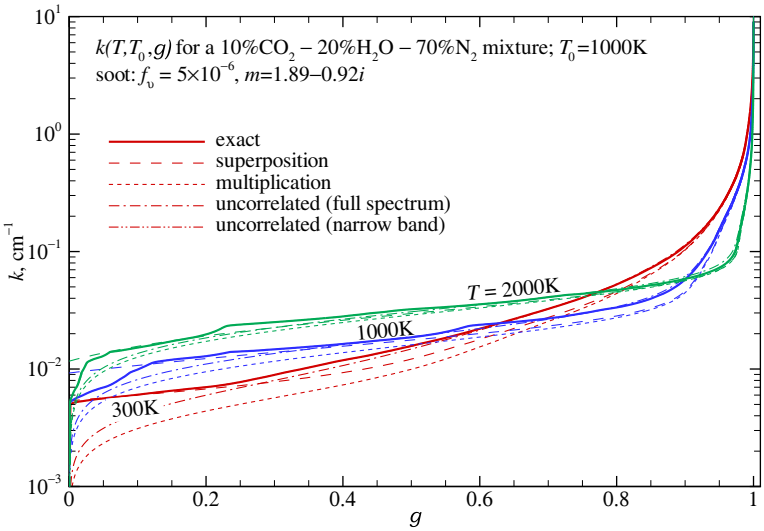

FIGURE 20-16
Full-spectrum *k*-distributions for a 10% CO_2–20% H_2O–70% N_2 mixture with soot, for various Planck function temperatures (absorption coefficient evaluated at 1000 K).

employed; finally, *(v)* mixing was done on a narrow band basis, using the Modest and Riazzi scheme, equation (11.125), after which the full spectrum distribution was obtained from equation (20.152). Figure 20-15 shows that all approximate methods predict the correct distribution very well for large values of k. For very small values of k substantial overlap between species is to be expected, and the superposition method fails. The product method, on the other hand, appears to give good accuracy for nearly all conditions. The uncorrelated transmissivity scheme of Modest and Riazzi, when applied on a full-spectrum basis, displays good accuracy similar to the multiplication scheme, but outperforms it for very small values of k. When applied at the narrow band level, the uncorrelated mixing rule is virtually exact (lines become indistinguishable). Note that the $k(g)$ levels decrease with temperature, because of the strong effect of the rotational band of water vapor at long wavelengths, favoring low temperatures. When applied to evaluate the radiative source within a homogeneous slab [124] (for which directly calculated *k*-distributions return exact answers), the multiplication scheme incurred errors of 4% and 5% when mixing on narrow band and full spectrum levels, respectively, while the Modest and Riazzi mixing scheme resulted in 0% and 1% error, respectively. These findings were corroborated by Demarco et al. [125], who tested several spectral models (WSGG with parameters from Smith and coworkers [71]; statistical narrow band using the EM2C database [55]; and SLW and FSCK using the EM2C database [55] to assemble full-spectrum *k*-distributions) as well as mixing models (superposition, multiplication and uncorrelated mixing), and found that the combination of FSCK with the Modest and Riazzi mixing scheme gave the most accurate results.

The methods were also tested for gas mixtures with nonscattering soot, using equation (12.123) with a volume fraction of $f_v = 5 \times 10^{-6}$ and a refractive index $m = 1.89 - 0.92i$. Clearly, none of the first four methods should work terribly well, since strong overlap is assured, and the soot absorption coefficient is anything but random. That Fig. 20-16, nonetheless, shows reasonable agreement is a consequence of the fact that the soot *k*-distribution dominates the mixture, especially at high Planck function temperatures (favoring short wavelengths with strong soot and weak gas radiation). For the same reason $k(g)$ values now *increase* with temperature. None of the assumptions underlying scheme *(v)* are violated, and it again displays superb accuracy (with its line indistinguishable from the exact one).

Example 20.13. Repeat Example 20.11 using individual *k*-distributions for CO_2 and H_2O obtained from the correlations in Tables 20.3 and 20.4, together with the superposition, multiplication, and uncorrelated methods.

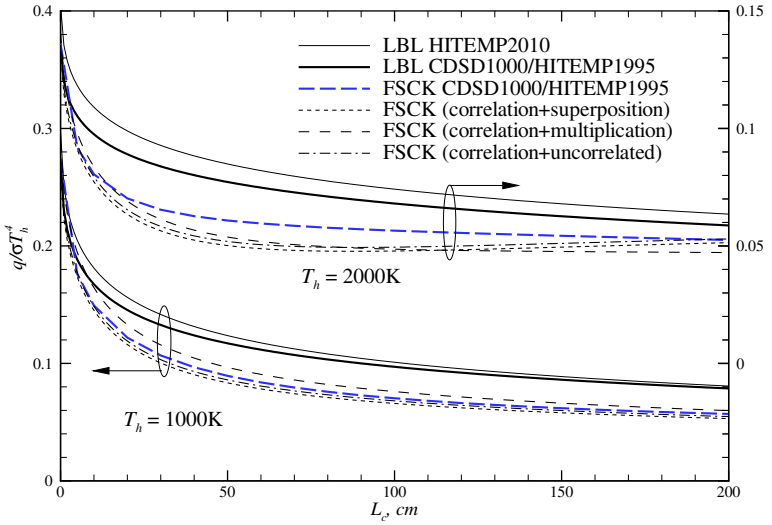

FIGURE 20-17
Heat loss from the cold column of a two-column 10% CO_2–20% H_2O–70% N_2 mixture at different temperatures (T_h = 1000 K and 2000 K, L_h = 50 cm; T_c = 300 K, L_c variable; uniform p = 1 bar, cold and black walls), from LBL and FSCK models; LBL from HITEMP 2010 database and CDSD1000(CO_2)/HITEMP 1995(H_2O); FSCK using individual k-distributions for CO_2 from CDSD1000 and the Modest and Singh correlation [117]/H_2O from HITEMP 1995 and the Modest and Mehta correlation [118].

Solution

The solution proceeds identically to that of Example 20.11, except that the five k-distributions are evaluated differently.

Subroutines `fskdco2` and `fskdh2o` are provided in Appendix F to calculate the individual k-distributions for CO_2 and H_2O, respectively. Combined k-distributions are then obtained using program `fskdistmix`, choosing the proper mixing option, i.e., applying equations (20.162) (superposition), (20.163) (multiplication), or (20.167) (uncorrelated mixture). Results from the FSCK method are shown in Fig. 20-17 and are compared with LBL results, all using the identical spectroscopic databases (CDSD-1000 for CO_2 and HITEMP 1995 for H_2O) that were used for the correlations given in Tables 20.3 and 20.4. As was observed in Fig. 20-12 for this problem the FSCK scheme is less accurate than FSSK, giving fair answers for a hot medium temperature of T_h = 1000 K, but rather poor answers for T_h = 2000 K. For T_h = 1000 K the agreement between the directly calculated FSCK and those from the correlations is good for all three mixing schemes, with—as expected—the uncorrelated mixture scheme of equation (20.167) giving the best results. At T_h = 2000 K there is a considerable difference between directly calculated FSCK results and those from the correlations, indicating that one or both of the correlations loses accuracy (probably the H_2O correlation, which—due to neglect of T_P-dependence—becomes inaccurate for the small values of k important here). For both cases the superposition method returns the least-accurate answers and should be avoided. While the uncorrelated-mixture approach always is the most accurate, the multiplication scheme returns respectable results with less effort and, given the inaccuracies of the correlations, may be sufficient.

The exiting flux for this example was also calculated using the NBKDIR database given in Appendix F, i.e., the FSCK result compiled from databased narrow band k-distributions for CO_2 and H_2O mixed at the narrow band level with the Modest and Riazzi (uncorrelated mixture) scheme. Those results are virtually indistinguishable from the directly calculated FSCK line in Fig. 20-17, attesting to the accuracy of this mixing model.

Also shown in Fig. 20-17 are LBL results obtained with the latest HITEMP 2010 database [2] (for both CO_2 and H_2O) yielding a noticeably higher heat flux at T_h = 2000 K, due to the inclusion of many more high-temperature lines for water vapor. On the other hand, the LBL flux given in Fig. 20-12 is quite a bit larger for the higher temperature, in this case due to errors in HITEMP 1995 that manifest themselves for $T > 1000$ K (incorrectly strong high-temperature lines for CO_2, as discussed in Chapter 11).

20.12 HIGHER ORDER *k*-DISTRIBUTION METHODS

The FSK method is exact for homogeneous media, and also for materials with a "correlated" absorption coefficient, i.e., media where spectral minima and maxima always occur at the same wavenumbers everywhere inside the spatial domain. We noticed that this premise is violated in media with large temperature disparities, because of the rise of "hot lines" in high-temperature regions (spectral lines from elevated vibrational energy levels, which are not present in colder gas). In such cases the gas becomes "uncorrelated" and the FSK method breaks down, and likewise the SLW and ADF schemes (see Fig. 20-12). The problem is exacerbated if the medium also contains strong concentration changes, with spectral lines of one species (say, a hydrocarbon fuel, such as methane) in one part of the domain, and other species (such as combustion products CO_2 and H_2O) elsewhere. There is no reason to believe spectral lines of two different gas species would occur at the same wavenumbers, and the gas mixture becomes uncorrelated. In fact, this uncorrelatedness between species is the basis for some of the *k*-distribution mixing models of the previous section.

The accuracy of the FSK methods for nonhomogeneous media (and similarly, that of the SLW and ADF methods) can be improved by breaking up the absorption coefficient of the gas into spectral scales or groups, each of which is assumed to be correlated or scaled, and solving separate RTEs for each scale or group. This was first recognized by researchers in France for the case of strong temperature inhomogeneities. They grouped *spectral lines* according to the values of their lower level energies into a number of "fictitious gases," first for narrow band *k*-distributions [10, 111] (cf. Section 11.9), and then for the ADF scheme, calling it the ADFFG (absorption distribution function fictitious gases) method [8].

While grouping spectral lines according to their lower level energies is straightforward, it does have the disadvantage that the absorption coefficients of the different scales overlap. The ADFFG treats this overlap exactly, by evaluating conditional probability density functions (i.e., the joint event that $k_1 = \kappa_{1\eta}$ while also $k_2 = \kappa_{2\eta}$, etc.). This makes the method uneconomical beyond two or three fictitious gases, requiring N^M RTE evaluations, where M is the number of fictitious gases or scales and N is the number of gray gases for each scale. Zhang and Modest [14] also used this scheme to extend the validity of the FSK approach, calling it the "multiscale" MSFSK method. However, recognizing that overlap between scales (separate species or groups of species, or a single gas broken up into temperature scales) tends to be relatively minor, they opted for an approximate approach to determine overlap, arguing that a small error in overlap treatment would result in near-negligible overall error. In this way the MSFSK method requires only $N \times M$ RTE evaluations, making it much more economical than the ADFFG approach. Zhang and Modest applied their method to gas mixtures without wall emission, using both the FSSK and FSCK schemes. They noted that—even for the worst-possible temperature steps—already a two-scale model returns near-exact answers with little difference between the scaled FSSK and the correlated FSCK. Since the FSCK is somewhat more straightforward to apply, only this scheme was pursued in further work. Wang and Modest [126] extended the MSFSK scheme to allow determination of the required *k*-distributions from narrow band databases, such as the one by Wang and Modest [112], and, finally, the method was further developed to allow for gray surface emission as well as for nongray particles [127, 128].

A somewhat different approach to improve the accuracy of the FSK method in the presence of strong temperature disparities is the "multigroup" or MGFSK approach [15, 16], in which *spectral positions* are grouped together according to their absorption coefficient's temperature and pressure dependence (i.e., the contributions from *all* spectral lines at *one* spectral location, as opposed to *individual* lines contributing to *all* wavenumbers in the multiscale/fictitious gas approach). Since there is no overlap between spectral groups, there is no need to evaluate an overlap factor with the presumption of uncorrelatedness among scales (somewhat questionable for lines from the same species). The method also requires only $N \times M$ RTE evaluations, but

without additional approximations, and was shown to reach line-by-line accuracy with as few as $N = 4$ spectral groups.

Recently, Pal and coworkers [129,130] combined the advantages of the multigroup approach (breaking up the absorption coefficient of a single species according to temperature behavior, without overlap issues between groups), with those of the multiscale scheme (treating different species or groups of species as separate scales, exploiting their uncorrelatedness to accurately evaluate overlap effects). They generated a four-group narrow band database for the two most important species (H_2O and CO_2), which can be used for four-group simulations or combined for two-group and single-group calculations, and it can be employed in conjunction with Wang and Modest's [112] narrow band database for other species.

For illustrative purposes we will present here only the (relatively) simple case of the MSFSK approach applied to a gas mixture without wall emission [126]. Readers interested in gas–particulate mixtures and/or wall emission should consult [127, 128], and those striving for the greatest accuracy obtainable by the hybrid multigroup–multiscale scheme are referred to [129,130].

If one separates the contributions to κ_η from the M scales (such as component gases, or groups of species) and breaks up the radiative intensity I_η accordingly, i.e.,

$$\kappa_\eta = \sum_{m=1}^{M} \kappa_{m\eta}, \quad I_\eta = \sum_{m=1}^{M} I_{m\eta}, \tag{20.171}$$

then the RTE equation (20.97) (without particle absorption and scattering) is transformed into M component RTEs, one for each species or scale. For each scale this leads to

$$\frac{dI_{m\eta}}{ds} = \kappa_{m\eta}(\boldsymbol{\phi}) I_{b\eta} - \kappa_\eta(\boldsymbol{\phi}) I_{m\eta} +, \quad \text{for } m = 1, \ldots, M. \tag{20.172}$$

Physically, the intensity $I_{m\eta}$ for the mth scale is due to emission from the mth species but subject to absorption by all species.

If there is no particle or wall emission present in the medium, the spectral locations where κ_η contributes to the absorption of $I_{m\eta}$ (i.e., absorption by all the gas scales) are only those wavenumbers for which $\kappa_{m\eta}$ is nonzero. Therefore, the overlap region is only a subset of those wavenumbers with $\kappa_{m\eta} \neq 0$, across which absorption from other gases occurs as well. The MSFSK formulation takes advantage of the fact that the overlap regions for each scale are relatively small compared to the total emission/absorption spectrum of each scale.

In the absence of wall emission, equation (20.98) for scale m can be written as

$$I_{m\eta} = I_{wm\eta} = (1 - \epsilon_w) \frac{1}{\pi} \int_{\hat{\mathbf{n}} \cdot \hat{\mathbf{s}} < 0} I_{m\eta} \, |\hat{\mathbf{n}} \cdot \hat{\mathbf{s}}| \, d\Omega, \tag{20.173}$$

where $I_{wm\eta}$ is the spectral intensity leaving the enclosure wall, due to diffuse, gray reflection.

We now apply the FSK scheme to the RTE of each scale: First equation (20.172) is multiplied by Dirac's delta function $\delta(k_m - \kappa_{m\eta}(\boldsymbol{\phi}_0))$, followed by division with

$$f_m(T_0, \boldsymbol{\phi}_0, k_m) = \frac{1}{I_b(T_0)} \int_0^\infty I_{b\eta}(T_0) \, \delta\left(k_m - \kappa_{m\eta}(\boldsymbol{\phi}_0)\right) d\eta, \tag{20.174}$$

where $\boldsymbol{\phi}_0$ and T_0 refer to a reference state. The resulting equation is then integrated over the entire spectrum, leading to

$$\frac{dI_{mg}}{ds} = k_m a_m I_b - \lambda_m I_{mg}, \quad \text{for } m = 1, \ldots, M, \tag{20.175}$$

where

$$I_{mg} = \int_0^\infty I_{m\eta}\,\delta\left(k_m - \kappa_{m\eta}(\boldsymbol{\phi}_0)\right)\,d\eta \Big/ f_m\left(T_0, \boldsymbol{\phi}_0, k_m\right), \tag{20.176}$$

subscript g pertains to the cumulative k-distribution for the mth scale,

$$g_m = \int_0^{k_m} f_m(T_0, \boldsymbol{\phi}_0, k)\,dk, \tag{20.177}$$

a_m is the nongray stretching factor,

$$a_m = \frac{f_m(T, \boldsymbol{\phi}_0, k_m)}{f_m(T_0, \boldsymbol{\phi}_0, k_m)}, \tag{20.178}$$

and λ_m is the overlap parameter of the mth scale with all other scales, defined by

$$\lambda_m I_{mg} = k_m I_{mg} + \int_0^\infty \left(\sum_{n\neq m} \kappa_{n\eta}\right) I_{m\eta}\,\delta\left(k_m - \kappa_{m\eta}(\boldsymbol{\phi}_0)\right)\,d\eta \Big/ f_m\left(T_0, \boldsymbol{\phi}_0, k_m\right) \tag{20.179}$$

Similarly, FSK reordering is performed on boundary condition(s) with respect to $\kappa_{m\eta}(\boldsymbol{\phi}_0)$, which results in

$$I_{mg} = \frac{1-\epsilon}{\pi} \int_{2\pi} I_{mg}\,|\hat{n}.\hat{s}|\,d\Omega, \quad \text{for } m = 1, \ldots, M. \tag{20.180}$$

The last term in equation (20.175) describes the overlap of the absorption coefficient of the mth scale, $\kappa_{m\eta}$, with those of all other scales, which occurs over part of the spectrum. In the MSFSK method the overlap parameter λ_m is evaluated in an approximate way, such that the emitted intensity emanating from a homogeneous nonscattering layer bounded by black walls is predicted exactly. The so-determined λ_m is a function of the state variables as well as of k_m (or g_m).

In equation (20.175) the reordering is performed in terms of the absorption coefficient of one scale $\kappa_{m\eta}$, and the interaction between $\kappa_{m\eta}$ and κ_η during the reordering process is lumped into the overlap parameter λ_m. The reordering of equation (20.172) can also be performed in terms of κ_η, which, for a homogeneous layer at temperature T, leads to

$$\frac{dI^*_{mg}}{ds} = \frac{k^*_m I_b}{f(T, \boldsymbol{\phi}, k)} - kI^*_{mg}, \quad \text{for } m = 1, \ldots, M, \tag{20.181}$$

where

$$f(T, \boldsymbol{\phi}, k) = \frac{1}{I_b(T)} \int_0^\infty I_{b\eta}(T)\,\delta\left(k - \kappa_\eta(\boldsymbol{\phi})\right)\,d\eta, \tag{20.182}$$

$$I^*_{mg} = \int_0^\infty I_{m\eta}\delta\left(k - \kappa_\eta(\boldsymbol{\phi})\right)\,d\eta \Big/ f\,(T, \boldsymbol{\phi}, k), \tag{20.183}$$

$$k^*_m = \frac{1}{I_b} \int_0^\infty I_{b\eta}(T)\kappa_{m\eta}\delta\left(k - \kappa_\eta(\boldsymbol{\phi})\right)\,d\eta. \tag{20.184}$$

In equation (20.181) the interaction between $\kappa_{m\eta}$ and κ_η is lumped into k^*_m. The solutions to equations (20.175) and (20.181) for a homogeneous layer at temperature T bounded by black walls (for which $a_m \equiv 1$) can be obtained analytically, and the total exiting intensities from the gas scales at $s = L$ are

$$I_m = \int_0^1 I_{mg}\,dg_m = \int_0^\infty \frac{k_m}{\lambda_m} I_b\left[1 - \exp(-\lambda_m s)\right] f_m(T, \boldsymbol{\phi}, k_m)\,dk_m, \quad \text{for } m = 1, \ldots, M, \tag{20.185}$$

and

$$I_m^* = \int_0^1 I_{mg}^* \, dg = \int_0^\infty \frac{k_m^*}{k} I_b \left[1 - \exp(-ks)\right] dk, \quad \text{for } m = 1, \ldots, M, \tag{20.186}$$

respectively. The spectrally integrated intensity, I_m, should be equal to I_m^*, and this requirement leads to

$$\lambda_m = k, \quad \text{and} \quad k_m f_m(T, k_m)\, dk_m = k_m^*(T, k)\, dk, \tag{20.187}$$

or

$$k_m^*(T, \lambda_m)\, d\lambda_m = k_m f_m(T, k_m)\, dk_m = k_m(g_m)\, dg_m. \tag{20.188}$$

Equation (20.188) provides the relationship between λ_m and k_m that is required to solve equation (20.175). One convenient way of determining λ_m is using a partly integrated form

$$\int_0^{g_m(k_m)} k_m(g_m)\, dg_m = \int_0^{k=\lambda_m} k_m^*(T, k)\, dk. \tag{20.189}$$

The overlap parameter can be determined efficiently and accurately from a database of narrow band k-distributions of individual species (scales). One advantage of using narrow band k-distributions is that assembling mixture full spectrum k-distributions from narrow band k-distributions of individual gas species mixed at the narrow band level is more accurate than mixing entire full spectrum k-distributions of individual species. In addition, the use of narrow band k-distributions of individual species allows the inclusion of nongray absorbing particles in the participating medium, by employing equation (11.120).

For the mth scale, substituting equation (20.184), into equation (20.189) the right-hand side (RHS) may be rewritten in terms of narrow band k_m^* as

$$\text{RHS} = \int_0^{k=\lambda_m} \sum_{i=1}^{N_{\text{nb}}} \frac{I_{bi}}{I_b} \frac{1}{\Delta\eta} \int_{\Delta\eta} \kappa_{m\eta}\, \delta(k - \kappa_\eta)\, d\eta\, dk = \sum_{i=1}^{N_{\text{nb}}} \frac{I_{bi}}{I_b} \int_0^{k=\lambda_m} k_{m,i}^*(k)\, dk, \tag{20.190}$$

where $k_{m,i}^*$ is the narrow band counterpart of k_m^*, N_{nb} is the number of narrow bands comprising the entire spectrum, and the narrow band Planck function I_{bi} is defined by equation (20.153). In order to evaluate the integrals involving $k_{m,i}^*$ in equation (20.190) in terms of narrow band k-distributions, we consider the quantity

$$Q_m = \frac{1}{\Delta\eta} \int_{\Delta\eta} \kappa_{m\eta} \exp(-\kappa_\eta L)\, d\eta \tag{20.191}$$

for the ith narrow band. Physically, Q_m is related to narrow band emission from scale m, attenuated over path L by the entire gas mixture. Using the definition of the Dirac-delta function, equation (11.99), Q_m can be rewritten as

$$Q_m = \frac{1}{\Delta\eta} \int_{\Delta\eta} \kappa_{m\eta} \int_0^\infty \exp(-kL)\, \delta(k - \kappa_\eta)\, dk\, d\eta = \int_0^\infty k_{m,i}^* \exp(-kL)\, dk = \mathscr{L}(k_{m,i}^*), \tag{20.192}$$

i.e., Q_m is the Laplace transform of $k_{m,i}^*$. It was observed in Section 20.11 that, on a narrow band basis, the spectral behavior of different species is essentially statistically uncorrelated. With this assumption, Q_m can also be written as

$$\begin{aligned} Q_m &= \frac{1}{\Delta\eta} \int_{\Delta\eta} \kappa_{m\eta} \exp(-\kappa_{m\eta} L) \prod_{n \neq m} \exp(-\kappa_{n\eta} L)\, d\eta \\ &\approx \frac{1}{\Delta\eta} \int_{\Delta\eta} \kappa_{m\eta} \exp(-\kappa_{m\eta} L)\, d\eta \prod_{n \neq m} \left(\frac{1}{\Delta\eta} \int_{\Delta\eta} \exp(-\kappa_{n\eta} L)\, d\eta \right). \end{aligned} \tag{20.193}$$

The second step follows by recognizing that the integration in the first step is an averaging operator, together with the assumption that the absorption coefficients of different scales are statistically uncorrelated. The k-distribution method can then be applied to equation (20.193) and we obtain

$$\begin{aligned} Q_m &\approx \int_0^1 k_{m,i} \exp(-k_{m,i}L)\, dg_m \prod_{n\neq m} \left(\int_0^1 \exp(-k_{n,i}L)\, dg_n \right) \\ &= \int_{g_1=0}^1 \cdots \int_{g_M=0}^1 k_{m,i} \exp\left(-\sum_{n=1}^M k_{n,i}L \right) dg_1 \cdots dg_M. \end{aligned} \tag{20.194}$$

Equating equations (20.192) and (20.194), we have

$$\mathscr{L}(k^*_{m,i}) \approx \int_{g_1=0}^1 \cdots \int_{g_M=0}^1 k_{m,i} \exp\left(-\sum_{n=1}^M k_{n,i}L \right) dg_1 \cdots dg_M, \tag{20.195}$$

and, using the integral property of the Laplace transform,

$$\mathscr{L}\left(\int_0^{k=\lambda_m} k^*_{m,i}(k)\, dk \right) \approx \int_{g_1=0}^1 \cdots \int_{g_M=0}^1 k_m \frac{\exp(-\sum_{n=1}^M k_n L)}{L}\, dg_1 \cdots dg_M. \tag{20.196}$$

Finally, taking the inverse Laplace transform, we obtain

$$\int_0^{k=\lambda_m} k^*_{m,i}(k)\, dk \approx \int_{g_1=0}^1 \cdots \int_{g_M=0}^1 k_m H\left(k - \sum_{n=1}^M k_n \right) dg_1 \cdots dg_M, \tag{20.197}$$

where H is the Heaviside step function.

The left-hand side of equation (20.189) is also readily expressed in terms of narrow band k-distributions, as defined by equation (11.98), as

$$\begin{aligned} \text{LHS} &= \int_0^{k_m} k_m \frac{1}{I_b} \int_0^\infty I_{b\eta}\, \delta(k_m - \kappa_{m\eta})\, d\eta\, dk_m = \sum_{i=1}^{N_{\text{nb}}} \frac{I_{bi}}{I_b} \int_0^{k_m} k_m \frac{1}{\Delta\eta} \int_{\Delta\eta} \delta(k_m - \kappa_{m\eta})\, d\eta\, dk_m \\ &= \sum_{i=1}^{N_{\text{nb}}} \frac{I_{bi}}{I_b} \int_0^{g_{m,i}(k_m)} k_{m,i}\, dg_m. \end{aligned} \tag{20.198}$$

Equating the left- and right-hand sides, we obtain a generic expression for the determination of the overlap coefficient λ_m based on narrow band k-distributions of individual gases as

$$\sum_{i=1}^{N_{\text{nb}}} \frac{I_{bi}}{I_b} \int_0^{g_{m,i}(k_m)} k_{m,i}\, dg_m = \sum_{i=1}^{N_{\text{nb}}} \frac{I_{bi}}{I_b} \int_{g_{1,i}=0}^1 \cdots \int_{g_{M,i}=0}^1 k_{m,i} H\left(\lambda_m - \sum_{n=1}^M k_{n,i} \right) dg_1 \cdots dg_M, \quad \text{for } m = 1, \ldots, M. \tag{20.199}$$

In this expression the k_m and λ_m are global values; all others ($k_{m,i}$, g_m, etc.), are for the ith narrow band. In particular, the integration in equation (20.198) is taken over the k-distribution of the ith narrow band until $k_{m,i}$ reaches the global value $k_{m,i} = k_m$. In practice, $\lambda_m(k_m)$ is found by evaluating the left- and right-hand sides of equation (20.199) independently for many values of k_m and λ_m once and for all for each cell. Required values of $\lambda_m(k_m)$ for g-quadrature are then found by interpolation.

A few extreme one-dimensional examples are shown in Figs. 20-18 and 20-19, all considering a mixture of CO_2, H_2O, and N_2 confined between two cold black walls [126, 130]. The mixture

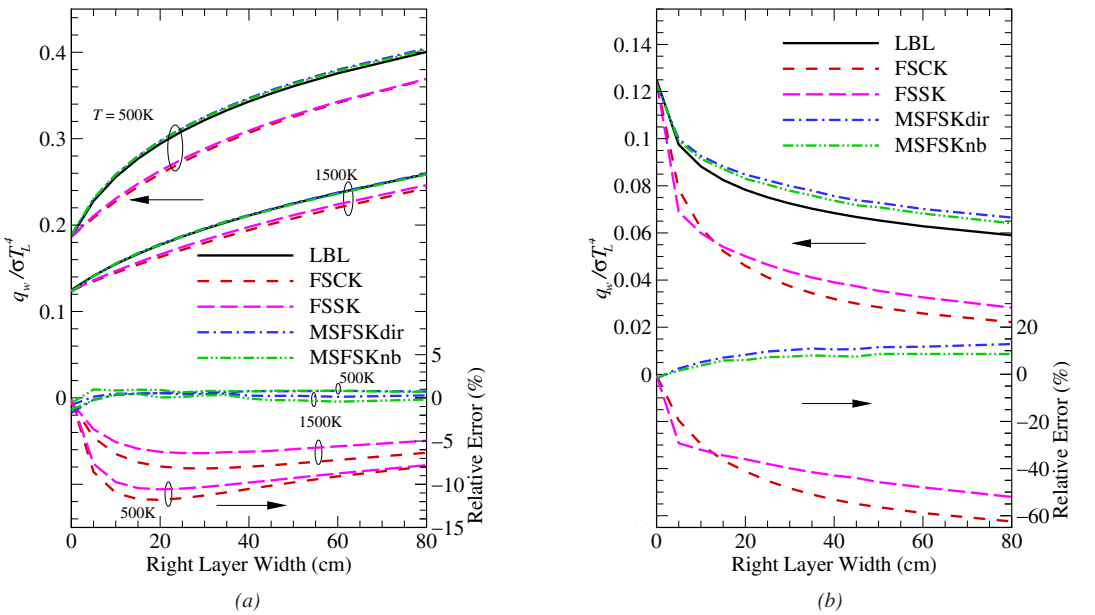

FIGURE 20-18
Relative errors of the FSCK, FSSK, MSFSKdir, and MSFSKnb calculations with step changes in mole fraction. Left layer: 2% CO_2 and 20% H_2O; right layer: 20% CO_2 and 2% H_2O. *(a)* Medium at uniform temperature (500 K or 1500 K); *(b)* medium with step temperature (left layer at 1500 K, right at 500 K) [126].

is at a total pressure of 1 bar and consists of two different homogeneous layers (denoted as left and right layer). The left layer has a fixed width of $L_L = 50$ cm, and the right layer a variable width of L_R. The radiative heat flux leaving from the right layer is calculated. Five methods are used to calculate the exiting flux: the LBL, FSK (using both the correlated-k, FSCK, and the scaled-k, FSSK, approaches), and MSFSK (using correlated-k, both, with the overlap coefficient calculated directly from the spectral database, MSFSKdir, and calculated from the NBKDIR narrow band database, MSFSKnb) methods. In the LBL calculations, the HITEMP 1995 and CDSD-1000 spectral databases were used for the absorption coefficients of H_2O and CO_2, respectively. In the FSK calculations, the k–g distributions are constructed directly from the spectral databases; the reference states and the scaling functions were determined according to equations (20.142) and (20.143). Only correlated-k was considered for the present MSFSK examples. For the MSFSKdir calculations the overlap coefficients (and k-distributions) were obtained directly from HITEMP 1995 and CDSD-1000; for the MSFSKnb calculation the overlap coefficients and k-distributions were obtained from narrow band k–g distributions read from the narrow band k–g database of Wang and Modest [112]. A 10-point Gaussian quadrature scheme was used for the spectral integrations in all FSCK, FSSK, MSFSKdir, and MSFSKnb calculations.

In Fig. 20-18*a* the temperatures of both layers (T_L and T_R) are set equal, but the species mole fractions change sharply: the left layer contains 20% CO_2 and 2% H_2O, while the right layer has 2% CO_2 and 20% H_2O. The nondimensional heat flux exiting from the right layer is plotted in the upper half of Fig. 20-18*a* as a function of the right layer width (i.e., the optical thickness of the right layer). The figure includes the results for two mixture temperatures (1500 and 500 K). The heat flux increases with increasing thickness of the right layer as emission from the right layer builds up. The MSFSK results follow the LBL calculations closely, while the FSK methods show significant departures. The relative errors of the FSCK, FSSK, MSFSKdir, and MSFSKnb calculations compared to LBL calculations are shown in the lower half of the figure. For the case of homogeneous temperature with strongly inhomogeneous gas concentration, the MSFSK

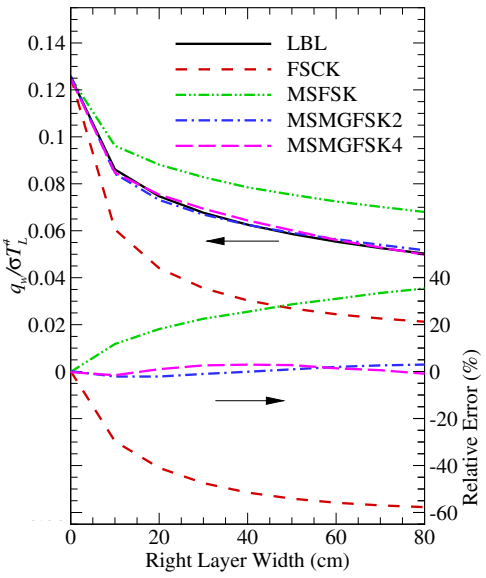

FIGURE 20-19
Relative errors of the FSCK, MSFSK, and MGMSFSK (two and four groups) calculations for the two-layer slab of Fig. 20-18*b* with 0.1 ppm nongray soot added to right layer [130].

method gives errors less than 1% with 10 quadrature points (and, thus, RTE evaluations) for various optical thicknesses, while the FSCK and FSSK methods reach errors of 10% to 12%. As the width of the right layer increases, the FSCK and FSSK errors decrease, indicating that emission from the homogeneous right layer becomes dominant, and that limit can be predicted exactly by the FSCK and FSSK methods.

In Fig. 20-18*b*, in addition to a step change in species mole fraction, a step change in mixture temperature is introduced: the temperature of the left layer is set to 1500 K, and the right layer to 500 K, with the same mixture as given in Fig. 20-18*a*. Thus, in this example the absorption coefficients of both layers are uncorrelated due to, both, species concentration and temperature effects. Heat flux leaving the right layer is now due to emission by the left hot layer, which is attenuated by the (strongly uncorrelated) right layer. The nondimensional heat fluxes calculated by the LBL, FSCK, FSSK, MSFSKdir, and MSFSKnb methods are shown in Fig. 20-18*b* against the width of the right layer. In the MSFSK calculations, the reference states are determined separately for each scale. The heat flux decreases with increasing width of the right absorption layer. For this extreme case of strong inhomogeneity in both species concentration and temperature, the FSCK and FSSK methods fail completely, while the present MSFSK method, although designed for just dealing with strong inhomogeneities in gas concentration, has a maximum error of only about 12% with 10 quadrature points for various optical thickness. The difference between MSFSKdir and MSFSKnb calculations is small, indicating that the scheme of using a database of narrow band *k*-distributions to evaluate overlap coefficients is robust.

Finally, in Fig. 20-19 we consider the same two-layer slab as in Fig. 20-18*b*, but with 0.1 ppm soot added to the right layer [130]. Nongray soot absorption coefficients were calculated from equation (12.53), with the complex index of refraction given by Chang and Charalampopoulos [131], equation (12.116). Again, LBL, FSCK, and MSFSK results are shown, the latter using 3 scales (one each for CO_2, H_2O, and soot) within the extended MSFSK model of Pal and Modest [128]. Also included are hybrid multigroup–multiscale results [130] (three scales, two or four groups each for CO_2 and H_2O). It is seen that the FSCK incurs a maximum error of close to 60%, but even the three-scale MSFSK displays large errors, indicating that the method cannot always cope with severe temperature and concentration inhomogeneity in multiphase mixtures. The hybrid model, on the other hand, never has errors exceeding 5%, with the two-group model requiring $2 \times 10(CO_2) + 2 \times 10(H_2O) + 10(\text{soot}) = 50$ RTE evaluations.

It should be understood that these examples (with discontinuities in temperature, concen-

trations, and/or soot levels) are extreme, and are never encountered in realistic systems. For the vast majority of industrial applications the MSFSK method can be expected to produce excellent results. Pal and Modest have investigated several realistic combustion situations, applying the FSCK and MSFSK approaches to an artificial methane flame [128, 132] and all higher order methods to an ethylene flame [130] first studied experimentally by Kent and Honnery [133]. In the Kent and Honnery flame radiation from ethylene (C_2H_4), H_2O, CO_2, CO, and nongray soot was considered, using the FSCK scheme (10 spectral RTE evaluations), the MSFSK scheme (treating C_2H_4, CO, and soot as separate scales, and combining H_2O and CO_2 into a single scale, for a total of four scales, or 4×10 spectral RTE evaluations), and the MSMGFSK scheme (also separating H_2O and CO_2 and breaking each into two groups, for a total of 7×10 spectral RTE evaluations). The basic FSCK scheme displayed good accuracy over most of the domain, but had errors of up to 35% (in terms of maximum $\nabla \cdot \mathbf{q}$) near the inlet; the MSFSK and MSMGFSK schemes reduced the maximum error to 6% and 3%, respectively. It was also demonstrated that the methods, including the Modest and Riazzi mixing scheme, remain accurate at high pressures [132].

We close our discussion in this section by observing that narrow band *k*-distributions were first applied in the field of atmospheric sciences, before the development of full spectrum *k*-distributions in the heat transfer field; and that the full-spectrum versions have since then found their way back to the atmospheric sciences [134, 135]. The concept may be applied to any system with strong spectrally varying radiation, and has most recently also been applied to nonequilibrium radiation in hypersonic plasmas [122, 136, 137].

References

1. Rothman, L. S., I. E. Gordon, A. Barbe, D. C. Benner, P. F. Bernath, M. Birk, V. Boudon, L. R. Brown, A. Campargue, J.-P. Champion, K. Chance, L. H. Coudert, V. Dana, V. M. Devi, S. Fally, J.-M. Flaud, R. R. Gamache, A. Goldman, D. Jacquemart, I. Kleiner, N. Lacome, W. J. Lafferty, J.-Y. Mandin, S. T. Massie, S. N. Mikhailenko, C. E. Miller, N. Moazzen-Ahmadi, O. V. Naumenko, A. V. Nikitin, J. Orphal, V. I. Perevalov, A. Perrin, A. Predoi-Cross, C. P. Rinsland, M. Rotger, M. Simeckova, M. A. H. Smith, K. Sung, S. A. Tashkun, J. Tennyson, R. A. Toth, A. C. Vandaele, and J. V. Auwera: "The HITRAN 2008 molecular spectroscopic database," *Journal of Quantitative Spectroscopy and Radiative Transfer*, vol. 110, pp. 533–572, 2009.
2. Rothman, L. S., I. E. Gordon, R. J. Barber, H. Dothe, R. R. Gamache, A. Goldman, V. I. Perevalov, S. A. Tashkun, and J. Tennyson: "HITEMP, the high-temperature molecular spectroscopic database," *Journal of Quantitative Spectroscopy and Radiative Transfer*, vol. 111, no. 15, pp. 2139–2150, 2010.
3. Denison, M. K., and B. W. Webb: "An absorption-line blackbody distribution function for efficient calculation of total gas radiative transfer," *Journal of Quantitative Spectroscopy and Radiative Transfer*, vol. 50, pp. 499–510, 1993.
4. Denison, M. K., and B. W. Webb: "A spectral line based weighted-sum-of-gray-gases model for arbitrary RTE solvers," *ASME Journal of Heat Transfer*, vol. 115, pp. 1004–1012, 1993.
5. Denison, M. K., and B. W. Webb: "The spectral-line-based weighted-sum-of-gray-gases model in nonisothermal nonhomogeneous media," *ASME Journal of Heat Transfer*, vol. 117, pp. 359–365, 1995.
6. Rivière, P., A. Soufiani, M.-Y. Perrin, H. Riad, and A. Gleizes: "Air mixture radiative property modelling in the temperature range 10000–40000 K," *Journal of Quantitative Spectroscopy and Radiative Transfer*, vol. 56, pp. 29–45, 1996.
7. Pierrot, L., A. Soufiani, and J. Taine: "Accuracy of narrow-band and global models for radiative transfer in H_2O, CO_2, and H_2O–CO_2 mixtures at high temperature," *Journal of Quantitative Spectroscopy and Radiative Transfer*, vol. 62, pp. 523–548, 1999.
8. Pierrot, L., P. Rivière, A. Soufiani, and J. Taine: "A fictitious-gas-based absorption distribution function global model for radiative transfer in hot gases," *Journal of Quantitative Spectroscopy and Radiative Transfer*, vol. 62, pp. 609–624, 1999.
9. Scutaru, D., L. Rosenmann, and J. Taine: "Approximate band intensities of CO_2 hot bands at 2.7, 4.3 and 12 μm for high temperature and medium resolution applications," *Journal of Quantitative Spectroscopy and Radiative Transfer*, vol. 52, pp. 765–781, 1994.
10. Rivière, P., A. Soufiani, and J. Taine: "Correlated-*k* and fictitious gas model for H_2O infrared radiation in the Voigt regime," *Journal of Quantitative Spectroscopy and Radiative Transfer*, vol. 53, pp. 335–346, 1995.
11. Marin, O., and R. O. Buckius: "Wide band correlated-*k* approach to thermal radiative transport in nonhomogeneous media," *ASME Journal of Heat Transfer*, vol. 119, no. 4, pp. 719–729, 1997.
12. Solovjov, V. P., and B. W. Webb: "SLW modeling of radiative transfer in multicomponent gas mixtures," *Journal of Quantitative Spectroscopy and Radiative Transfer*, vol. 65, pp. 655–672, 2000.

13. Modest, M. F., and H. Zhang: "The full-spectrum correlated-*k* distribution and its relationship to the weighted-sum-of-gray-gases method," in *Proceedings of the IMECE 2000*, vol. HTD-366-1, ASME, Orlando, FL, pp. 75–84, 2000.
14. Zhang, H., and M. F. Modest: "A multi-scale full-spectrum correlated-*k* distribution for radiative heat transfer in inhomogeneous gas mixtures," *Journal of Quantitative Spectroscopy and Radiative Transfer*, vol. 73, no. 2–5, pp. 349–360, 2002.
15. Zhang, H., and M. F. Modest: "Scalable multi-group full-spectrum correlated-*k* distributions for radiative heat transfer," *ASME Journal of Heat Transfer*, vol. 125, no. 3, pp. 454–461, 2003.
16. Zhang, H., and M. F. Modest: "Multi-group full-spectrum *k*-distribution database for water vapor mixtures in radiative transfer calculations," *International Journal of Heat and Mass Transfer*, vol. 46, no. 19, pp. 3593–3603, 2003.
17. Rothman, L. S., R. B. Wattson, R. R. Gamache, J. Schroeder, and A. McCann: "HITRAN, HAWKS and HITEMP high temperature databases," *Proceedings of SPIE*, vol. 2471, pp. 105–111, 1995.
18. Solovjov, V. P., and B. W. Webb: "Radiative transfer model parameters for carbon monoxide at high temperature," in *Proceedings of the 11th International Heat Transfer Conference*, vol. 7, Kyongju, Korea, pp. 445–450, 1998.
19. Tang, K. C., and M. Q. Brewster: "K-distribution analysis of gas radiation with nongray, emitting, absorbing and anisotropic scattering particles," *ASME Journal of Heat Transfer*, vol. 116, no. 4, pp. 980–985, 1994.
20. Tang, K. C., and M. Q. Brewster: "Analysis of molecular gas radiation: Real gas property effects," in *7th AIAA/ASME Joint Thermophysics and Heat Transfer Conference*, vol. HTD-357-1, ASME, pp. 23–32, 1998.
21. Park, C.: "Nonequilibrium air radiation (NEQAIR) program: User's manual," NASA/Ames Research Center, Moffett Field, CA 94035-1000, 1985.
22. Olynick, D. R., W. D. Henline, L. Hartung-Chambers, and G. V. Candler: "Comparison of coupled radiative flow solutions with project Fire II flight data," *Journal of Thermophysics and Heat Transfer*, vol. 9, no. 4, pp. 586–594, 1995.
23. Olynick, D. R., Y.-K. Chen, and M. E. Tauber: "Aerothermodynamics of the Stardust sample return capsule," *Journal of Spacecraft and Rockets*, vol. 36, no. 3, pp. 442–462, 1999.
24. Olejniczak, J., M. Wright, D. Prabhu, N. Takashima, B. R. Hollis, and E. V. Zoby: "An analysis of the radiative heating environment for aerocapture at Titan," *AIAA Paper No. 2003-4953*, 2003, 39th AIAA/ASME/SAE/ASEE Joint Propulsion Conference and Exhibit, Huntsville, Alabama.
25. da Silva, M. L.: "An adaptive line-by-line–statistical model for fast and accurate spectral simulations in low-pressure plasmas," *Journal of Quantitative Spectroscopy and Radiative Transfer*, vol. 108, pp. 106–125, 2007.
26. Feldick, A. M., M. F. Modest, and D. A. Levin: "Closely coupled flowfield–radiation interactions during hypersonic reentry," *Journal of Thermophysics and Heat Transfer*, vol. 25, no. 4, pp. 481–492, 2011.
27. Hartung, L., and H. A. Hassan: "Radiation transport around axisymmetric blunt body vehicles using a modified differential approximation," *Journal of Thermophysics and Heat Transfer*, vol. 7, no. 2, pp. 220–227, 1993.
28. Hottel, H. C.: "Radiant heat transmission," in *Heat Transmission*, ed. W. H. McAdams, 3rd ed., ch. 4, McGraw-Hill, New York, 1954.
29. Hottel, H. C., and A. F. Sarofim: *Radiative Transfer*, McGraw-Hill, New York, 1967.
30. Dunkle, R. V.: "Geometric mean beam lengths for radiant heat transfer calculations," *ASME Journal of Heat Transfer*, vol. 86, no. 1, pp. 75–80, 1964.
31. Andersen, K. M., and S. Hadvig: "Geometric mean beam lengths for the space between two coaxial cylinders," *ASME Journal of Heat Transfer*, vol. 111, no. 3, pp. 811–812, 1989.
32. Andersen, F. M. B.: "Geometric mean beam lengths between two concentric spheres," *ASME Journal of Heat Transfer*, vol. 119, no. 2, pp. 379–380, 1997.
33. Viskanta, R.: "Concerning the definitions of the mean absorption coefficient," *International Journal of Heat and Mass Transfer*, vol. 7, no. 9, pp. 1047–1049, 1964.
34. Finkleman, D., and K. Y. Chien: "Semigrey radiative transfer," *AIAA Journal*, vol. 6, no. 4, pp. 755–758, 1968.
35. Finkleman, D.: "Numerical studies in semigray radiative transfer," *AIAA Journal*, vol. 7, pp. 1602–1605, 1969.
36. Finkleman, D.: "A note on boundary conditions for use with the differential approximation to radiative transfer," *International Journal of Heat and Mass Transfer*, vol. 12, pp. 653–656, 1969.
37. Traugott, S. C.: "Radiative heat-flux potential for a nongrey gas," *AIAA Journal*, vol. 4, no. 3, pp. 541–542, 1966.
38. Traugott, S. C.: "On grey absorption coefficients in radiative transfer," *Journal of Quantitative Spectroscopy and Radiative Transfer*, vol. 8, pp. 971–999, 1968.
39. Modest, M. F., and K. K. Sikka: "The application of the stepwise-gray P-1 approximation to molecular gas–particulate mixtures," *Journal of Quantitative Spectroscopy and Radiative Transfer*, vol. 48, no. 2, pp. 159–168, 1992.
40. Modest, M. F.: "The weighted-sum-of-gray-gases model for arbitrary solution methods in radiative transfer," *ASME Journal of Heat Transfer*, vol. 113, no. 3, pp. 650–656, 1991.
41. Chandrasekhar, S.: "The radiative equilibrium of the outer layers of a star with special reference to the blanketing effects of the reversing layer," *Monthly Notices Royal Astron. Soc.*, vol. 96, pp. 21–42, 1935.
42. Siewert, C. E., and P. F. Zweifel: "An exact solution of equations of radiative transfer for local thermodynamic equilibrium in the non-gray case: Picket fence approximation," *Ann. Phys. (N.Y.)*, vol. 36, pp. 61–85, 1966.
43. Kung, S. C., and M. Sibulkin: "Radiative transfer in a nongray gas between parallel walls," *Journal of Quantitative Spectroscopy and Radiative Transfer*, vol. 9, pp. 1447–1461, 1969.

44. Reith, R. J., C. E. Siewert, and M. N. Özişik: "Non-grey radiative heat transfer in conservative plane-parallel media with reflecting boundaries," *Journal of Quantitative Spectroscopy and Radiative Transfer*, vol. 11, pp. 1441–1462, 1971.
45. Greif, R.: "Energy transfer by radiation and conduction with variable gas properties," *International Journal of Heat and Mass Transfer*, vol. 7, pp. 891–900, 1964.
46. Modest, M. F.: "A simple differential approximation for radiative transfer in non-gray gases," *ASME Journal of Heat Transfer*, vol. 101, pp. 735–736, 1979.
47. Thynell, S. T.: "Radiation due to CO_2 or H_2O and particles in cylindrical media," *Journal of Thermophysics and Heat Transfer*, vol. 4, no. 4, pp. 436–445, 1990.
48. Kaminski, D. A., X. D. Fu, and M. K. Jensen: "Numerical and experimental analysis of combined convective and radiative heat transfer in laminar flow over a circular cylinder," *International Journal of Heat and Mass Transfer*, vol. 38, no. 17, pp. 3161–3169, 1995.
49. Seo, T., M. K. Jensen, and D. A. Kaminski: "Combined convection and non-gray radiation in simultaneously developing turbulent flow and heat transfer," in *Proceedings of the 11th International Heat Transfer Conference*, vol. 7, Kyongju, Korea, pp. 337–342, 1998.
50. Mazumder, S., and M. F. Modest: "A PDF approach to modeling turbulence–radiation interactions in nonluminous flames," *International Journal of Heat and Mass Transfer*, vol. 42, pp. 971–991, 1999.
51. Mazumder, S., and M. F. Modest: "Turbulence–radiation interactions in nonreactive flow of combustion gases," *ASME Journal of Heat Transfer*, vol. 121, pp. 726–729, 1999.
52. Van Wylen, G. H., and R. E. Sonntag: *Fundamentals of Classical Thermodynamics*, John Wiley & Sons, New York, 1985.
53. Grosshandler, W. L.: "Radiative transfer in nonhomogeneous gases: A simplified approach," *International Journal of Heat and Mass Transfer*, vol. 23, pp. 1447–1457, 1980.
54. Grosshandler, W. L.: "RADCAL: a narrow-band model for radiation calculations in a combustion environment," Technical Report NIST Technical Note 1402, National Institute of Standards and Technology, 1993.
55. Soufiani, A., and J. Taine: "High temperature gas radiative property parameters of statistical narrow-band model for H_2O, CO_2 and CO, and correlated-k model for H_2O and CO_2," *International Journal of Heat and Mass Transfer*, vol. 40, no. 4, pp. 987–991, 1997.
56. Kim, T. K., J. A. Menart, and H. S. Lee: "Nongray radiative gas analyses using the S-N discrete ordinates method," *ASME Journal of Heat Transfer*, vol. 113, no. 4, pp. 946–952, 1991.
57. Menart, J. A., H. S. Lee, and T. K. Kim: "Discrete ordinates solutions of nongray radiative transfer with diffusely reflecting walls," *ASME Journal of Heat Transfer*, vol. 115, no. 1, pp. 184–193, 1993.
58. Menart, J. A., and H. S. Lee: "Nongray gas analyses for reflecting walls utilizing a flux technique," *ASME Journal of Heat Transfer*, vol. 115, no. 3, pp. 645–652, 1993.
59. Cherkaoui, M., J.-L. Dufresne, R. Fournier, J.-Y. Grandpeix, and A. Lahellec: "Radiative net exchange formulation within one-dimensional gas enclosures with reflective surfaces," *ASME Journal of Heat Transfer*, vol. 120, no. 1, pp. 275–278, 1998.
60. Liu, F., O. L. Gülder, G. J. Smallwood, and Y. Ju: "Non-grey gas radiative transfer analyses using the statistical narrow-band model," *International Journal of Heat and Mass Transfer*, vol. 41, no. 14, pp. 2227–2236, 1998.
61. Ju, Y., K. Takita, M. Goro, F. Liu, and H. Guo: "Analyses of extinction and flammability limit of stretched premixed flames using the statistical narrow-band model," in *Proceedings of the 11th International Heat Transfer Conference*, vol. 7, Kyongju, Korea, pp. 301–306, 1998.
62. Liu, F.: "Numerical solutions of three-dimensional non-grey gas radiative transfer using the statistical narrow-band model," *ASME Journal of Heat Transfer*, vol. 121, no. 1, pp. 200–203, 1999.
63. Edwards, D. K., and A. Balakrishnan: "Slab band absorptance for molecular gas radiation," *Journal of Quantitative Spectroscopy and Radiative Transfer*, vol. 12, pp. 1379–1387, 1972.
64. Edwards, D. K.: "Molecular gas band radiation," in *Advances in Heat Transfer*, vol. 12, Academic Press, New York, pp. 115–193, 1976.
65. Wassel, A. T., and D. K. Edwards: "Molecular gas band radiation in cylinders," *ASME Journal of Heat Transfer*, vol. 96, pp. 21–26, 1974.
66. Hutchison, J. R., and R. F. Richards: "Effect of nongray gas radiation on thermal stability in carbon dioxide," *Journal of Thermophysics and Heat Transfer*, vol. 13, no. 1, pp. 25–32, 1999.
67. Modest, M. F.: "Radiative heat transfer in a plane-layer mixture of non-gray particulates and molecular gases," *Journal of Quantitative Spectroscopy and Radiative Transfer*, vol. 26, pp. 523–533, 1981.
68. Cumber, P. S., M. Fairweather, and H. S. Ledin: "Application of wide band radiation models to non-homogeneous combustion systems," *International Journal of Heat and Mass Transfer*, vol. 41, no. 11, pp. 1573–1584, 1998.
69. Liu, F., G. J. Smallwood, and O. L. Gülder: "Application of statistical narrowband model to three-dimensional absorbing–emitting–scattering media," *Journal of Thermophysics and Heat Transfer*, vol. 13, no. 3, pp. 285–291, 1999.
70. Maruyama, S., and Z. Guo: "Radiative heat transfer in arbitrary configurations with nongray absorbing, emitting, and anisotropic scattering media," *ASME Journal of Heat Transfer*, vol. 121, no. 3, pp. 722–726, 1999.
71. Smith, T. F., Z. F. Shen, and J. N. Friedman: "Evaluation of coefficients for the weighted sum of gray gases model," *ASME Journal of Heat Transfer*, vol. 104, pp. 602–608, 1982.

72. Farag, I. H., and T. A. Allam: "Gray-gas approximation of carbon dioxide standard emissivity," *ASME Journal of Heat Transfer*, vol. 103, pp. 403–405, 1981.
73. Truelove, J. S.: "The zone method for radiative heat transfer calculations in cylindrical geometries," HTFS Design Report DR33 (Part I: AERE-R8167), Atomic Energy Authority, Harwell, 1975.
74. Taylor, P. B., and P. J. Foster: "Some gray gas weighting coefficients for CO_2–H_2O–soot mixtures," *International Journal of Heat and Mass Transfer*, vol. 18, pp. 1331–1332, 1975.
75. Yin, C., L. C. R. Johansen, L. A. Rosendahl, and S. K. Kär: "New weighted sum of gray gases model applicable to computational fluid dynamics (CFD) modeling of oxy-fuel combustion: Derivation, validation, and implementation," *Energy & Fuels*, vol. 24, pp. 6275–6282, 2010.
76. Johansson, R., K. Andersson, B. Leckner, and H. Thunman: "Models for gaseous radiative heat transfer applied to oxy-fuel conditions in boilers," *International Journal of Heat and Mass Transfer*, vol. 53, pp. 220–230, 2010.
77. Bressloff, N. W.: "The influence of soot loading on weighted sum of grey gases solutions to the radiative transfer equation across mixtures of gases and soot," *International Journal of Heat and Mass Transfer*, vol. 42, no. 18, pp. 3469–3480, 1999.
78. Ramamurthy, H., S. Ramadhyani, and R. Viskanta: "A two-dimensional axisymmetric model for combusting, reacting and radiating flows in radiant tubes," *Journal of the Institute of Energy*, vol. 67, pp. 90–100, 1994.
79. Mesyngier, C., and B. Farouk: "Turbulent natural convection–nongray gas radiation analysis in a square enclosure," *Numerical Heat Transfer – Part A: Applications*, vol. 29, no. 7, pp. 671–687, 1996.
80. Liu, F., H. A. Becker, and Y. Bindar: "A comparative study of radiative heat transfer modelling in gas-fired furnaces using the simple grey gas and the weighted-sum-of-grey-gases models," *International Journal of Heat and Mass Transfer*, vol. 41, no. 22, pp. 3357–3371, 1998.
81. Baek, S. W., J. H. Park, and C. E. Choi: "Investigation of droplet combustion with nongray gas radiation effects," *Combustion Science and Technology*, vol. 142, no. 1, pp. 55–79, 1999.
82. Kühlert, K., and U. Renz: "A comprehensive radiation model for numerical simulations of pulverised coal flames," in *Proceedings of the 11th International Heat Transfer Conference*, vol. 7, Kyongju, Korea, pp. 307–312, 1998.
83. Yu, M. J., S. W. Baek, and J. H. Park: "An extension of the weighted sum of gray gases non-gray gas radiation model to a two phase mixture of non-gray gas with particles," *International Journal of Heat and Mass Transfer*, vol. 43, no. 10, pp. 1699–1713, 2000.
84. Omori, T., S. Yamaguchi, and T. Fusegi: "Computational heat transfer analysis of a furnace using the WSGG model," in *Proceedings of 2000 IMECE*, vol. HTD-366-1, ASME, pp. 103–108, 2000.
85. Denison, M. K., and B. W. Webb: "*k*-Distributions and weighted-sum-of-gray gases: A hybrid model," in *Tenth International Heat Transfer Conference*, Taylor & Francis, pp. 19–24, 1994.
86. Denison, M. K., and B. W. Webb: "Development and application of an absorption line blackbody distribution function for CO_2," *International Journal of Heat and Mass Transfer*, vol. 38, pp. 1813–1821, 1995.
87. Denison, M. K., and B. W. Webb: "The spectral-line weighted-sum-of-gray-gases model for H_2O/CO_2 mixtures," *ASME Journal of Heat Transfer*, vol. 117, pp. 788–792, 1995.
88. Solovjov, V. P., and B. W. Webb: "An efficient method of modeling radiative transfer in multicomponent gas mixtures with soot," *ASME Journal of Heat Transfer*, vol. 123, pp. 450–457, 2001.
89. Dembele, S., A. Delmas, and J.-F. Sacadura: "A method for modeling the mitigation of hazardous fire thermal radiation by water spray curtains," *ASME Journal of Heat Transfer*, vol. 119, pp. 746–753, 1997.
90. Dembele, S., and J. X. Wen: "Investigation of a spectral formulation for radiative heat transfer in a one-dimensional fires and combustion system," *International Journal of Heat and Mass Transfer*, vol. 43, pp. 4019–4030, 2000.
91. Liu, F., G. J. Smallwood, and O. L. Gülder: "Application of the statistical narrow-band correlated-*k* method to low-resolution spectral intensity and radiative heat transfer calculations – effects of the quadrature," *International Journal of Heat and Mass Transfer*, vol. 43, pp. 3119–3135, 2000.
92. Liu, F., and G. J. Smallwood: "An efficient approach for the implementation of the SNB based correlated-*k* method and its evaluation," *Journal of Quantitative Spectroscopy and Radiative Transfer*, vol. 84, pp. 465–475, 2004.
93. Tessé, L., F. Dupoirieux, B. Zamuner, and J. Taine: "Radiative transfer in real gases using reciprocal and forward Monte Carlo methods and a correlated-k approach," *International Journal of Heat and Mass Transfer*, vol. 45, pp. 2797–2814, 2002.
94. Lee, P. Y. C., G. D. Raithby, and K. G. T. Hollands: "The "reordering" concept of the absorption coefficient for modelling nongray gases," in *Radiative Heat Transfer: Current Research*, vol. HTD-276, ASME, pp. 21–30, 1994.
95. Lee, P. Y. C., K. G. T. Hollands, and G. D. Raithby: "Reordering the absorption coefficient within the wide band for predicting gaseous radiant exchange," *ASME Journal of Heat Transfer*, vol. 118, no. 2, pp. 394–400, 1996.
96. Parthasarathy, G., J. C. Chai, and S. V. Patankar: "A simple approach to nongray gas modeling," *Numerical Heat Transfer*, vol. 29, pp. 394–400, 1996.
97. Denison, M. K., and W. A. Fiveland: "A correlation for the reordered wave number of the wideband absorptance of radiating gases," *ASME Journal of Heat Transfer*, vol. 119, pp. 853–856, 1997.
98. Ströhle, J.: "Assessment of the re-ordered wide band model for non-grey radiative transfer calculations in 3D enclosures," *Journal of Quantitative Spectroscopy and Radiative Transfer*, vol. 109, no. 10, pp. 1622–1640, 2008.
99. Marin, O., and R. O. Buckius: "Wide band correlated-*k* method applied to absorbing, emitting and scattering media," *Journal of Thermophysics and Heat Transfer*, vol. 10, pp. 364–371, 1996.
100. Marin, O., and R. O. Buckius: "A model of the cumulative distribution function for wide band radiative properties," *Journal of Quantitative Spectroscopy and Radiative Transfer*, vol. 59, pp. 671–685, 1998.

101. Marin, O., and R. O. Buckius: "A simplified wide band model of the cumulative distribution function for water vapor," *International Journal of Heat and Mass Transfer*, vol. 41, pp. 2877–2892, 1998.
102. Marin, O., and R. O. Buckius: "A simplified wide band model of the cumulative distribution function for carbon dioxide," *International Journal of Heat and Mass Transfer*, vol. 41, pp. 3881–3897, 1998.
103. Rothman, L. S., R. R. Gamache, R. H. Tipping, C. P. Rinsland, M. A. H. Smith, D. C. Benner, V. M. Devi, J.-M. Flaud, C. Camy-Peyret, A. Perrin, A. Goldman, S. T. Massie, L. R. Brown, and R. A. Toth: "The HITRAN molecular database: Editions of 1991 and 1992," *Journal of Quantitative Spectroscopy and Radiative Transfer*, vol. 48, no. 5/6, pp. 469–507, 1992.
104. Modest, M. F., and H. Zhang: "The full-spectrum correlated-*k* distribution for thermal radiation from molecular gas–particulate mixtures," *ASME Journal of Heat Transfer*, vol. 124, no. 1, pp. 30–38, 2002.
105. Modest, M. F.: "Narrow-band and full-spectrum *k*-distributions for radiative heat transfer—correlated-*k* vs. scaling approximation," *Journal of Quantitative Spectroscopy and Radiative Transfer*, vol. 76, no. 1, pp. 69–83, 2003.
106. Solovjov, V. P., D. Lemonnier, and B. W. Webb: "The SLW-1 model for efficient prediction of radiative transfer in high temperature gases," *Journal of Quantitative Spectroscopy and Radiative Transfer*, vol. 112, no. 7, pp. 1205–212, 2011.
107. Solovjov, V. P., and B. W. Webb: "A local-spectrum correlated model for radiative transfer in non-uniform gas media," *Journal of Quantitative Spectroscopy and Radiative Transfer*, vol. 73(2–5), pp. 361–373, 2002.
108. Solovjov, V. P., and B. W. Webb: "The cumulative wavenumber method for modeling radiative transfer in gas mixtures with soot," *Journal of Quantitative Spectroscopy and Radiative Transfer*, vol. 93(1-3), pp. 273–287, 2005.
109. Solovjov, V. P., and B. W. Webb: "Application of CW local correction approach to SLW modeling of radiative transfer in non-isothermal gaseous media," *Journal of Quantitative Spectroscopy and Radiative Transfer*, vol. 111, no. 2, pp. 318–324, 2010.
110. Barlow, R. S.: *International Workshop on Measurement and Computation of Turbulent Nonpremixed Flames (TNF)* website: http://www.sandia.gov/TNF/abstract.html.
111. Rivière, P., A. Soufiani, and J. Taine: "Correlated-*k* and fictitious gas methods for H_2O near 2.7 μm," *Journal of Quantitative Spectroscopy and Radiative Transfer*, vol. 48, pp. 187–203, 1992.
112. Wang, A., and M. F. Modest: "High-accuracy, compact database of narrow-band *k*-distributions for water vapor and carbon dioxide," *Journal of Quantitative Spectroscopy and Radiative Transfer*, vol. 93, pp. 245–261, 2005.
113. Tashkun, S. A., V. I. Perevalov, A. D. Bykov, N. N. Lavrentieva, and J.-L. Teffo: *Carbon Dioxide Spectroscopic databank (CDSD)*: available from ftp://ftp.iao.ru/pub/CDSD-1000, 2002.
114. Denison, M. K., and B. W. Webb: "The absorption-line blackbody distribution function at elevated pressure," in *Proceedings of the First International Symposium on Radiation Transfer*, ed. M. P. Mengüç, Begell House, pp. 228–238, 1996.
115. Hartmann, J.-M., R. Levi Di Leon, and J. Taine: "Line-by-line and narrow-band statistical model calculations for H_2O," *Journal of Quantitative Spectroscopy and Radiative Transfer*, vol. 32, no. 2, pp. 119–127, 1984.
116. Zhang, H., and M. F. Modest: "Full-spectrum *k*-distribution correlations for carbon dioxide mixtures," *Journal of Thermophysics and Heat Transfer*, vol. 17, no. 2, pp. 259–263, 2003.
117. Modest, M. F., and V. Singh: "Engineering correlations for full spectrum *k*-distribution of h_2o from the HITEMP spectroscopic databank," *Journal of Quantitative Spectroscopy and Radiative Transfer*, vol. 93, pp. 263–271, 2005.
118. Modest, M. F., and R. S. Mehta: "Full spectrum *k*-distribution correlations for CO_2 from the CDSD-1000 spectroscopic databank," *International Journal of Heat and Mass Transfer*, vol. 47, pp. 2487–2491, 2004.
119. Pal, G., A. Wang, and M. F. Modest: "A *k*-distribution-based spectral module for radiation calculations in multiphase mixtures," in *Proceedings of ASME Summer Heat Transfer Conference, Paper HT2009-88245*, 2009.
120. Abramowitz, M., and I. A. Stegun (eds.): *Handbook of Mathematical Functions*, Dover Publications, New York, 1965.
121. Press, W. H., B. P. Flannery, S. A. Tenkolsky, and W. T. Vetterling: *Numerical Recipes – The Art of Scientific Computing*, 1st ed., Cambridge, New York, 1989.
122. Bansal, A., M. F. Modest, and D. A. Levin: "Multigroup correlated-k distribution method for nonequilibrium atomic radiation," *Journal of Thermophysics and Heat Transfer*, vol. 24, no. 3, pp. 638–646, 2010, DOI: 10.2514/1.46641.
123. Taine, J., and A. Soufiani: "Gas IR radiative properties: From spectroscopic data to approximate models," in *Advances in Heat Transfer*, vol. 33, Academic Press, New York, pp. 295–414, 1999.
124. Modest, M. F., and R. J. Riazzi: "Assembly of full-spectrum *k*-distributions from a narrow-band database; effects of mixing gases, gases and nongray absorbing particles, and mixtures with nongray scatterers in nongray enclosures," *Journal of Quantitative Spectroscopy and Radiative Transfer*, vol. 90, no. 2, pp. 169–189, 2005.
125. Demarco, R., J. L. Consalvi, A. Fuentes, and S. Melis: "Assessment of radiative property models in non-gray sooting media," *International Journal of Thermal Sciences*, vol. 50, pp. 1672–1684, 2011.
126. Wang, L., and M. F. Modest: "Narrow-band based multi-scale full-spectrum *k*-distribution method for radiative transfer in inhomogeneous gas mixtures," *ASME Journal of Heat Transfer*, vol. 127, pp. 740–748, 2005.
127. Wang, L., and M. F. Modest: "Treatment of wall emission in the narrow-band based multi-scale full-spectrum *k*-distribution method," *ASME Journal of Heat Transfer*, vol. 129, no. 6, pp. 743–748, 2007.
128. Pal, G., and M. F. Modest: "A multi-scale full-spectrum *k*-distribution method for radiative transfer in nonhomogeneous gas–soot mixture with wall emission," *Computational Thermal Sciences*, vol. 1, pp. 137–158, 2009.

129. Pal, G., M. F. Modest, and L. Wang: "Hybrid full-spectrum correlated *k*-distribution method for radiative transfer in strongly nonhomogeneous gas mixtures," *ASME Journal of Heat Transfer*, vol. 130, pp. 082701–1–082701–8, 2008.
130. Pal, G., and M. F. Modest: "A narrow-band based multi-scale multi-group full-spectrum *k*- distribution method for radiative transfer in nonhomogeneous gas–soot mixture," *ASME Journal of Heat Transfer*, vol. 132, pp. 023307–1–023307–9, 2010.
131. Chang, H., and T. T. Charalampopoulos: "Determination of the wavelength dependence of refractive indices of flame soot," *Proceedings of the Royal Society (London) A*, vol. 430, no. 1880, pp. 577–591, 1990.
132. Pal, G., and M. F. Modest: "*k*-distribution methods for radiation calculations in high pressure combustion," *50th Aerospace Sciences Meeting, Paper No. AIAA-2012-0529*, 2012.
133. Kent, J. H., and D. Honnery: "Modeling sooting turbulent jet flames using an extended flamelet technique," *Combustion Science and Technology*, vol. 54, pp. 383–397, 1987.
134. Pawlak, D. T., E. E. Clothiaux, M. F. Modest, and J. N. S. Cole: "Full spectrum correlated-*k* for shortwave atmospheric radiative transfer," *Journal of the Atmospheric Sciences*, vol. 61, pp. 2588–2601, 2004.
135. Hogan, R. J.: "The full-spectrum correlated-*k* method for longwave atmospheric radiative transfer using an effective Planck function," *Journal of the Atmospheric Sciences*, vol. 67, pp. 2086–2100, 2010.
136. Bansal, A., M. F. Modest, and D. A. Levin: "Multi-scale k-distribution model for gas mixtures in hypersonic nonequilibrium flows," *Journal of Quantitative Spectroscopy and Radiative Transfer*, vol. 112, no. 7, pp. 1213–1221.
137. Bansal, A., and M. F. Modest: "Narrow-band k-distribution database for atomic radiation in hypersonic nonequilibrium flows," *ASME Journal of Heat Transfer*, p. 122701, 2011.

Problems

20.1 A long, cylindrical furnace bounded by a cold, black wall of 1 m radius contains pure CO_2 that is isothermal at 1700 K and at a pressure of p atm. Using the mean-beam-length method, determine the nondimensional wall heat flux $\Psi = q_w/\sigma T^4$ as a function of pressure. Plot Ψ *vs.* p (actual calculations for $p = 0.001$, 0.01, 0.1, and 1.0 should suffice).

20.2 A high-pressure isothermal mixture ($p > 40$ atm) of 80% N_2 and 20% CO at 2000 K is contained between two large, parallel, cold black plates, spaced 1 m apart. If the radiative flux to each wall may not exceed 100 kW/m^2, what is the maximum pressure the gas mixture may be raised to? Use the mean-beam-length method.

20.3 An isothermal mixture of N_2 and soot ($m = 2.5 - 0.15i$) at 2000 K is contained between two large, parallel, cold black plates, spaced 1 m apart. If the radiative flux to each wall may not exceed 100 kW/m^2, what is the maximum volume fraction of soot, f_v, allowed? Use the mean-beam-length method.

20.4 Two parallel, infinite, black plates at constant temperatures T_1 and T_2 are separated by a nongray medium of geometrical thickness $d = 10$ cm that is at radiative equilibrium. The absorption characteristics of the medium are such that they can be approximated by

$$\kappa_\lambda = \begin{cases} \overline{\kappa} = 1\,\text{cm}^{-1} & 3\,\mu\text{m} < \lambda < 7\,\mu\text{m}, \\ 0 & \text{elsewhere.} \end{cases}$$

Calculate the nondimensional heat flux, $q/\sigma(T_1^4 - T_2^4)$, for a number of T_2 ($T_2 = 500$ K, 750 K, 1000 K, 1500 K, and 2000 K) and $T_1 = 300$ K by

(*a*) the differential approximation, using a gray gas with Planck-mean absorption coefficient κ_P,
(*b*) the nongray differential approximation.

For the evaluation of κ_P you may use $T_m = (T_1 + T_2)/2$. Plot, compare, and discuss your results.

20.5 A cold-walled cylindrical furnace of 1 m radius contains pure CO_2 that is isothermal at 1700 K and at a pressure of p atm. Using the (*i*) gray and (*ii*) nongray differential approximation with single band strength $\overline{\kappa}$, determine the nondimensional wall heat flux $\Psi = q_w/\sigma T^4$ as a function of pressure. Plot Ψ *vs.* p (actual calculations for $p = 0.001$, 0.01, 0.1, and 1.0 should suffice; for simplification, you may assume that band width is not a function of p).

20.6 Repeat Problem 20.5, adding steam at 0.1 atm partial pressure to the medium. You may assume that only the 2.7 and 6.3 μm bands are of importance.

20.7 An infinitely long cylinder of radius $R = 10\,\text{cm}$ is bounded by a cold black wall. Inside the cylinder there is uniform heat generation of $\dot{Q}''' = 38{,}136\,\text{W/m}^3$. Estimate wall heat fluxes and temperature distributions using the P_1-approximation if

(*a*) the medium has a band at $\lambda = 4\,\mu\text{m}$ of width $\Delta\lambda = 1\,\mu\text{m}$; across the band it has a constant absorption coefficient such that $\overline{\kappa}R = 100$,

(*b*) the medium is gray with an "appropriately" chosen κ_P, say by evaluating κ_P at the volume-averaged temperature T_{av}, that is

$$T_{\text{av}}^4 = \frac{1}{V}\int_V T^4\,dV.$$

20.8 The new planet in an adjacent solar system recently found by Penn State (and other) researchers has been determined to have an atmosphere consisting of nitrogen with 1% by volume NO. The planet's surface has an emittance of $\epsilon = 0.5$, and a temperature of $T_s = 900\,\text{K}$. The atmosphere's total pressure is known to be $p(z) = p_s\,e^{-z/L}$ (surface pressure $p_s = 5\,\text{bar}$, characteristic length $L = 10\,\text{km}$). Assuming radiative equilibrium prevails, what is the heat loss from the planet? You may assume that for NO line broadening is unaffected by temperature.

(a) To make a coarse approximation, replace the atmosphere by a constant pressure (p_s) layer of a thickness that would contain the correct total pressure path length. Evaluate radiative properties as if the atmosphere's temperature were constant at T_s.

(b) The problem is to be solved by the P_1-approximation combined with the box model. Find the appropriate absorption coefficient(s) and other necessary parameters. You may assume that the spectral width of bands for NO is unaffected by altitude (evaluate at surface conditions). Set up equation(s) and boundary condition(s).

(c) Determine the heat loss from the planet.

(d) What would change if an infinitely thick atmosphere with exponentially decaying pressure were considered?

20.9 A high-pressure isothermal mixture ($p > 40\,\text{atm}$) of 80% N_2 and 20% CO at 2000 K is contained between two large, parallel, cold black plates, spaced 1 m apart. If the radiative flux to each wall may not exceed $100\,\text{kW/m}^2$, what is the maximum pressure the gas mixture may be raised to? Use the box model together with *(a)* the P_1-approximation as well as *(b)* the exact formulation.

20.10 The coal particles of Problem 12.3 are burnt in a long cylindrical combustion chamber of $R = 1\,\text{m}$ radius. The combustor walls are gray and diffuse, with $\epsilon_w = 0.8$, and are at 800 K. Since it is well stirred, combustion results in uniform heat generation throughout of $\dot{Q}''' = 720\,\text{kW/m}^3$.

(a) Determine the maximum temperature in the combustor, using the P_1/differential approximation, assuming radiation is the only mode of heat transfer (use $\kappa = 4.5\ \text{m}^{-1}$ and $\sigma_s = 0.5\,\text{m}^{-1}$ if the results of Problem 12.3 are not available).

(b) How will the answer change if, instead, the combustion gas is responsible for the radiation with

$$\kappa_\lambda = \begin{cases} 10\,\text{cm}^{-1}, & 4\,\mu\text{m} < \lambda < 5\,\mu\text{m} \\ 0, & \text{elsewhere} \end{cases}; \quad \sigma_s = 0?$$

(c) What if both are present?

20.11 Consider a sphere of very hot molecular gas of radius 50 cm. The gas has a single vibration–rotation band at $\eta_0 = 3000\,\text{cm}^{-1}$, is suspended magnetically in a vacuum within a large cold container and is initially at a uniform temperature $T_g = 3000\,\text{K}$. For this gas $(\rho_a\alpha)(T) = 500\,\text{cm}^{-2}$, $\omega(T) = 100\sqrt{T/100\,\text{K}}\,\text{cm}^{-1}$, and $\beta \gg 1$. These properties imply that the absorption coefficient may be determined from

$$\kappa_\eta = \kappa_0\,e^{-2|\eta-\eta_0|/\omega}, \quad \kappa_0 = \frac{\rho_a\alpha}{\omega}$$

and the band absorptance from

$$A(s) = \omega A^* = \omega[E_1(\kappa_0 s) + \ln(\kappa_0 s) + \gamma_E], \qquad \gamma_E = 0.577216.$$

Using the stepwise-gray model together with the P_1-approximation and neglecting conduction and convection, specify the total heat loss per unit time from the entire sphere at time $t = 0$. Outline the solution procedure for times $t > 0$.
Hint: Solve the governing equation by introducing a new dependent variable $g(\tau) = \tau(4\pi I_b - G)$.

20.12 Repeat Problem 20.11 using the exact integral relations together with the exponential wide band model.

20.13 Repeat Problem 20.11 using the weighted-sum-of-gray gases approach together with the P_1-approximation.

20.14 Repeat Problem 20.11 for varying line overlap β, say $\beta = 0.01,\ 0.1,\ 1$, and 10. Plot heat loss at $t = 0$ *vs.* β.
Hint: Use Table 11.2 or some other correlation for the band absorptance.

20.15 An infinitely long cylinder of radius $R = 10$ cm is bounded by a wall that is isothermal at $T_w = 1500$ K and has a gray emittance of $\epsilon = 0.3$. Inside the cylinder there is uniform heat generation of $\dot{Q}''' = 38{,}136\ \mathrm{W/m^3}$. The cylinder is filled with a mixture of combustion gases at $p = 1$ atm, containing 10% by volume CO_2 and 20% water vapor. Assuming the gas to be well-stirred (i.e., isothermal) determine the gas temperature using the weighted-sum-of-gray-gases approach, using the data of Table 20.2. This problem will require an iteration and, thus, is most conveniently solved on a computer.

(a) Set up all necessary equations and explain the procedure. You may use the exact relations of Section 14.6 or the P_1-approximation.

(b) Write a small computer code to find the gas temperature.

Note for the P_1-approximation: The solution to the ODE

$$\frac{1}{r}\,\frac{d}{dr}\left(r\frac{df}{dr}\right) - \nu^2 f = 0$$

is

$$f(r) = C_1 I_0(\nu r) + C_2 K_0(\nu r),$$

where I_0 and K_0 are modified Bessel functions. Note also that $K_0(0) \to \infty$ and $I_0'(x) = I_1(x)$.

20.16 Repeat Problem 20.7 for the case that the medium is a mixture of 30% water vapor in nitrogen, using the SLW method with four gray gases, together with the correlation of Denison and Webb. To determine an appropriate reference temperature, first make a more approximate gray calculation, using a Planck mean absorption coefficient from Fig. 11-31.

20.17 A spherical container of 1 m diameter is filled with pure CO_2 and is initially at 2000 K, 1 bar. While the CO_2 is continuously stirred (i.e., stays isothermal), the walls of the container are cooled such that the gray, diffuse wall ($\epsilon_w = 0.6$) remains at a constant $T_w = 400$ K. Determine the time it takes for the gas to cool down to 500 K, using the FSK method together with the Denison and Webb correlation. Assume a constant reference condition of $T_{\mathrm{ref}} = 1000$ K, and use the P_1 method to solve the RTE.

20.18 Repeat Problem 20.17 adding small gray particles with an absorption coefficient of $\kappa_p = 0.1\ \mathrm{m^{-1}}$ and an (isotropic) scattering coefficient of $\sigma_p = 1\ \mathrm{m^{-1}}$.

20.19 Repeat Problem 20.17 adding H_2O and N_2 to the mixture, so that the final mixture has 20% CO_2 and 40% N_2 (by volume).

20.20 Repeat Problem 20.19 using the WSGG approach together with the correlation of Truelove.

20.21 Repeat Problem 20.19 using the SLW method with four gray gases. Compare with results from the previous problem.

20.22 Repeat Problem 20.19 for the case of radiative equilibrium without stirring.

20.23 Repeat Problem 20.21 for the case of radiative equilibrium without stirring.